LATERAL TORSIONAL BUCKLING OF WOOD I-JOIST

BY

RÉMI ST-AMOUR

A THESIS SUBMITTED TO THE

FACULTY OF GRADUATE AND POSTDOCTORAL STUDIES

IN PARTIAL FULFILLMENT OF THE REQUIREMENTS FOR THE

MASTER OF APPLIED SCIENCE IN CIVIL ENGINEERING

OTTAWA-CARLETON INSTITUTE FOR CIVIL ENGINEERING

FACULTY OF CIVIL ENGINEERING

UNIVERSITY OF OTTAWA

ABSTRACT

Engineered wood I-joists have grown in popularity as flooring and roofing structural systems in the past 30 years, replacing solid sawn lumber joists. Typical wood I-joists are manufactured with a very slender section, which is desirable to achieve higher flexural capacities and longer spans; however, this makes them susceptible to lateral torsional buckling failure. Continuous beam spans and uplift forces on roof uplift are potential scenarios where lateral instability can occur and reflects the need to investigate the lateral torsional buckling behavior of wood I-joists. Within this context, the present study conducts an experimental investigation on the material properties and the critical buckling load of 42 wood I-joist specimens. A 3D finite element model is built using the experimentally determined material parameters to effectively predict the observed buckling behavior of the specimens while also accounting for initial imperfections in the joists. The adequacy of other analytical models to predict the critical buckling load of wood I-joists are also investigated. It is demonstrated that the American design standard underestimates the critical buckling load of wood I-joists while the classical theory provides an adequate estimate of the buckling capacity. Furthermore, the effects of initial imperfections on the lateral torsional buckling behavior are discussed. The developed and verified FE model is used to reproduce the nonlinear buckling behavior of the wood I-joist and also to provide an accurate estimate of the lateral torsional buckling capacity using the linear buckling analysis.

ACKNOWLEDGMENT

I would like to express my sincere gratitude towards my research director, Dr. Ghasan Doudak, whose advice and guidance allowed me to develop my expertise in timber engineering and complete this research.

I can never thank enough colleagues that provided crucial help during my research especially, Mr. Yang Du, Mr. Qiuwu Xiao, Mr. Dominic Cote, Ms. America Lopez, Mr. Arthur Manieri, Mr. Benoît Pelletier and Mr. Christian Viau.

Finalement, je veux exprimer ma profonde reconnaissance à l'égard de ma mère et de mon père pour voir cru en moi ainsi que pour leur appui tout au long de mes études universitaires.

TABLE OF CONTENTS

LIST OF TABLES

LIST OF FIGURES

CHAPTER 1

INTRODUCTION

Recent initiatives to build "greener" structures (e.g. Wood First Act (BC, 2009), La Charte du bois (QC, 2013) has turned the attention of the engineering community towards engineered wood products, especially those that can produce larger spans while still maintaining a relatively low self-weight. This chapter presents a description of the problem, a general background on the lateral torsional buckling failure, provides research objectives and the methodology and describes the thesis structure.

1.1 Description of the problem

Engineered wood products are commonly used in the residential sector. Wood I-joists gradually replaced conventional lumber joists in flooring and roofing applications since the 1980s. Engineered wood includes any wood-based product that has been manipulated to enhance its mechanical properties. Wood I-joists fall into this category as they consist of a composite assembly of wooden flanges, usually made of machine stress-rated lumber or laminated veneer lumber, and a web panel made of oriented strand board (OSB). The resulting I-shape possesses an increased moment of inertia about the strong axis, making them efficient members to resist strong axis bending, where the flanges resist axial bending forces and, the web provides shear resistance. Through the use of finger joints, engineered wood I-joists can be used in any length allowing longer spans with small lumber pieces.

The slender nature of wood I-joists may be desirable for flexural resistance but comes at the price of lateral instability as they become susceptible to lateral torsional buckling (LTB) failure. Engineered wood I-joists are typically sheathed with subflooring and are therefore considered to be braced against lateral instability. However, several examples of construction details exist, where the wood I-joist is not adequately braced, such as:

continuous beams, cantilevers and cases where wind uplift on roofs govern the design. North American timber design standards recognize lateral torsional buckling as a potential failure mode for long and slender members. However, design against such failure in wood I-joists is taken into account in a cursory manner (NDS, 2015) or not addressed at all (CSA, 2014a). In this context, the current research aims to study the lateral instability behavior of engineered wood I-joists and to assess the validity of various analytical models to predict the critical buckling load considering the anisotropic and composite nature of I-joist elements.

1.1.1 Constitutive material properties of wood I-joists

Wood I-joist is anisotropic material but can be simplified and modelled as an orthotropic material with distinct material properties along three orthogonal axes defined by the wood fiber and the annual growth rings (FPL, 2010). Figure 1-1 illustrates the orthotropic axes of wood including the longitudinal direction that follows the wood's fiber direction, the radial direction that is perpendicular to the growth rings, and the tangential direction that is tangent to the growth rings.

The mechanical properties in the tangential and radial directions are very close for a large variety of species (FPL, 2010). Furthermore, it is impractical to determine the orientation of the growth rings for each lumber piece, prior to its use. Therefore, the mechanical properties of the radial and tangential directions are generally assumed to be identical. For this reason, design standards refer to the properties of wood in the directions parallel and perpendicular to the grain.

Albeit wood can be modelled as an orthotropic material, not all its mechanical properties are involved in the resistance to lateral torsional buckling. It has been demonstrated that only the longitudinal modulus of elasticity (MOE) and the transverse shear modulus influence the elastic lateral torsional buckling response of wooden beams (Xiao et al., 2014).

The I-joist web panel is made of oriented strand board which consists of wood strands bonded with a waterproof adhesive. The orientation of the inner layer dictates the weak axis, whereas the outer layer's strand orientation dictates the strongest axis. It is common to find the strong axis oriented along the transverse direction of the wood I-joist in order to enhance its shear capacity. Although data on the modulus of elasticity of OSB panel has been provided in the literature (Thomas, 2011), limited data is available on the shear properties and the Poisson's ratio of OSB. Methods for determining the shear modulus of structural composite panels (ASTM D2718 & D2719) involve planar shear and shear through the thickness.

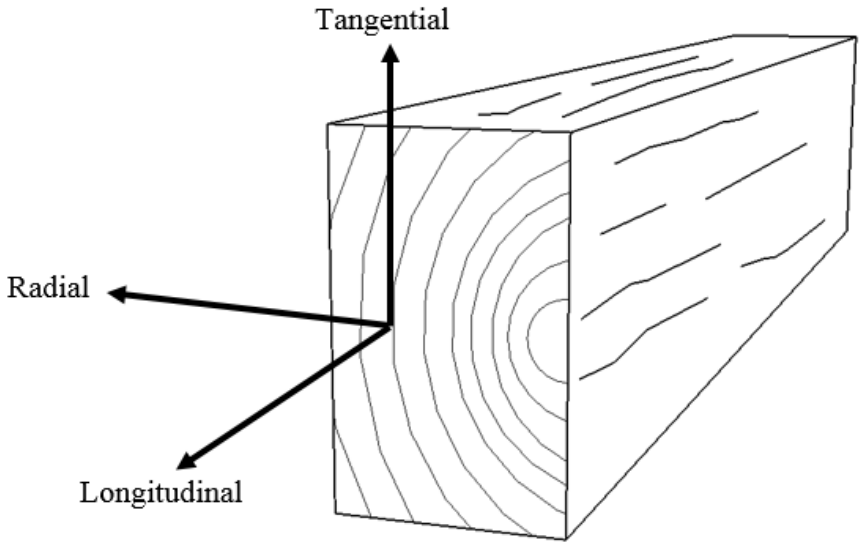

Figure 1-1 Wood orthotropic principal axes

1.1.2 Behavior of I-shaped beams subjected to lateral instability

Given a slender section, an I-shaped beam can develop a tendency to undergo lateral torsional buckling when it is bent about its major axis, if it is not laterally and/or torsionally restrained. As the beam deflects, axial stresses develop in the flanges and as a result, one flange experiences compressive stresses and the other tension stresses. The compression flange tends to buckle out of plane while the tension flange resists this tendency. The tension flange's restoring force is not enough to prevent buckling but contributes to the overall resistance and the section starts to deflect laterally and twist (Figure 1-2). The twisting motion about the longitudinal axis involves the torsional and warping stiffness of the section and is mostly influenced by its flange dimensions (NSC, 2006). The lateral deflection involves the lateral bending stiffness which includes the moment of inertia about the weak-axis that is also influenced mostly by the flange cross-section; especially the flange width.

Several factors influence the lateral torsional buckling resistance of an I-section, including the section type (such as mono symmetric, z sections etc.), the moment distribution along the span, the boundary conditions and the position of the applied loads relative to the shear center (Timoshenko & Gere, 1961). A load applied above the shear center has a destabilizing effect that will decrease the lateral torsional buckling resistance of a section, while a load applied below the shear center would have a stabilizing effect.

The development of a closed form solution for the lateral torsional buckling of an I-section can be derived for a simply supported configuration and a uniform moment. Formulated using the principle of total potential energy (Timoshenko & Gere, 1961), it provides the basis for most design provisions. The total potential energy of an I-beam of length *l* having a weak-axis bending stiffness EI_y, a torsional rigidity GJ and a warping stiffness EC_w subjected to a uniform moment M undergoing lateral torsional buckling can be written as

$$\pi = \frac{1}{2}\int_0^l EI_y w''^2 dx + \frac{1}{2}\int_0^l GJ\theta'^2 dx + \frac{1}{2}\int_0^l EC_w\theta''^2 dx + \int_0^l M\theta w'' dx \qquad (1\text{-}1)$$

Where $w(x)$ and $\theta(x)$ denote the lateral displacement and angle of twist functions. In the process of derivation of a closed form solution for Equation 1-1, applicable assumptions include: conservative loads, no initial imperfections in the member, a linear elastic material, negligible inertia effects (static analysis), negligible shear deformations and the cross-section that remains rigid throughout buckling (Vlasov, 1961). By applying the stationary conditions $\left(\frac{\partial \pi}{\partial w''}\right)\delta w'' + \left(\frac{\partial \pi}{\partial \theta}\right)\delta\theta + \left(\frac{\partial \pi}{\partial \theta'}\right)\delta\theta' + \left(\frac{\partial \pi}{\partial \theta''}\right)\delta\theta'' = 0$, one obtains the equilibrium and boundary conditions which can be solved. Alternatively, Equation 1-1 can be solved using approximate energy methods which assume two sinusoidal functions for the lateral and angle of twist displacement functions. The critical moment M_{cr} for a simply supported I-beam of unsupported length L subjected to a uniform moment M is given as:

$$M_{cr} = \frac{\pi}{L}\sqrt{EI_yGJ + \left(\frac{\pi E}{L}\right)^2 I_y C_w} \qquad (1\text{-}2)$$

Closed form solutions for boundary conditions, moment distribution and load eccentricity effect other than Equation 1-2 are unattainable. One can resort to numerical methods and finite element analysis, for instance, to estimate the critical buckling load of a structural element with specific boundary conditions and loading pattern other than those that lay the basis for Equation 1-2. Finite element modelling has become a critical tool when it comes to providing general provisions on the lateral buckling that address various loading and boundary conditions scenarios. To account for different loading and boundary conditions, the Canadian Design Standards for steel construction (CSA, 2014b) uses a moment gradient factor (ω_2) to account for various moment distributions and an effective length factor (L_e) to account for load position effects.

An underlying assumption in the derivation of the lateral torsional buckling capacity of an I-beam (Equation 1-2) assumes that the member has no initial imperfection, leading to a bifurcation where it undergoes lateral torsional buckling (Figure 1-3). In reality, I-beams have minor imperfections such as crook and bow that promote lateral displacement and

twist of the section as soon as the loading is applied, resulting in a nonlinear behavior (Kirby & Nethercot, 1979).

The Southwell plot method (Southwell, 1931) determines the critical buckling load of a strut based on force-displacement experimental data. By plotting the displacement versus the ratio of displacement to force and computing the inverse of the resulting slope one can find the critical buckling load, regardless of the nonlinear behavior of the real strut that contains initial imperfections. This method as been supported by several researchers and a variant was proposed to convert this technique for lateral torsional buckling of beams. However, Mandal and Calladine (2002) argued that the original Southwell plot technique is still more reliable in the analysis for lateral torsional buckling of beams, based on experimental and analytical proofs.

The stability of imperfect thin-walled composite beams was studied by Machado (2010). Considering the initial imperfections, a static non-linear analysis was conducted to evaluate the effects of imperfection on the pre-buckling, buckling and post-buckling response of thin-walled composite beams based on large displacements and rotations formulation. Numerical results showed that the initial geometric imperfection reduces the load-carrying capacity of thin-walled members and its effects on the nonlinear response to the loading becomes larger as the initial imperfections increase.

A study on the effect of random imperfection in steel I-beams were conducted by Kala (2013). Mathematical models and numerical simulations are developed for both perfect and beams with initial imperfections. The influence of various imperfections profiles is discussed and it is concluded that initial imperfection reduced significantly the ultimate load-bearing capacity in lateral buckling, compared to the theoretical model that assumed a perfect beam. The author also emphasized that the steel I-beam can suffer from material yielding prior to undergo global buckling as a result of initial imperfections.

Ascione (2014) investigated the influence of initial geometric imperfections on the lateral buckling of thin-walled pultruded GFRP I-profile beams. Two manufacturing

imperfections were considered; the minor axis out-of-straightness and the web/flange non-orthogonality. Numerical analysis showed that these imperfections can affect the pre-buckling behavior and implied that out of straightness should be considered in design, especially for serviceability requirements.

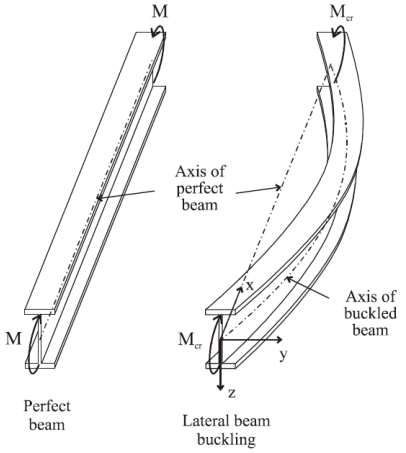

Figure 1-2 I-section undergoing lateral torsional buckling (Kala, 2013)

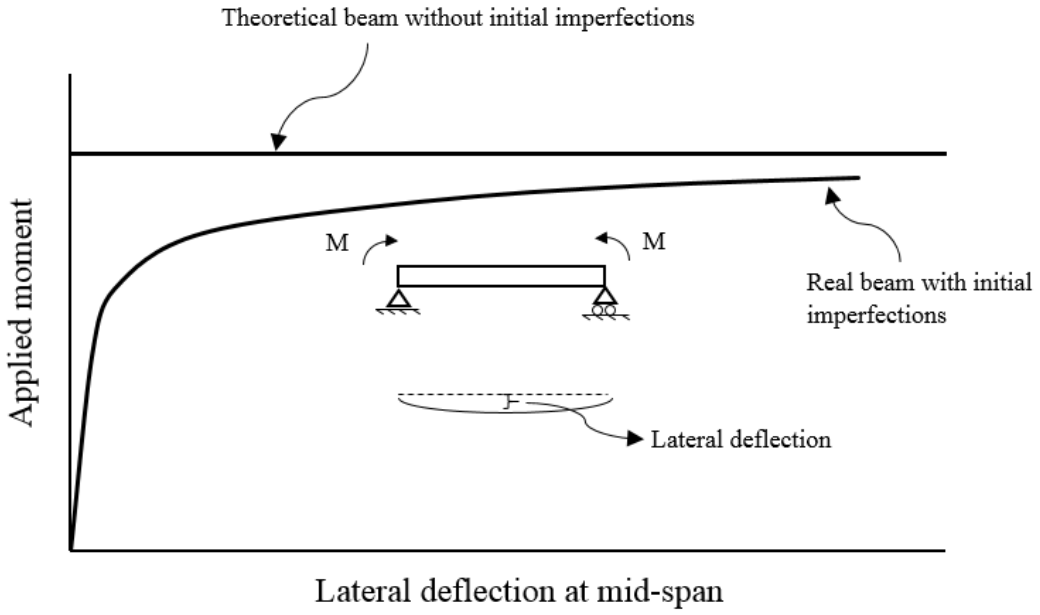

Figure 1-3 Lateral buckling of theoretical and realistic I-beams

1.1.3 Canadian design standard for steel construction

The elastic critical moment of an I-section subjected to lateral instability in the Canadian steel standard (CSA, 2014b) is given by Equation 1-3:

$$M_u = \omega_2 \frac{\pi}{L} \sqrt{EI_y GJ + \left(\frac{\pi E}{L}\right)^2 I_y C_w} \qquad (1\text{-}3)$$

Where ω_2 is a moment gradient factor given by Equation 1-4:

$$\omega_2 = \frac{4M_{max}}{\sqrt{M_{max}^2 + 4M_a^2 + 7M_b^2 + 4M_c^2}} \leq 2.5 \qquad (1\text{-}4)$$

Where M_{max} represents the maximum bending moment in the beam segment, M_b denotes the bending moment at mid-span of the beam segment and M_a & M_c are the bending moment at quarter span of the beam segments.

1.1.4 American design standard for wood construction

The American design standard for wood construction (NDS, 2015) proposes a method to calculate the critical moment of a wood I-joist subjected to lateral instability as per Clause 7.3.5.3. This method consists of idealizing the wood I-joist as a column restrained in the plane of the I-joist's web undergoing lateral buckling and using the section properties of the I-joist's compression flange. The moment resistance is factored with the stability factor of a column C_p showed in Equation 1-5:

$$C_p = \frac{1+(F_{cE}/F_c^*)}{2c} - \sqrt{\left[\frac{1+(F_{cE}/F_c^*)}{2c}\right]^2 - \frac{(F_{cE}/F_c^*)}{c}} \qquad (1\text{-}5)$$

Where $F_{cE} = \frac{0.822E'_{min}}{(l_e/d)^2}$, F_c^* is the specified compression strength of the flange and c is a reliability factor.

1.1.5 Twisting of I-beams

Provided that the warping deformations in the flanges are free to occur, the I-section undergoing twist involves only the Venant torsional shear stresses. In the case where warping is prevented, axial stresses develop in the flanges and the latter experiences a combination of warping and St-Venant torsional shear stresses (Kirby & Nethercot, 1979). The warping constant C_w of an open section with thick flanges must consider global and local warping actions (Gjelsvik, 1981). For an I-section with thin flanges, local warping is generally neglected. However, when it comes to wood I-joists which have thick flanges, local warping may be considerable.

The warping constant C_w for an I-section with thick flanges having a flange width b, web height d' (taken between flange centroids), flange thickness t, a web thickness w and a moment of inertia about the weak axis I_y, can be computed as the summation of the global (C_{wg}) and the local (C_{wl}) warping components:

$$C_w = \{C_{wg}\} + \{C_{wl}\} = \{I_y d'^2/\,4\} + \{2t^3 b^3/144 + w^3 d'^3/144\} \qquad (1\text{-}6)$$

While warping stresses can be neglected for I-beams with narrow and thin flanges (Timoshenko & Gere, 1936), the warping contribution will still be considered for the wood I-joist in this study since the span to depth ratio of the test specimens will vary and likely attain small values, which promotes warping deformations in the member. Gjelsvik also proposed an approximate form for the St-Venant constant J given by $J = \sum_{i=1,2,3} \frac{b_i h_i^3}{3}$. A more precise value for the St-Venant constant J_e is given by:

$$J_e = \sum_{i=1,2,3} \left(\frac{b_i h_i^3}{3}\right) \left[1 - \frac{192 h_i}{\pi^5 b_i} \sum_{n=1,3\ldots}^{\infty} \frac{1}{n^5} \tanh\left(\frac{n\pi b_i}{2h_i}\right)\right] \qquad (1\text{-}7)$$

where b is the width and h the height of the considered component.

1.1.6 Transformed section properties for composite I-beams

Transformed section properties for composite I- beams that have two distinct materials for the flanges and the web can be derived from the theorem of internal strain energy and the Vlasov theory (Du, 2016). Assuming the I-beam consists entirely of the flange material, the transformed St-Venant constant $J_{e\,tr}$, warping constant $C_{w\,tr}$ and the moment of inertia about the weak axis $I_{y\,tr}$ are given as

$$I_{y\,tr} = I_{y,f} + n_1 I_{y,w} \qquad (1\text{-}8)$$

$$C_{w\,tr} = C_{w,f} + n_1 C_{w,w} \qquad (1\text{-}9)$$

$$J_{e\,tr} = J_{e,f} + n_2 J_{e,w} \qquad (1\text{-}10)$$

where $n_1 = E_{web}/E_{flange}$ and $n_2 = G_{web}/G_{flange}$, E denoting the modulus of elasticity and G the shear modulus, $I_{y,f}$ is the weak axis moment of inertia of the flanges, $I_{y,w}$ is the weak axis moment of inertia of the web, $C_{w,f}$ is the warping constant of the flanges, $C_{w,w}$ is the warping constant of the web, $J_{e,f}$ is the St-Venant constant of the flanges and $J_{e,w}$ is the St-Venant constant fo the web.

1.2 Research objectives

The current research project aims at investigating the lateral torsional buckling behavior of wood I-joists. Specific goals include:

- Conducting an experimental investigation on the mechanical properties of wood I-joist components;
- Studying the lateral torsional buckling behavior of wood I-joists in the elastic range through full-scale experiments;

- Developing a finite element model using commercially available software packages to predict the behavior of wood I-joist in lateral torsional buckling and validating the models using full-scale test results;
- Conducting a sensitivity analysis of the modulus of elasticity, shear modulus and Poisson's ratio on the buckling response;
- Evaluating the adequacy of current timber code provisions on lateral stability of engineered wood I-joists.

1.3 Methodology

The approaches taken to meet the above-mentioned research objectives are outlined as follows.

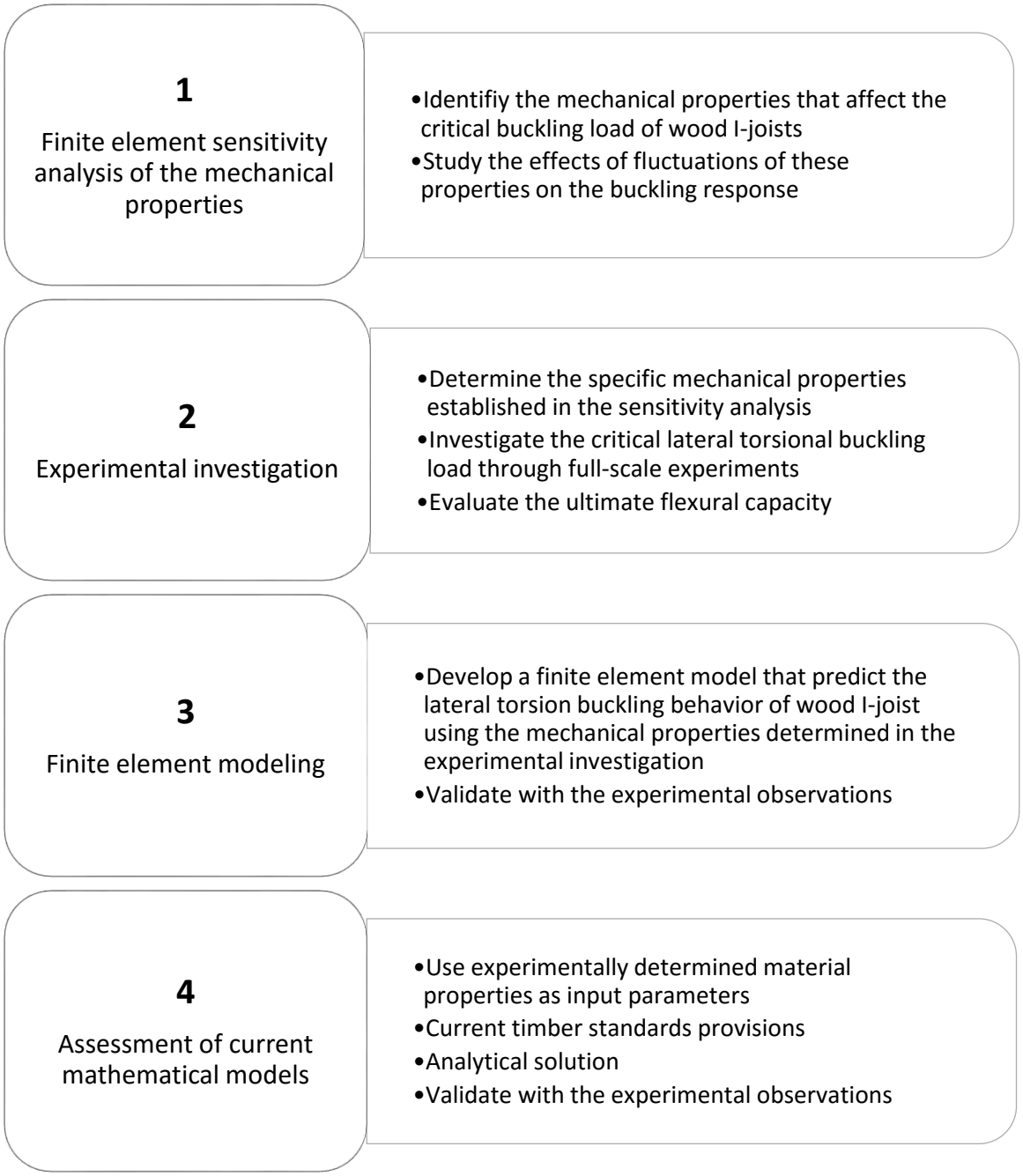

1.4 Outline of the thesis

Chapter 1 introduces the engineered wood product under the scope of this study, the research needs, objectives and methodology.

Chapter 2 presents the available literature on lateral instability of wooden beams and wood I-joists and provides an overview of the conducted experimental research in this field.

Chapter 3 conducts a finite element sensitivity analysis on the material parameters of the wood I-joists that affect the response to lateral torsional buckling.

Chapter 4 elaborates on the experimental investigation and presents the methods used for determination of the mechanical properties, the critical lateral torsional buckling load and the ultimate flexural capacity.

Chapter 5 presents results of the experiment investigation on the mechanical properties, the critical buckling load and the ultimate flexural capacity.

Chapter 6 describes the finite element modelling.

Chapter 7 discusses the results obtained from the experimental investigations and validates the various analytical models used in this study.

Chapter 8 presents a summary of the research, relevant findings and conclusions as well as recommendations for further research.

CHAPTER 2

LITERATURE REVIEW

This chapter presents a review of experimental researches that investigated the lateral instability of wooden beams. Research studies presented in Section 2.1 emphasize on rectangular wood beams while those presented in Section 2.2 focus on wood I-joists. Considering the scope of this study, this review primarily focuses on the experimental methods used for the determination of the critical buckling load as well as the developed analytical models for predicting the critical buckling loads of wood beams and wood I-joists.

2.1 Lateral instability of wood beams

Hooley and Madsen (1964) conducted bending tests on glued-laminated beam specimens without lateral restraints along the span to investigate the lateral torsional buckling failure of wood beams. The goal was to validate the empirical solution for lateral torsional buckling of rectangular wooden beams. The experimental data agreed well with the theory and the study concluded that the slenderness ratio Ld/b^2 governs the lateral stability of the beams, rather than d/b which was then assumed by many building standards. The concept of short, intermediate and long beams was introduced, which combined the flexural mode of failures of pure flexural, inelastic buckling and elastic buckling in one relationship for design purposes. The tests in this study showed that this approach yielded a safety factor ranging from 2.5 to 3, depending on the beam slenderness.

Zahn (1973) analyzed the effect of decking on the buckling capacity of beams through energy-based solutions. The shear resistance provided by the deck system is incorporated and a closed form solution is obtained to investigate various loading and support conditions. Zahn (1984) studied the effectiveness of lateral and twisting bracing on beam-deck in a sway model under gravity loads.

Bell and Eggen (2001) investigated the approach taken by the Norwegian and European timber codes to evaluate the capacities of beam-columns subjected to lateral instability. Linear and non-linear buckling models were developed, using simply supported rectangular wood beam configuration, axial force and two equal and opposite moments at the ends. The geometric non-linear analysis incorporated initial imperfections in the members and was used in the determination of the critical buckling moment. Critical buckling loads for the axial force and the bending moments acting alone from the non-linear analysis were found to be 10% lower than the linear buckling analyses. Combined loading interaction curves from the linear and non-linear model were compared against the two code approach for beam-columns capacity. The normalized linear and non-linear interaction curves were found to be very similar. It was shown that the Norwegian code which assumes a linear relationship between the normalized flexural and axial capacities was very conservative. On the other hand, it is demonstrated that Eurocode 5 overestimate the capacity by as much as 30 %, for certain values of axial force and bending moment. According to the analytical results, the authors propose a nonlinear combined loading formula. They also investigate the effectiveness of bracing on beam stability. The bracing height and stiffness effects were analyzed using a spring. It was demonstrated that the buckling capacity improvement was proportional to the lateral bracing distance above the shear center, where the extreme compression fiber was the optimal position that requires the smallest spring stiffness. Other researchers also investigated the behavior of beam-columns stability such as Steiger and Fontana (2005), Song and lam (2006) and Song and Lam (2009) with emphasis on numerical solutions.

AFPA (2003) issued a technical report that addresses the design of wood members for lateral torsional buckling. The effect of beam slenderness, loading and support conditions were discussed. The effective length and equivalent moment factor approaches for adjusting the buckling capacity were outlined and compared. The report proposed conservative values to be used for support configurations other than cantilevered and continuous beams. Closed form solutions for lateral torsional buckling of beams were derived using differential equations, infinite series approximation and strain energy

approximation methods. Based on an energy formulation, the load eccentricity expression was also derived. The solution was based on several simplifying assumptions such as the member having a rectangular section, warping can be neglected and the vertical displacement of the load function is sinusoidal.

Hindman (2005a) studied the lateral torsional buckling behavior of various structural composite lumber products such as machine stress rated lumber (MSR), laminated veneer lumber (LVL), parallel strand lumber (PSL) and laminated strand lumber (LSL). Their distinct elastic constant ratios and torsional rigidity resulted in a critical buckling load behavior that is different from solid sawn wood members. Emphasis was put on modifying the code equations to incorporate the experimentally determined material properties and to produce more reliable predictions of the critical buckling load for structural composite lumber. The test configuration consisted of a cantilevered beam with a concentrated load positioned at the free end. The critical buckling load was identified by a clear bifurcation point on the force-angular displacement plot. Experimental data showed some increase in the capacity after the bifurcation point.

Suryoatmono and Tjondro (2008) investigated the lateral torsional buckling behavior of simply supported rectangular wooden beams subjected to a concentrated force at mid-span. Finite element models were developed using isotropic and orthotropic materials. The experimental results agreed well with the finite element model for some of the wood species whereas the buckling capacity of the others were considerably underestimated by the finite element model.

Xiao (2014) investigated the orthotropic material properties that affect the lateral torsional buckling response of rectangular wooden beams through a finite element sensitivity analysis. The outcomes of this study suggested that the buckling capacity is primarily affected by the longitudinal modulus of elasticity and the transverse shear modulus. The Poisson’s ratio and the remaining material properties were shown to have negligible effect on the critical moment. Full-scale lateral torsional buckling experiments were conducted on simply supported rectangular lumber joists using a concentrated load at mid-span. The

experimental data was then used to validate a finite element model and agreed well with the predictions. Using the validated FE model, a finite element parametric study was conducted. An analysis of the load position relative to the shear center revealed results that are in good agreement with the load eccentricity factor proposed by AFPA (2003). The parametric study also demonstrates that the location of end supports with respect to the shear center did not significantly affect the critical buckling moments.

Du (2016) investigated the behavior of wooden beam-deck systems subjected to lateral torsional buckling. Closed form solutions, analytical solutions, energy-based approximate solution and finite element solutions were formulated for a sway and non-sway models that account for various boundary conditions and moment distributions. The sway model had partial lateral restraint while the non-sway model assumed a fully restrained lateral motion of the beam and only allowed angular displacements. The effects of beam and deck spans, load type and height, lateral and twisting restraints, lateral restraint height and stiffness and continuous beams on the critical buckling load of the system were assessed through a parametric study. It was shown that the non-sway model could undergo lateral torsional buckling only for uplift forces while the sway model was subjected to lateral instability for both gravity and uplift forces. For the uplift scenario, the non-sway model predicted a higher capacity than the sway model. Partial or full bracing action of deck boards significantly enhanced the critical buckling load of the beam-deck assembly. Furthermore, the buckling resistance decreased as the deck span increases. Load height significantly affected the buckling capacity for short span beams and long span decks. Continuous beams demonstrated a slight increase in the critical buckling load compared to a single-span system.

2.2 Lateral instability of wood I-joists

2.2.1 Mechanical properties

Hindman (2003) investigated the material properties of structural composite lumber products using an isotropic and orthotropic formulations. The material tested were machine stress-rated lumber (MSR), laminated-veneer lumber (LVL), parallel strand lumber (PSL), laminated strand lumber (LSL), which are materials commonly used in wood I-joist flanges. The test methods included the five points bending test for determining the modulus of elasticity and the shear modulus of the studied materials. The results showed a modulus of elasticity to shear modulus ratio E:G for the SCL, OSB and MSR products to be significantly lower than that of solid sawn lumber, questioning the conservatism of the design code provisions which generally assumed an E:G ratio of 16. The torsional rigidity of whole wood I-joists were also investigated. Mathematical models based on an isotropic and orthotropic formulations were used to predict the torsional stiffness of the various tested materials. The MSR and LSL materials showed good agreement between the measured torsional stiffness (GJ) data and the isotropic model while the LVL, PSL and I-joist materials were best predicted by the orthotropic model.

Grandmont (2011) studied the effect that the material properties of the web have on the deflection of wood I-joist, using a finite element model. The resulting sensitive material properties were determined experimentally. It was demonstrated that the density variations along the OSB panels affect the shear resistance of wood I-joist and that the properties determined from small-scale specimens differed significantly from those of large scale specimens. It was also concluded that the material properties, of which the most influential is the shear modulus in the plane of the panel, did not contribute significantly to the in-plane deflection of wood I-joist in the elastic range.

2.2.2 Lateral instability

Hindman (2005b) conducted an experimental study on the lateral buckling of cantilevered wood I-joist subjected to a concentrated force at the free end. A comparison between the experimental buckling load and that predicted by various mathematical models was undertaken. Two types of wood I-joists were studied including 60 specimens of various lengths. The experimental critical buckling load was defined as the point where a significant increase appears on the force-angular displacement plot. It was shown that the elastic buckling beam theory (Timoshenko & Gere, 1961) yielded the most accurate results, although there was a significant difference in the range of 12 to 43.4 %. The authors argued that such differences between the experimental and predicted buckling loads lie in the fundamental inaccurate assumption that a wood I-joist can be treated as a homogenous isotropic material. The models based on the US timber design standard (NDS, 2003) model grossly underestimated the wood-joist critical buckling loads by about 70%.

Zhu et al. (2005) studied the buckling behavior of wood I-joists by comparing experimental tests to finite element simulations in ABAQUS. Both global buckling of the wood I-joist and local buckling of the web were investigated. The specimen population included a total of 17 wood I-joists with dimensions ranging from 300 to 450 mm in depth, 1,5 to 5 m in length and flanges of 72 x 45 mm in cross section. The test specimens were simply supported and subjected to two concentrated load applied on the top flange with five discrete lateral bracing points along the span that restrained the top flange from lateral movement. Linear and non-linear buckling analyses were conducted which incorporated measured initial imperfections of the test specimens. An empirical formula was derived for the buckling capacity of the web. The authors concluded that the global buckling of wood I-joist was driven by the span, the flange size and the location of lateral restraints. Finite element simulation overestimated critical buckling loads, whereas a model including geometrical non-linearity provided predictions that agreed more with experimental data. The material properties used for the finite element model were determined from tension and compression tests of the flange and web materials. It was also concluded that the web

buckling capacity was influenced by the presence of stiffeners and that the overall capacity of wood I-joist was dictated by global buckling, web buckling or material strength.

Burow et al. (2006) investigated the behavior of wood I-joists in lateral buckling through a cantilever and a simply supported configuration. The specimen population for the cantilever configuration included 22 wood I-joists and the simply supported test included a total of 9 specimens. All specimens were 241 mm deep, with an unbraced length ranging from 610 to 7000 mm and 38 x 38 mm flanges. Three mathematical models based on elastic theoretical stability solution of beams and American code provisions were developed and incorporated various loading and lateral bracing configurations. The models incorporated the bending stiffness and the torsional rigidity of the wood I-joists that were determined experimentally. The torsional rigidity was measured using a torsional stress analyzer (TSA) machine and calculated with the empirical torsional stiffness expression for a circular shaft. From non-linear experimental force-angular displacement curves, the critical buckling load was defined as the point where the slope increment went beyond 0.2 degrees. It was also shown that the model in the American timber design standard (NDS, 2003) underestimated the experimental critical buckling loads (CBLs) by an average of 78 %. The modified Euler model consistently underestimated the CBLs by as much as 44 % while the equivalent moment factor model had predictions that varied between -18.6% and 53.4 %. The study suggests modifications to enhance these provisions to provide more realistic predictions.

Aguilar (2012) investigated the lateral buckling behavior of wood I-joist under human walking loads. Emphasis was put on the derivation of mathematical models to predict the dynamic lateral torsional buckling load induced by workers walking on floors. These models considered various end support conditions and bracing systems based on actual I-joist hangers and braces used in the construction industry. These model predictions agreed well with the experimental data. The author concluded that the critical buckling loads were influenced by the end support condition and the location of the braces and that the critical point of instability from a dynamic loading pattern was the I-joist mid-span.

Hindman et al. (2014) studied the effect of bracing stiffness, construction experience and human participants weight on the lateral torsional buckling behavior of wood I-joist. The study focused on three 16-inch-deep wood I-joists braced together with five different braces stiffness and two bracing configurations, involving human test subject to simulate the dynamic load induced by workers. The lateral accelerations, lateral displacement and angular displacements were recorded for the middle wood I-joist specimen. The brace stiffness inhibited the angular and lateral displacements of the wood I-joists subjected to a dynamic load induced by walking human subjects, while the brace configuration did not have an effect on the lateral acceleration.

2.3 Summary

This chapter presented the experimental studies on the lateral instability in rectangular wooden beams and wood I-joists. The development of present provisions on lateral torsional buckling of rectangular wood beams in the current Canadian design standard was based on the work of Hooley & Madsen (1964). Other researchers such as Bell and Eggen (2001), Hindman (2005a), Xiao 2014, Hindman (2005b) and Burow et al. (2006) validated the available provisions from the Canadian, American, European and Norwegian codes through experimental research. Burow et al. (2006) and Hindman (2005b) investigated the American design standards (NDS, 2015) model for stability of wood I-joists and concluded that it underestimates the critical buckling load.

The existing literature on lateral torsional buckling of wood I-joists was limited to a few studies and the knowledge base could still benefit from more experimental research in this field. The current research could add to the available data by investigating deeper and longer specimens than what has been published. This research will consider another approach to load the wood I-joist at mid-span which uses a platform designed to ensure that lateral restrain are not imposed by the loading mechanism. Differences in determining the point at which the critical buckling load should be determined was found in the literature. Some studies identified the critical buckling load as the bifurcation point where

a significant lateral displacement was observed in the elastic range (Hindman 2005b, Burow et al. 2006 & Aguilar, 2012), while other considered the ultimate capacity until inelastic deformations occurred (Xiao, 2014).

The current study will also consider the impact of initial imperfections present in the wood I-joist, an effect that was solely investigated by Zhu (2005) and that are inherent to wood I-joists. No consistency in the methods determining the material properties of the wood I-joist has been found in the literature. Given that wood is orthotropic in nature, there is no evidence in the literature on which of the material properties of wood I-joists affect the elastic lateral torsional buckling response and which method yields the most reliable data for analytical models. The current study aims to investigate through finite element modelling the material properties that affect the lateral torsional buckling response and the best suited experimental method in evaluating those properties.

CHAPTER 3

SENSITIVITY ANALYSIS

3.1 General

This chapter evaluates the effects of the material properties on the critical buckling load of wood I-joists. The identification of the sensitive material parameters will provide the basis for the experimental investigation of the wood I-joist specimens. Once these specific material properties are experimentally determined, they will be used as input parameters into various models for predicting the critical buckling load. Section 3.2 describes the finite element model used for the sensitivity study. Section 3.3 compares the response determined by the FE model with those predicted by the theoretical solution for lateral torsional buckling. Section 3.4 presents the results of the sensitivity analysis on the material properties.

3.1.1 Convention used for this study

The orientation of the principal axes of the wood I-joist used throughout this study is illustrated in Figure 3-1. The longitudinal axis (Axis 1) follows the I-joist length, the transverse axis (Axis 2) refers to the strong axis of the wood I-joist and the lateral axis (Axis 3) refers to the weak axis of the wood I-joist.

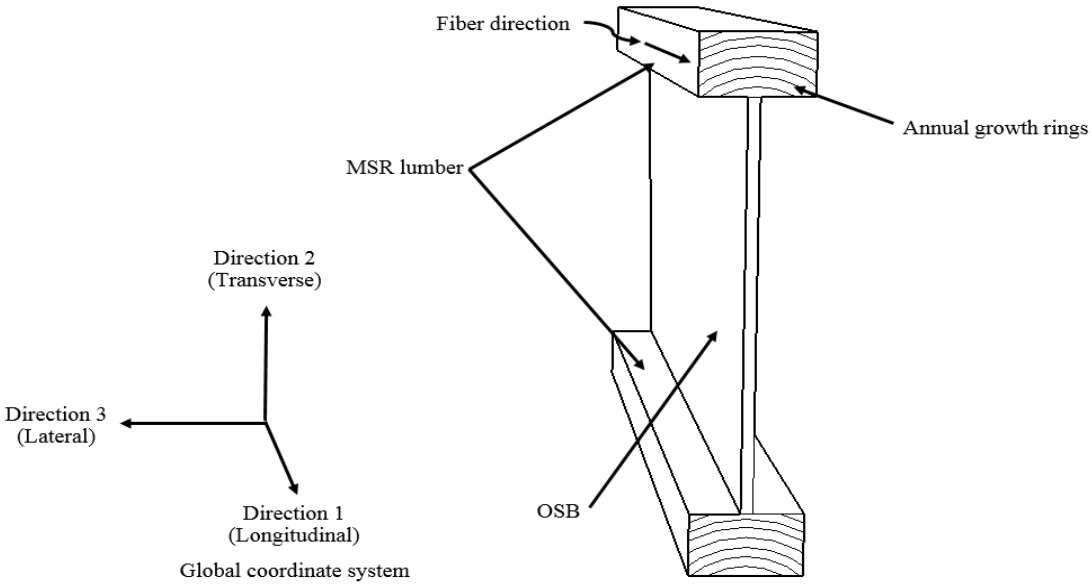

Figure 3-1 Convention used for the principal axes of wood I-joist

3.2 Model description

The model is built using the finite element software ABAQUS (Simulia, 2012), which is capable of conducting eigenvalue buckling analysis, and allows for various material elasticity definitions as well as shell and continuum elements which are useful for structural modelling applications. The formulation of the finite element model for the sensitivity analysis relies on the following assumptions:

- The I-joist acts as a composite beam made of two linear elastic materials;
- The flanges are fully connected to the web, i.e. no slippage occurs at the flange to web connection;
- The I-joist does not have initial imperfections;
- Pre-buckling deformations that could affect the critical moment are neglected;
- Loads are conservative;
- The member cross-section can be affected by distortion and shear deformations.

3.2.1 Cross-section dimensions

The model uses the dimensions of the smaller of the two wood I-joist types that are under the scope of the experimental investigation, presented in the subsequent chapter. The cross-section dimensions have a flange thickness of 38.0 mm, a flange width of 63.5 mm, a total height of 406 mm and a web thickness of 9.5 mm.

3.2.2 Element type

The element library in ABAQUS offers many options for the modelling of structural members, for instance, the S4R shell element that is suitable for describing the behavior of thin-walled structure such as the wood I-joists. This element has the ability to handle both thick and thin shells based on the thick shell theory and the Kirchhoff thin shell (Simulia, 2012). It is a conventional stress-displacement shell with 4 nodes that uses reduced integration with hourglass control. This general-purpose element considers transverse shear deformation for thick shell, however, it becomes negligible when the shell thickness is small. It has a total of 24 degrees of freedom per element (3 displacement and 3 rotation components per node). Furthermore, the ABAQUS library also offers solid elements such as C3D8R featuring a solid brick that consists of 24 degrees of freedom (3 translational degrees of freedom per node) with reduced integration and hourglass control. This element has been previously used in the literature to model wood beams and I-joist (Zhu, 2005 & Xiao, 2014). The I-joist model under the scope of this chapter uses S4R elements for the OSB web and C3D8R elements for the lumber flanges.

3.2.3 Mesh

A mesh sensitivity indicated that the critical load converges when using 232 elements along the length, eight elements for the flange width, five elements across the flange thickness and 16 elements for the web height. It yields an aspect ratio of 3:1 for the flange's elements

and 1:1 for the web's elements. Further mesh refinements did not result in significant improvement of the solution convergence.

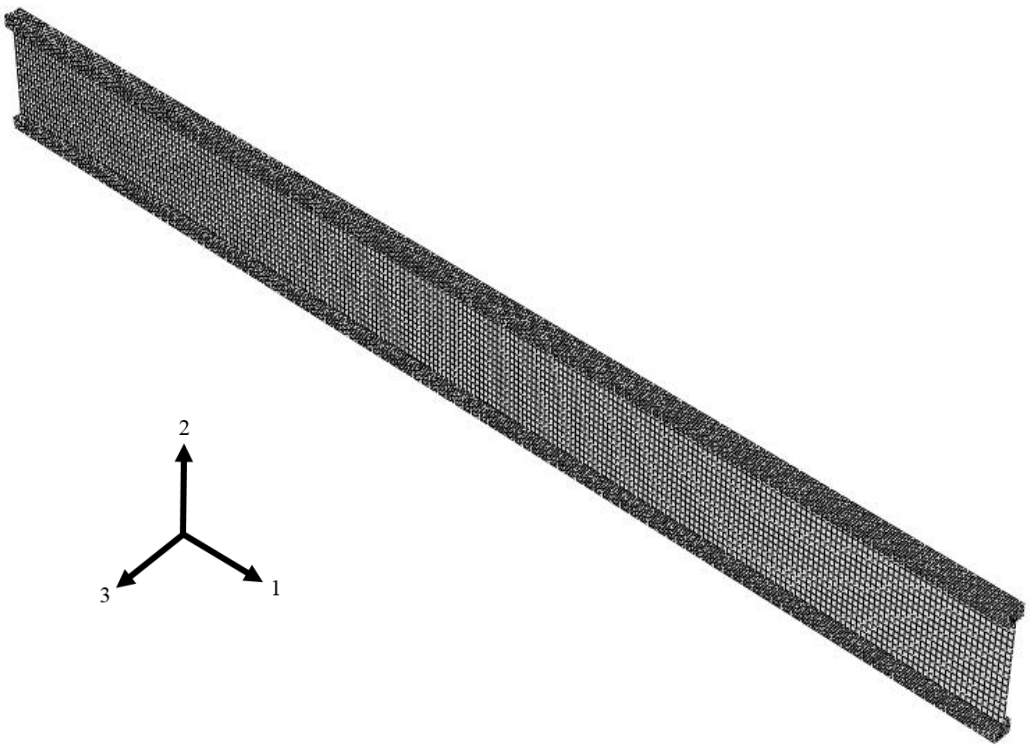

Figure 3-2 Finite element model mesh

3.2.4 Material properties

The wood I-joists in this research are composed of solid-sawn lumber and oriented strand which are both effectively described as rectangular orthotropic elastic materials. The mechanical properties of rectangular orthotropic materials are defined about three axes perpendicular to each other. Using the engineering constants feature in ABAQUS, the linear elasticity of orthotropic materials can be formulated as:

$$\begin{Bmatrix} \varepsilon_{11} \\ \varepsilon_{22} \\ \varepsilon_{33} \\ \gamma_{12} \\ \gamma_{13} \\ \gamma_{23} \end{Bmatrix} = \begin{bmatrix} 1/E_1 & -\nu_{21}/E_2 & -\nu_{31}/E_3 & 0 & 0 & 0 \\ -\nu_{21}/E_1 & 1/E_2 & -\nu_{32}/E_3 & 0 & 0 & 0 \\ -\nu_{13}/E_1 & -\nu_{23}/E_2 & 1/E_3 & 0 & 0 & 0 \\ 0 & 0 & 0 & 1/G_{12} & 0 & 0 \\ 0 & 0 & 0 & 0 & 1/G_{13} & 0 \\ 0 & 0 & 0 & 0 & 0 & 1/G_{23} \end{bmatrix} \begin{Bmatrix} \sigma_{11} \\ \sigma_{22} \\ \sigma_{33} \\ \tau_{12} \\ \tau_{13} \\ \tau_{23} \end{Bmatrix} \quad (3\text{-}1)$$

Where ε is the normal strain, γ is the shear strain, E is the elastic modulus, G is the shear modulus, σ is the normal stress and τ is the shear stress about the principal axes 1, 2 and 3. For the flanges, axis 1 is considered to be parallel to the wood fibers while axes 2 and 3 are perpendicular. It is known that the mechanical properties in the radial and tangential direction relative to the annual growth rings can be assumed to be identical (FPL, 2010), thus $E_2 = E_3$, $G_{12} = G_{13}$, $\nu_{12} = \nu_{13}$ and $\nu_{21} = \nu_{31}$. As a result, the wood flanges can be modelled as a transversely orthotropic material having a plane of isotropy about the axes 2-3. The material orientation of the flanges and web follows the global coordinate system presented in Figure 3-1. The flanges consist of machine-stress rated (MSR) lumber pieces that are longitudinally connected with finger joints. These joints are not included in the FE model, which assumes the flanges are made of continuous wooden pieces. Table 3-1 presents the material properties of the flanges that are based on the species Sitka Spruce, while the properties of the web are based on mean values found in the literature (FPL, 2010 & Thomas, 2010).

Table 3-1: Reference model mechanical properties

Part	**E_1 (MPa)**	**E_2 (MPa)**	**E_3 (MPa)**	**μ_{12}**	**μ_{13}**	**μ_{23}**	**G_{12} (MPa)**	**G_{13} (MPa)**	**G_{23} (MPa)**
Flanges	11200	678	678	0.372	0.467	0.435	700	700	33.6
Web	2500	5000	500	0.195	0.195	0.195	500	500	100

3.2.5 Boundary conditions

The sensitivity study relies on a simple beam configuration. To simulate this kind of support, Figure 3-3 illustrates the inactive translational DOFs at the member ends that provide a pinned-roller support in the transverse (axis 2) and the lateral direction (axis 3), and also restrain rotation about the longitudinal axis (axis 1). The web to flange connectivity nodes share the same DOFs as per the ‘’SHELL TO SOLID COUPLING’’ feature in ABAQUS.

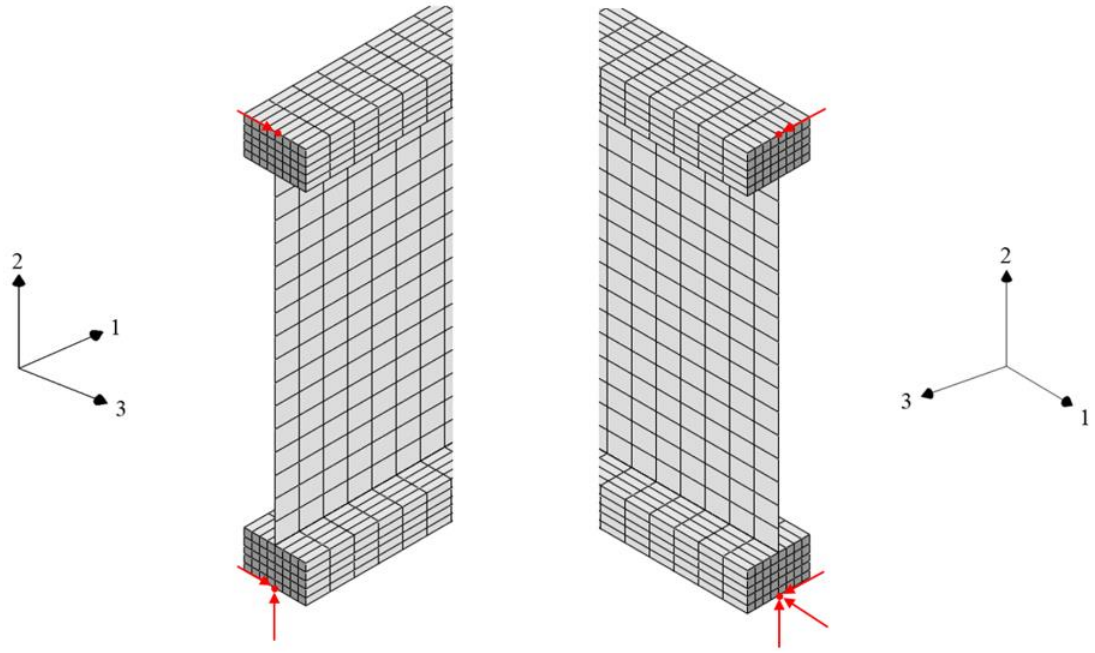

Figure 3-3 Inactive translational DOFs (RED arrows) at each end of a simply supported wood I-joist

3.2.6 Load application

The load application consists of a uniform moment about the strong axis. This loading configuration is used to study the response of the model to changes of the material properties. To apply a uniform moment about the strong axis, concentrated forces were

applied at the boundary nodes of the flanges which resulted in compression of the top flange and tension of the bottom flange (Figure 3-4). The wood I-joist self-weight is assumed to be too small compared to the buckling load, and was therefore neglected in the FE buckling analysis.

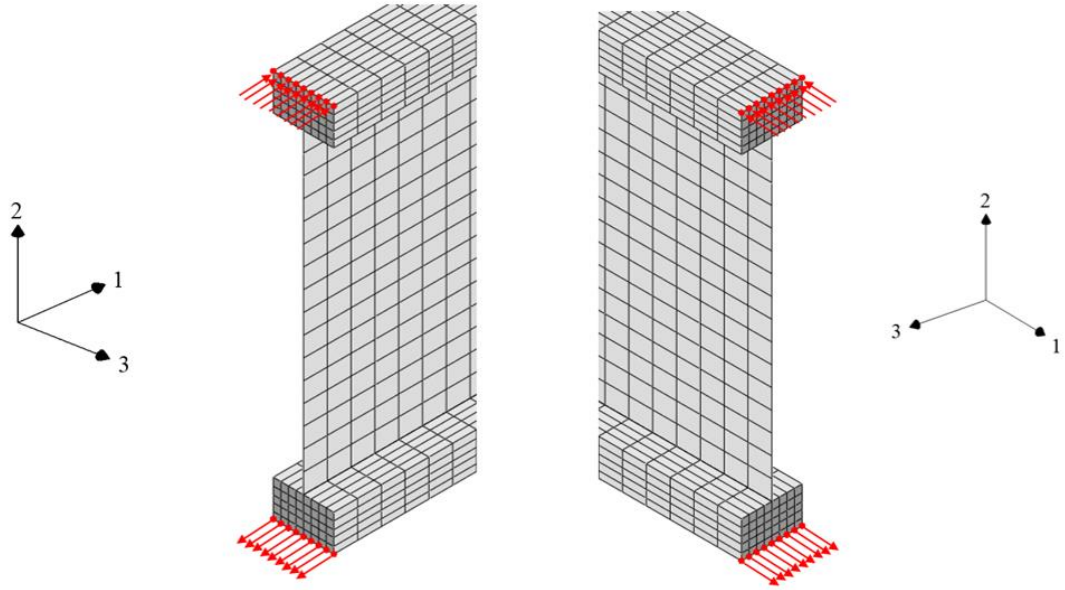

Figure 3-4 Loaded nodes at each end of a simply supported wood I-joist subjected to a uniform moment about its strong axis

3.2.7 Eigenvalue buckling analysis

An eigenvalue buckling analysis is used to evaluate the critical load at which the simply supported wood I-joist undergoes lateral torsional buckling. To find the critical load, the smallest eigenvalue λ_i is sought for which Equation 3-2 has a nontrivial solution:

$$([K^*] + \lambda_i[K_G])\{v_i\} = 0 \qquad (3\text{-}2)$$

Where $[K^*]$ denotes the stiffness matrix, $[K_G]$ is the geometric matrix and $\{v_i\}$ is the nodal displacement vector of the mode shape i.

3.3 Validation with the theoretical solution

The critical buckling moment for an I-section can be determined with the closed form solution using Equation 1-2. Assuming the reference case to have $E_{flange} = 11\,200\ MPa, G_{flange} = 700\ MPa, E_{web} = 2\,500\ MPa,$ and $G_{web} = 500\ MPa,$ the resulting critical moment is 2.58 kNm, which also involved using the transformed section properties (Du, 2016). The resulting critical moment for the reference case predicted by the FE model is 2.36 kNm. As expected, the predicted critical moment of the theoretical solution is slightly higher than the one predicted by the finite element model. This divergence can be explained by the fact that the finite element model allows distortion of the web, shear deformations and provides more degrees of freedom.

3.4 Results of the sensitivity analysis

The results of the sensitivity analysis on the wood I-joist material properties are presented in this section. These results provide information on which material parameters are relevant for the experimental investigation of the wood I-joist mechanical properties. As a reference case, this study considers a simply supported wood I-joist subjected to a uniform moment about its strong axis that has the material properties defined in Table 3-1, the cross-section dimensions outlined in Section 3.2.1 and a length of 5800 mm. The FE model response is analyzed as its material properties were changed from 50% to 150% for each parameter, while all other parameters were kept constant. This procedure is repeated for the modulus of elasticity (E), Poisson's ratio (μ) and the shear modulus (G) of each individual component (top flange, web and bottom flange) along the principal axes. From Table 3-2, it can be established that the critical moment is;

- Highly sensitive to fluctuations of the top flange's modulus of elasticity in the longitudinal direction (E_{1-TF});

- Moderately sensitive to fluctuations of the bottom flange's modulus of elasticity in the longitudinal direction (E_{1-BF});
- Moderately sensitive to fluctuations of top flange's shear modulus about planes 1-2 and 1-3 (G_{12-TF} & G_{13-TF});
- Moderately sensitive to fluctuations of bottom flange's shear modulus about planes 1-2 and 1-3 (G_{12-BF} & G_{13-BF});
- Slightly sensitive to fluctuations of the web's modulus of elasticity in the transverse direction (E_{w-2});
- Not sensitive to fluctuations of both flange's modulus of elasticity perpendicular to grain (E_2 & E_3), Poisson's ratio and shear modulus about plane 2-3 (G_{23});
- Not sensitive to fluctuations of the web's modulus of elasticity about the longitudinal and lateral direction (E_{w-1} & E_{w-3}), Poisson's ratio and shear modulus.

The sensitive parameters are further investigated by expanding the fluctuation range from 0% to 200% relative to the reference case, as seen in Figure 3-5. The analysis targeted the symmetric buckling mode shape illustrated in Figure 3-6. Effects of fluctuations of the material properties on the critical moment predicted by Equation 1-2 are also illustrated in Figure 3-5. It can be observed that the relationship between the critical moment and variations of the elastic modulus and shear modulus are similar to the behavior exhibited by the FE model.

The results that emerged from the sensitivity analysis therefore suggest that the wood I-joist can be treated as a composite beam made up from two isotropic materials for the flange and web. Ultimately, these conclusions form the basis of the current research in investigating the wood I-joist material properties in Chapter 4 and in developing a finite element model in Chapter 5.

Table 3-2 Finite element model response to material properties fluctuations

Model #	Mechanical property fluctuation									M_{cr} / M_{cr-ref}		
	$\frac{E_1}{E_{1\,ref}}$	$\frac{E_2}{E_{2\,ref}}$	$\frac{E_3}{E_{3\,ref}}$	$\frac{\mu_{12}}{\mu_{12\,ref}}$	$\frac{\mu_{13}}{\mu_{13\,ref}}$	$\frac{\mu_{23}}{\mu_{23\,ref}}$	$\frac{G_{12}}{G_{12\,ref}}$	$\frac{G_{13}}{G_{13\,ref}}$	$\frac{G_{23}}{G_{23\,ref}}$	Comp. flange	Tension flange	Web
Ref.	1	1	1	1	1	1	1	1	1	1.00	1.00	1.00
1	1.5	1	1	1	1	1	1	1	1	1.24	1.04	1.00
2	0.5	1	1	1	1	1	1	1	1	0.75	0.94	1.00
3	1	1.5	1	1	1	1	1	1	1	1.00	1.00	1.02
4	1	0.5	1	1	1	1	1	1	1	1.00	1.00	0.97
5	1	1	1.5	1	1	1	1	1	1	1.00	1.00	1.00
6	1	1	0.5	1	1	1	1	1	1	1.00	1.00	1.00
7	1	1	1	1.5	1	1	1	1	1	1.00	1.00	1.00
8	1	1	1	0.5	1	1	1	1	1	1.00	1.00	0.99
9	1	1	1	1	1.5	1	1	1	1	1.00	1.00	1.00
10	1	1	1	1	0.5	1	1	1	1	1.00	1.00	1.00
11	1	1	1	1	1	1.5	1	1	1	1.00	1.00	1.00
12	1	1	1	1	1	0.5	1	1	1	1.00	1.00	1.00
13	1	1	1	1	1	1	1.5	1	1	1.02	1.02	1.01
14	1	1	1	1	1	1	0.5	1	1	0.96	0.96	0.99
15	1	1	1	1	1	1	1	1.5	1	1.05	1.05	1.00
16	1	1	1	1	1	1	1	0.5	1	0.92	0.92	1.00
17	1	1	1	1	1	1	1	1	1.5	1.00	1.00	1.00
18	1	1	1	1	1	1	1	1	0.5	0.99	0.99	0.99

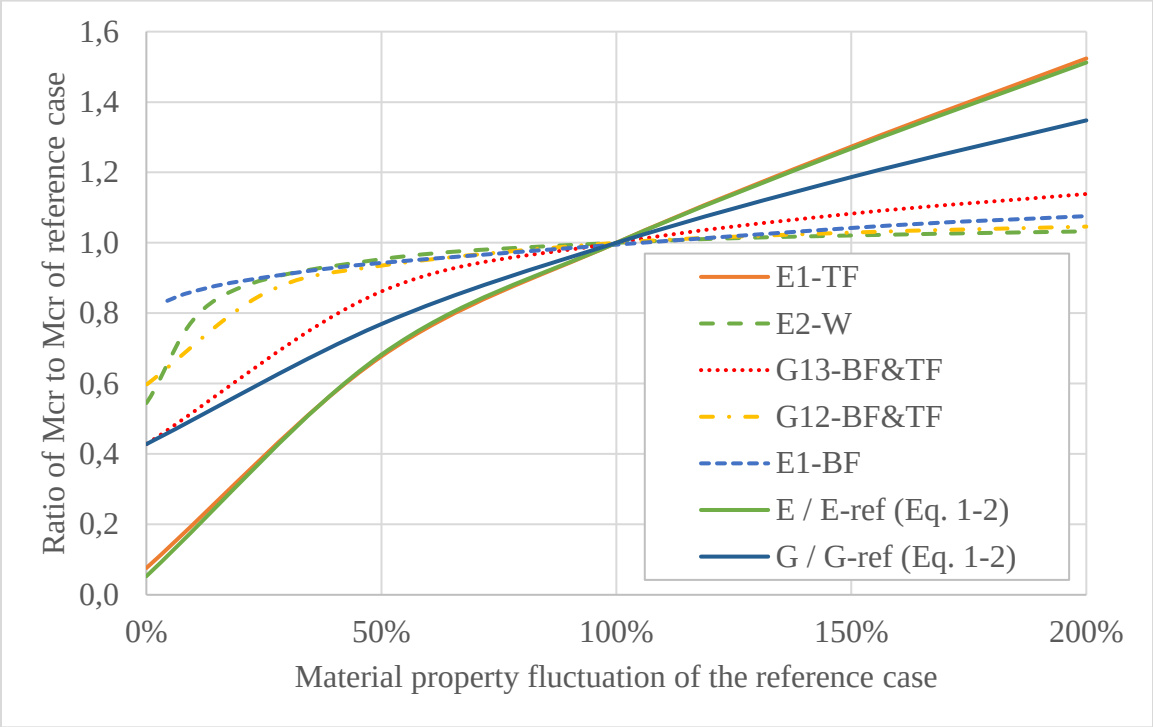

Figure 3-5 Responses of the critical moment to material properties fluctuations

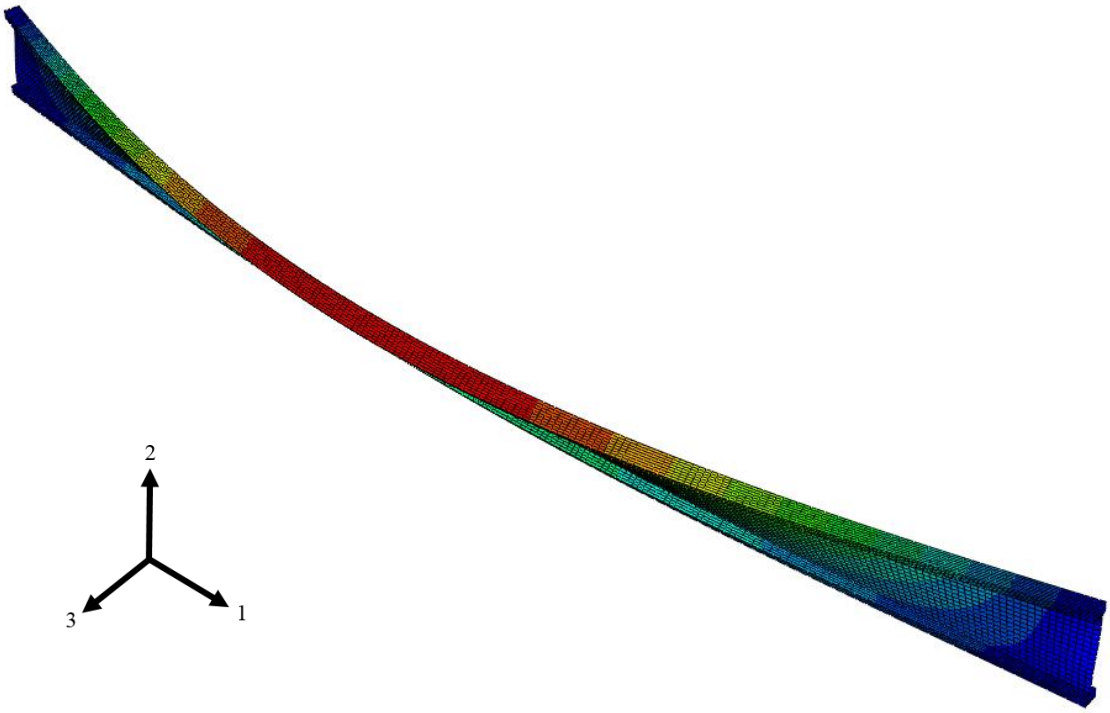

Figure 3-6 Sensitivity study buckled mode shape

CHAPTER 4

EXPERIMENTAL PROGRAM

The present chapter provides details on the I-joist test specimens and describes the testing procedures employed in this study. A discussion on various test methods used to find the specimens mechanical properties, the ultimate flexural capacity and the lateral torsional buckling critical load is also provided.

4.1 Specimen description

The I-joist consist of two different wood materials, which are manufactured using machine stress rated (MSR) lumber flanges and oriented strand board (OSB) webs and connected together with a waterproof, structural adhesive (Boise Cascade, 2014). The wood I-joists were received at a length of 6.1 m and cut at various lengths to produce the specimen breakdown presented in Table 4-1. The I-joist specimen moisture content was measured after 4 weeks from their arrival date to ensure that they are acclimatized to the ambient temperature and relative humidity. The average moisture content for each specimen length category is also presented in Table 4.1 along with the coefficient of variation. Figure 4-1 illustrates the two I-joist cross section dimensions while typical web and flange continuity joints are depicted in Figure 4-2.

Table 4-1 Wood I-joist specimen breakdown and moisture content

Sample group #	Specimen length m [feet]	I-joist section[1]	Number of specimens	Average moisture content (%)	COV (%)
1	1.83 [6]	0.4 m	10	12.7	4.67
2	2.44 [8]	0.4 m	10	13.0	7.03
3	3.05 [10]	0.4 m	10	12.6	5.51
4	3.66 [12]	0.4 m	10	12.8	6.48
5	4.27 [14]	0.4 m	10	12.6	2.73
6	4.88 [16]	0.4 m	5	12.8	4.57
7	5.49 [18]	0.4 m	5	12.5	2.13
8	6.10 [20]	0.4 m	26	12.6	3.52
9	1.83 [6]	0.6 m	10	15.8	4.61
10	2.44 [8]	0.6 m	10	15.9	6.69
11	3.05 [10]	0.6 m	10	14.8	6.23
12	3.66 [12]	0.6 m	10	16.0	6.99
13	4.27 [14]	0.6 m	10	15.3	2.96
14	4.88 [16]	0.6 m	5	15.3	7.34
15	5.49 [18]	0.6 m	5	15.5	4.14
16	6.10 [20]	0.6 m	11	15.4	7.15
Total	**----**	**----**	**157**	**----**	**----**

[1] Refer to Figure 4-1 for a description of the different I-joist sections

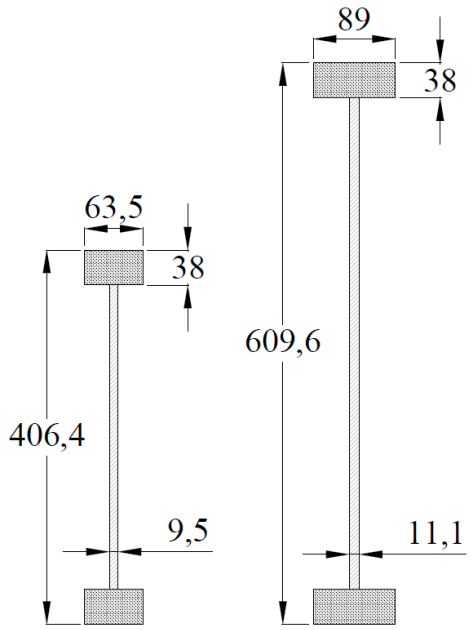

Figure 4-1 I-joist cross section dimensions (mm)

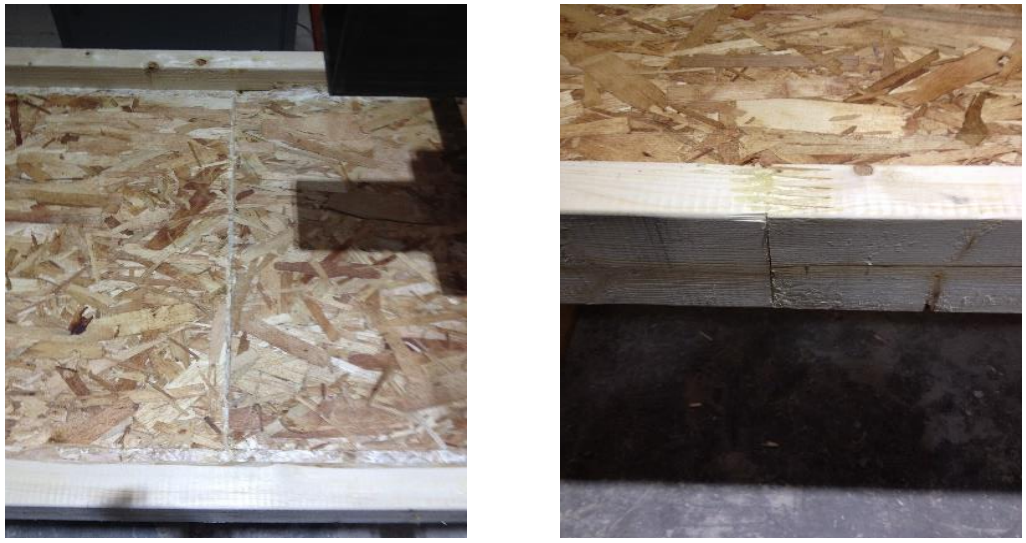

Figure 4-2 Web continuity joint (Left) and flange continuity joint (Right)

4.2 Testing program

The test program includes test methods to determine the lateral torsional buckling critical load of the wood I-joist specimens, their ultimate flexural capacity and their respective mechanical properties. The testing program described in Table 4-2 evaluates the I-joist lateral flexural stiffness (EI_y), the I-joist torsional rigidity (GJ), the lateral torsional buckling capacity, the flange's longitudinal MOE (E_{fl}), the flange's torsional shear modulus (G_t) and the transverse modulus of elasticity of the web E_t.

Table 4-2 Test program

1. Non-destructive lateral flexural stiffness tests	
▪ Include all the I-joist specimens except 15 specimens of sample #8 that are used for ultimate flexural capacity ▪ 2 repeats per specimen (one per side)	284 tests
2. Non-destructive torsional rigidity tests	
▪ Include the specimens of sample #6, #7, #8 and #16 ▪ 5 repeats per specimen at different span-depth ratios for the specimen sample #8 ▪ 1 repeat per specimen for sample #6 and #7 ▪ 3 repeats per specimen at various span-depth ratios for the sample #16	65 tests
3. Destructive lateral torsional buckling tests	
▪ Include the specimens of the sample #5, #6, #7, #8 and #16	42 tests
4. Non-destructive flange modulus of elasticity tests	
▪ Include the flanges of the specimens of sample #1, #5 and #16 ▪ 2 repeats per specimen (1 on each side)	124 tests
5. Non-destructive flange torsional shear modulus tests	
▪ Include the flanges of the specimens of sample #1, #5 and #16 ▪ 1 repeat per specimen	62 tests
6. Destructive web transverse modulus of elasticity test	
▪ Include the web of the specimens of sample #1, #5 and #16	31 tests
7. Destructive strong axis flexural tests	
▪ Include 15 specimens of the specimen sample #8	15 tests

4.2.1 I-joist lateral flexural stiffness

The I-joist lateral flexural stiffness test configuration is based on the American Standard Test methods of static tests of lumber in structural sizes (D198-14). This test method subjects the I-joist specimen to weak-axis two-point loading (Figure 4-3). The specimens were loaded at a prescribed rate of approximately 20 mm per minute and stopped at 25 % of the elastic region to ensure no inelastic deformations occurred. Applied load and deflection at mid span were measured with a 10 kN load cell and a wire-gauge attached to the specimen web.

The flanges were supported at each end with bearing plates to allow unrestricted longitudinal deformation and rotation during the loading phase. The hydraulic cylinder was attached to a solid frame anchored to the concrete floor (Figure 4-4). The test was conducted on both sides of each specimen in order to get a more accurate measure of the lateral flexural stiffness associated with the lateral buckling side.

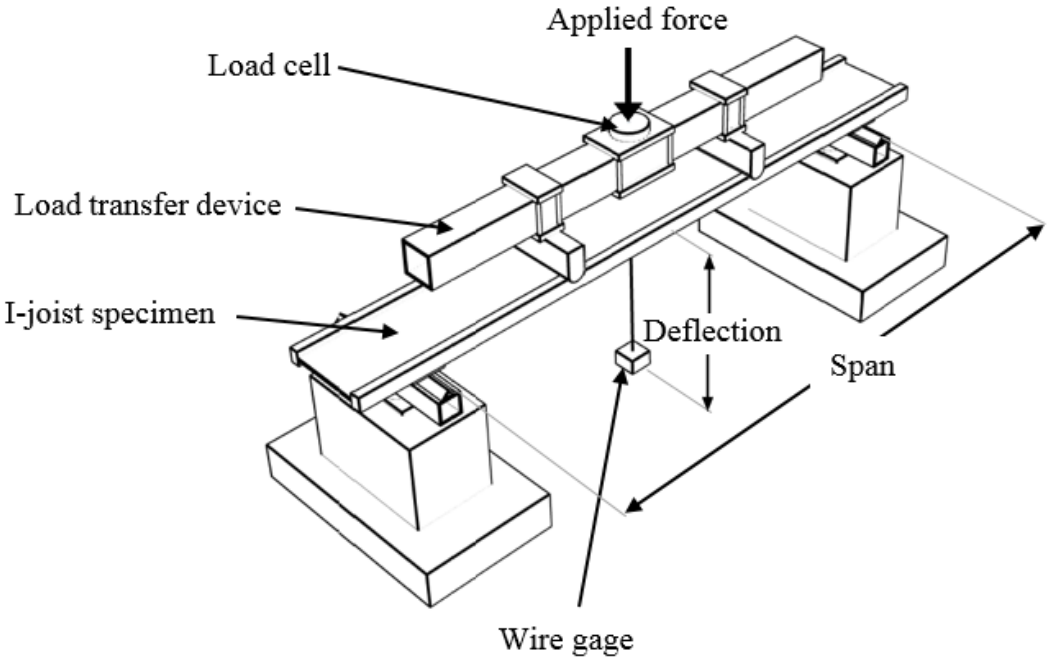

Figure 4-3 I-joist lateral flexural stiffness test configuration

Figure 4-4 I-joist lateral flexural stiffness laboratory test

4.2.2 I-Joist torsional rigidity

The I-joist torsional rigidity was evaluated as per the American Standard Test methods of static tests of lumber in structural sizes (D198-14). The torsion test machine (Figure 4-5) subjected the I-joist specimen to two equal and opposite torsional moments via a wood clamping devices. The latter had one arm resting on the ground support while the other supported the load transfer device. Inclinometers were installed 810 mm away from the clamps to avoid any grip effects on the measured angle of twist. A manual hydraulic pump activated a hydraulic cylinder, attached to a steel frame, that applied a downward force on a 10 kN load cell. The load and inclination were measured at each end. The loading was applied until the specimen reached approximately 8^{o} angle of twist to avoid any inelastic deformation.

The I-joist specimens from sample #8 were tested at 5 different span-to-depth ratios to evaluate the effect of change in torsional rigidity and determine the optimal testing span. Once the optimal testing span was determined, the test was conducted on the 16 and 18 feet specimens with one repeat per specimen. A rubber piece was placed at bearing locations to reduce slippage of the clamps. The initial inclination of the specimen at the beginning of the test was measured to account for the inclination of the load during the test. The wood arms were designed to clamp only the web of the I-joist specimen, to ensure warping deformation in the flanges could freely occur (Figure 4-6). Thus, it was assumed that no axial strains were developed in the flanges and that the torsional resistance involved only pure shear stresses (St-Venant).

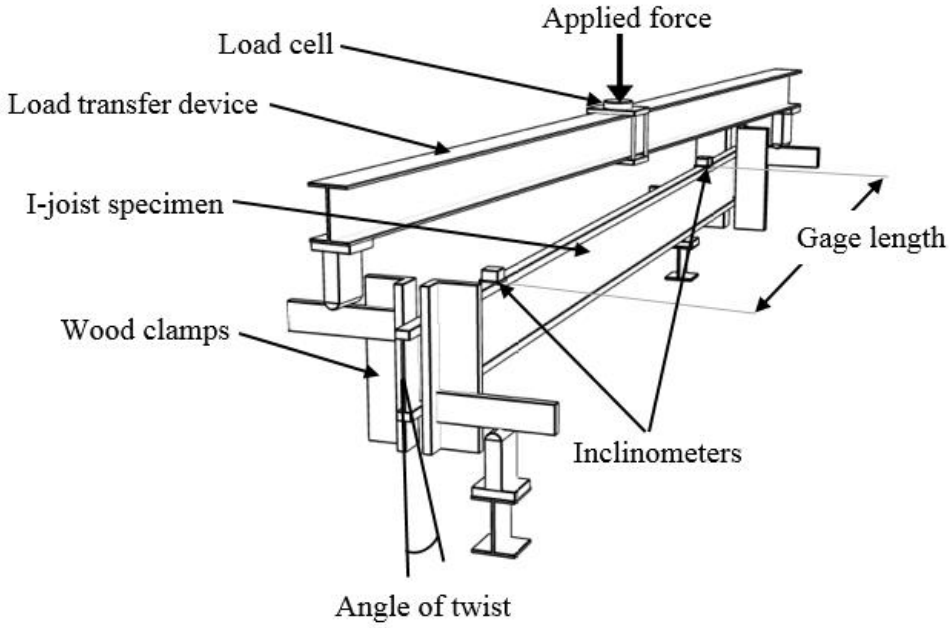

Figure 4-5 I-joist torsional rigidity test configuration

Figure 4-6 I-joist torsional rigidity test laboratory setup

4.2.3 Lateral torsional buckling capacity

The lateral torsional buckling capacity was evaluated using a simply supported beam configuration with a concentrated load at mid span applied on the specimen top flange (Figure 4-7). The test specimen was loaded manually by adding weights on a loading platform attached to a load transfer device mounted on the top flange. This allowed the loading apparatus to follow the I-joist through its buckling motion without providing any lateral restraint. Once the I-joist specimen was installed into the end supports, the initial out-of-straightness was measured using a chalk-line in order to estimate the initial geometric out-of-straightness. The vertical displacement at mid span, the top and bottom flange lateral displacements at mid span and the top flange lateral displacement at quarter span were recorded at each load increase with the aid of wire gauges. The initial state (zero displacements) included the specimen self-weight after which the loading platform apparatus and load increases were added until visible failure was observed. Once inelastic deformations were observed, the specimen was unloaded and deflection measurements were recorded for the final state.

The end supports were designed to simulate the boundary conditions of the simply supported reference case for lateral torsional buckling which restrains the vertical displacement, lateral displacement and rotation about the longitudinal axis. In contrast, the remaining displacement and rotational degrees of freedom are free to occur. To that purpose, the specimen was confined in a fitted HSS frame preventing vertical and lateral displacement while ensuring the frame was able to translate longitudinally. As a result, rotation about the longitudinal axis was prevented as well (Figure 4-8). The frame was placed on a thrust bearing to allow the specimen to rotate freely about the vertical axis. A steel shaft, welded to the frame base plate, was inserted through the thrust bearing into a steel base that had a fitted hole to prevent the HSS frame from translating in the lateral-longitudinal plane (Figure 4-9). The load transfer device was designed to transmit the load from the loading platform to the top flange as a concentrated force. A steel hinged support allowed the load to remain vertical during the buckling motion of the test specimen

(Figures 4-10 & 4-11), which is consistent with the underlying assumptions of the reference case for lateral torsional buckling. To achieve this configuration, the hinged support bottom was screwed on the specimen top flange while the upper part was welded to the load transfer device.

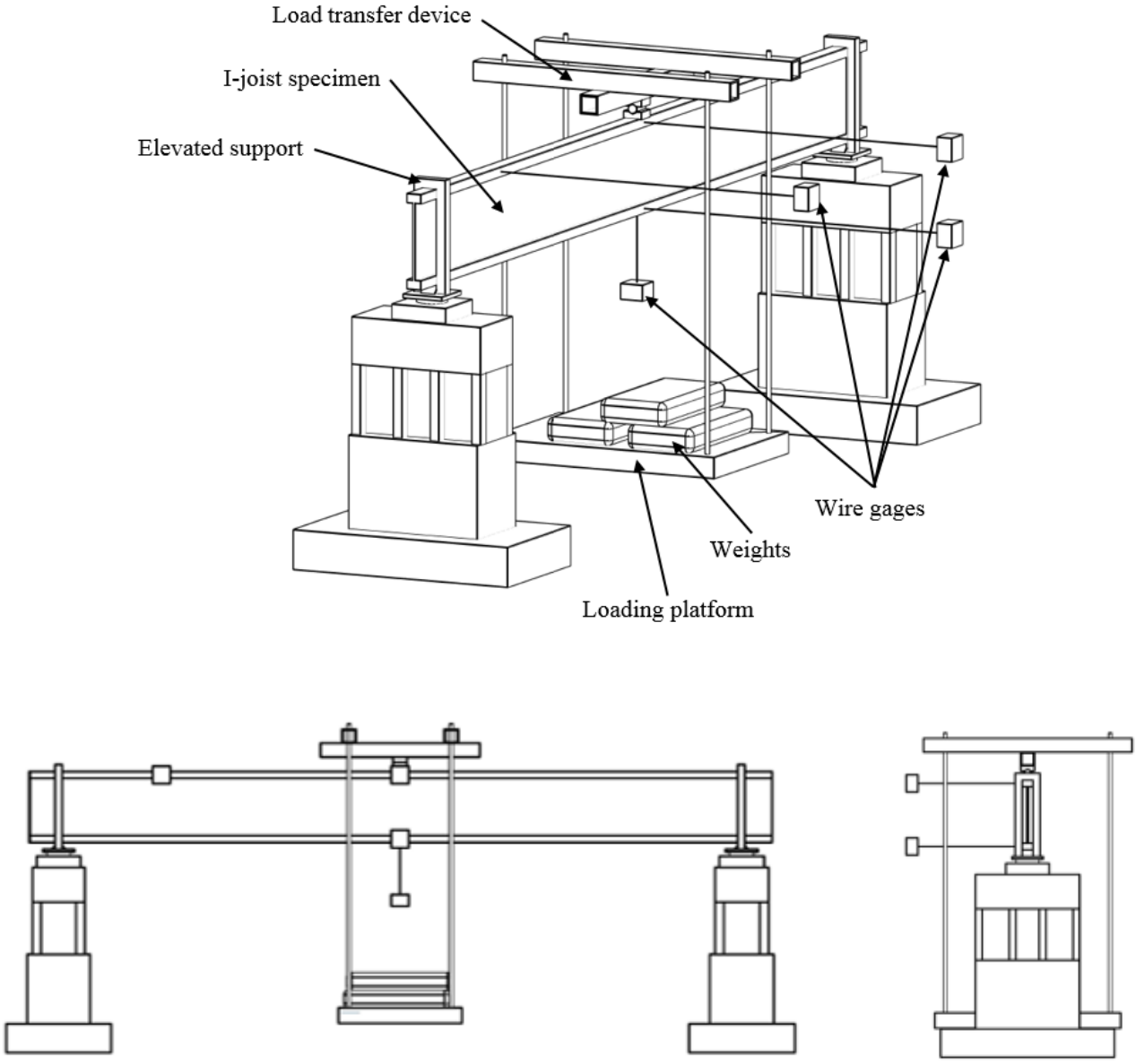

Figure 4-7 Schematic drawings of the lateral torsional buckling test configuration

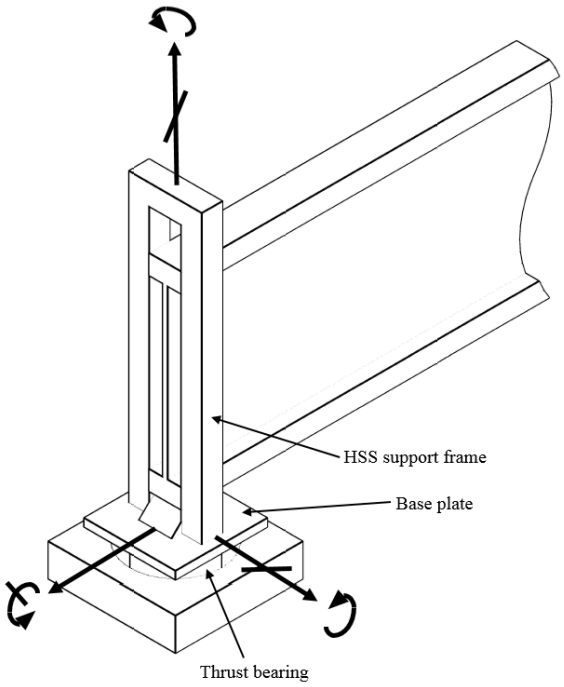

Figure 4-8 Lateral torsional buckling test end supports design and its restrained DOFs

Figure 4-9 Lateral torsional buckling end support apparatus

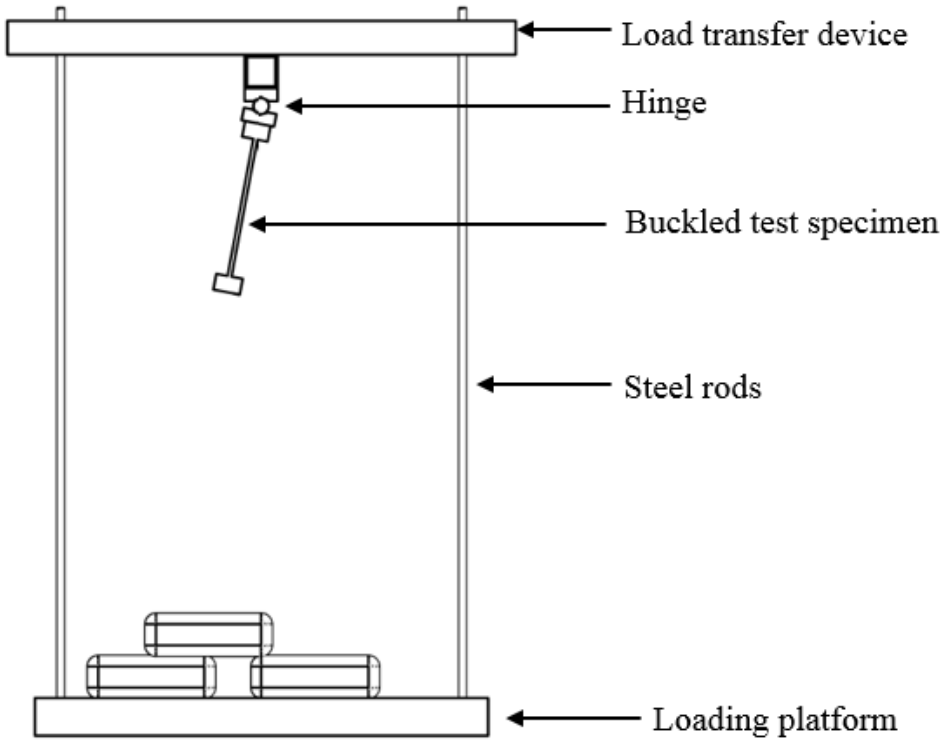

Figure 4-10 Lateral torsional buckling load transfer device design

Figure 4-11 Lateral torsional buckling test loading apparatus

4.2.4 Flange longitudinal modulus of elasticity

Following the lateral torsional buckling test, the flanges of selected specimens (Table 4-2) were cut from the web and tested to determine their longitudinal modulus of elasticity as per the American Standard Test Methods of static tests of lumber in structural sizes (D198-14). The test configuration used the same test apparatus as the lateral flexural stiffness test (Figure 4-12). The flange specimen was deflected at a constant rate while the force and vertical displacement at mid span were measured. The test was conducted on both sides of each specimen in order to get a more accurate measure of the lateral flexural stiffness. During the test, the flange specimen was bent about its strong axis in order to simulate the same bending action that occurs in lateral torsional buckling.

Figure 4-12 Flange longitudinal modulus of elasticity laboratory test setup

4.2.5 Flange torsional shear modulus

The flange torsional shear modulus of selected cut I-joist flanges were determined as per American Standard Test Method of static tests of lumber in structural sizes (D198-14). The

test configuration used the same test apparatus as for the torsional rigidity test (Figure 4-13). The flange specimen was loaded at a constant rate until it reached approximately 6º, while load and angle of twist were measured. The test specimen length varied between 6 and 7 feet, however, the gauge length was exactly 8 times the specimen depth.

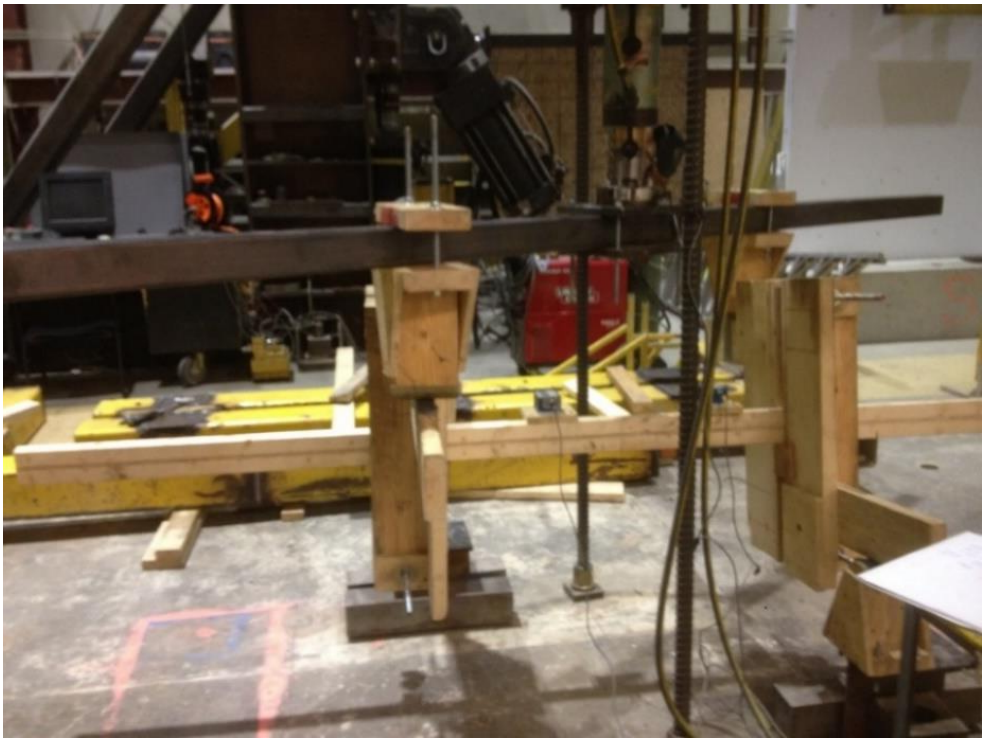

Figure 4-13 Flange torsional shear modulus laboratory test setup

4.2.6 Web transverse modulus of elasticity

The transverse modulus of elasticity of the web was determined based on the American Standard Test Methods for panel in flexure (D3043). A single point load was applied at the mid-span of a simply supported web test specimen until bending failure was observed (Figure 4-14). The web specimen was cut from selected I-joists after the lateral torsional buckling test was conducted. These cuts were taken in regions near the support to avoid any damage that may have occurred from the previous test. The specimen had a rectangular

shape of dimensions 280x102 mm for the 0.4 m I-joist specimen and 318x102 mm of the 0.6 m I-joist specimen. Load and deflection at mid span were recorded.

Figure 4-14 Web transverse modulus of elasticity test configuration

4.2.7 Flexural capacity

The specimen flexural capacity was evaluated as per the American Standard Test Methods of static tests of lumber in structural size (D198-14). A two-point loading was applied on the specimen top flange (Figure 4-15). The beam was deflected at a constant rate and corresponding load and deflection at mid span were recorded using a 10 kN load cell and a wire gauge. The experimental apparatus included lateral wood braces at each three feet interval along the length to prevent any lateral instability. A plastic strip was fastened on each wood brace to reduce friction between specimen and braces. A manual hydraulic pump was used to apply a downward force on a two-point loading transfer device (Figure

4-16). Steel hinge supports at the load-bearing location were installed to distribute the load and avoid local failure. Web stiffeners were installed at support and force application locations to promote bending failure.

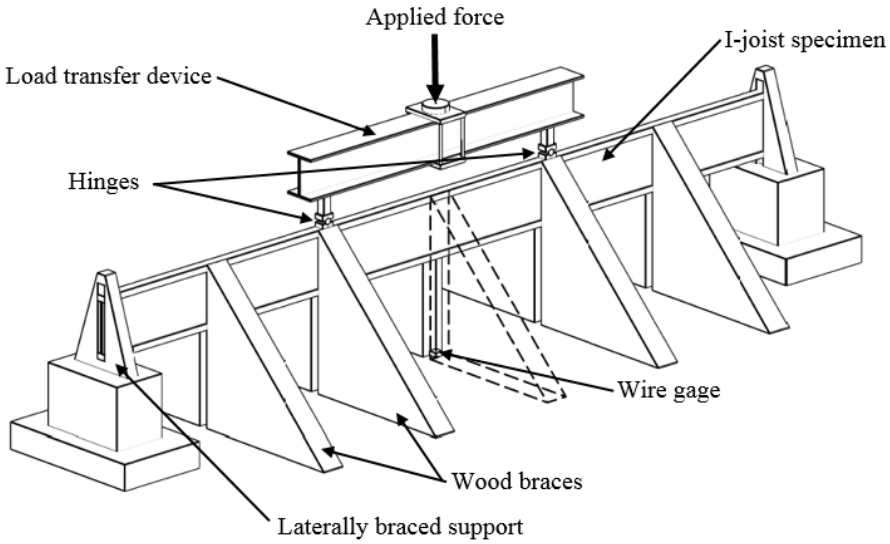

Figure 4-15 Ultimate flexural schematic drawing

Figure 4-16 Ultimate flexural capacity laboratory test setup

CHAPTER 5

EXPERIMENTAL RESULTS

5.1 General

This chapter presents the experimental results obtained for the wood I-joist mechanical properties, lateral torsional buckling capacity and the ultimate flexural capacity. It reports load and deflection data and modes of failure. The chapter also presents the experimental results of the lateral flexural stiffness and torsional rigidity of the wood I-joists, as well as the longitudinal MOE and the torsional shear modulus of the flanges and the transverse MOE of the web.

5.2 Mechanical properties

5.2.1 I-joist lateral flexural stiffness

The I-joist lateral flexural stiffness was evaluated for all the specimen groups. This property was measured using a two-point loading configuration, which allowed to measure the shear-free deflection at mid span. The load-deflection curves were obtained for both specimen sides. The shear-free lateral flexural stiffness EI_y was calculated using Equation (5-1):

$$EI_y = \left(\frac{P}{\Delta}\right)\frac{23L^3}{1296} \qquad (5\text{-}1)$$

where P/Δ is the slope of the load-deflection curve and L is the span length. Complete lateral flexural stiffness results for each specimen can be found in appendix B. The average lateral flexural stiffness was 2.10 x 10^{10} Nmm^2 for the 0.4 m wood I-joists with a COV of 0.087. The 0.6 m wood I-joists had an average lateral flexural stiffness of 5.27 x 10^{10} Nmm^2 with a COV of 0.072.

5.2.2 I-joist torsional rigidity

The torsional rigidity of entire I-joists specimens was found from the torque twist relationships using Equation 5-2:

$$GJ = \frac{TL}{\emptyset} \qquad (5\text{-}2)$$

where $T/\emptyset$ is the slope of the torque-twist curve and L is the gauge length from centre-centre points of the two inclinometers. A study was conducted on the length effect for specimens of the sample #8 and #16 to evaluate the fluctuation of the torsional rigidity over the span. The specimens of sample #8 were tested at span-depth ratios in the range of 4.5 to 13.5. For the specimens of sample #16 only span-depth ratios in the range of 4.5, to 9.5 were possible to test due to the greater depth of the I-joist cross-section and a limitation of the specimen's length. Table 5-1 and 5-2 display the torsional rigidity results for both I-joist sections. As shown in these tables, the computed torsional rigidity using Equation 5-2 is span dependent, with higher values for small spans and lower values for longer spans. Therefore, it suggests that warping was restrained until the torsional rigidity reached stable values such as observed for span to depth ratio of 11.5 in Table 5-1. In that case, Equation 5-2 is assumed to be valid as warping effects are assumed to be negligible at that span to depth ratio.

Table 5-1 Torsional rigidity of 0.4m wood I-joists

Sample #	**Specimen #**	**Span-depth ratio (GJ x 10^8 Nmm^2)**				
		4.5	**7.5**	**9.5**	**11.5**	**13.5**
6	1	----	----	----	12.5	----
6	2	----	----	----	13.4	----
6	3	----	----	----	12.1	----
6	4	----	----	----	12.0	----
6	5	----	----	----	10.3	----
7	1	----	----	----	10.4	----
7	2	----	----	----	10.8	----
7	3	----	----	----	11.3	----
7	4	----	----	----	11.7	----
7	5	----	----	----	11.5	----
8	1	52.1	18.3	15.6	12.9	8.70
8	2	47.1	12.3	17.0	8.40	7.90
8	3	50.8	----	15.3	9.90	8.70
8	4	50.9	18.5	15.0	8.60	9.90
8	5	50.1	19.2	16.3	9.80	13.7
8	6	49.2	20.8	16.2	14.0	14.1
8	7	33.1	18.6	16.5	14.8	16.6
8	8	50.5	20.3	13.3	9.80	12.8
8	9	57.6	18.9	16.1	9.30	12.1
8	10	45.8	19.8	18.0	11.8	9.80
8	11	50.9	18.8	12.0	7.60	12.2
Average	----	**48.9**	**18.5**	**15.5**	**11.1**	**11.5**
COV	----	**0.12**	**0.13**	**0.11**	**0.17**	**0.24**

Table 5-2 Torsional rigidity of 0.6m wood I-joists

Sample #	**Specimen #**	**Span-depth ratio (GJ x 10^8 Nmm^2)**				
		4.5	**7.5**	**9.5**	**11.5**	**13.5**
16	1	50.2	31.2	29.6	----	----
16	2	50.1	30.9	26.0	----	----
16	3	53.1	36.7	29.1	----	----
16	4	52.4	37.3	28.1	----	----
16	5	50.9	35.3	29.7	----	----
16	6	48.2	32.7	30.9	----	----
16	7	50.0	35.4	24.9	----	----
16	8	50.2	28.1	39.4	----	----
16	9	50.1	33.9	26.2	----	----
16	10	44.9	30.1	23.3	----	----
16	11	52.5	31.5	27.0	----	----
Average	----	**50.2**	**33.0**	**28.6**	----	----
COV	----	**0.04**	**0.09**	**0.15**	----	----

5.2.3 Wood I-joist components tests

After the lateral torsional buckling tests were conducted, selected I-joist specimens were dismantled and flanges and web specimens were cut, in order to evaluate the component's mechanical properties that will be used in the FE model. This testing phase included the specimens from the sample group #1, #5 and #16. Initially, the specimen from the sample group #5 were cut from 6.1 m long wood I-joists, which simultaneously generated the specimens of the sample group #1. To determine if the I-joist component's mechanical properties were affected by the destructive lateral torsional buckling test, the mechanical properties of the specimens of sample #5 were compared to that of the specimens of sample #1 that were not tested for buckling. The resulting longitudinal MOE, torsional shear modulus and web transverse MOE are reported in Tables 5-3, 5-4 and 5-5, respectively.

Table 5-3 Component mechanical properties of sample #1

Specimen #	**Longitudinal MOE (MPa)**			**Torsional shear modulus (MPa)**			**Web transverse MOE (MPa)**
	Bottom flange	**Top flange**	**Average**	**Bottom flange**	**Top flange**	**Average**	
3	13 533	13 580	13 557	763	720	742	3 058
4	14 077	12 008	13 043	1 080	807	944	3 681
5	12 871	15 042	13 957	832	1 354	1 093	3 374
6	10 625	12 550	11 588	886	1 157	1 022	4 128
8	13 756	14 790	14 273	807	1 043	925	4 441
9	11 925	13 029	12 477	932	1 141	1 037	3 397
Average	----	----	**13 149**	----	----	**960**	**3 680**
COV	----	----	**0.08**	----	----	**0.13**	**0.14**

Table 5-4 Component mechanical properties of sample #5

Specimen #	Longitudinal MOE (MPa)			Torsional shear modulus (MPa)			Web transverse MOE (MPa)
	Bottom flange	Top flange	Average	Bottom flange	Top flange	Average	
1	13 445	11 445	12 445	899	1 123	1 011	3 338
2	11 824	12 946	12 385	1 017	870	943	2 990
3	12 330	12 611	12 471	1 181	945	1 063	3 790
4	13 806	11 775	12 791	853	987	920	4 175
5	12 439	12 961	12 700	807	1 083	945	3 009
6	12 705	12 848	12 777	772	1 146	959	3 645
7	11 841	13 092	12 466	1 188	886	1 037	3 522
8	11 706	12 974	12 340	769	834	802	3 424
9	12 210	12 202	12 206	1 169	744	957	2 971
10	15 477	14 444	14 960	1 020	1 023	1 021	3 054
Average	----	----	**12 754**	----	----	**966**	**3 390**
COV	----	----	**0.06**	----	----	**0.08**	**0.12**

Table 5-5 Component mechanical properties of sample #16

Specimen #	Longitudinal MOE (MPa)			Torsional shear modulus (MPa)			Web transverse MOE (MPa)
	Bottom flange	Top flange	Average	Bottom flange	Top flange	Average	
1	12 212	13 457	12 835	499	696	597	2 828
2	11 995	11 921	11 958	764	759	761	2 748
3	12 931	11 419	12 175	677	642	659	3 220
4	11 986	12 829	12 408	608	724	666	2 616
5	11 308	11 800	11 554	271	855	563	2 234
6	12 488	13 300	12 894	416	823	619	2 463
7	13 027	13 681	13 354	427	683	555	2 939
8	13 702	13 068	13 385	764	641	702	2 373
9	13 562	12 929	13 245	772	1 095	934	2 507
10	12 231	13 757	12 994	921	921	921	2 620
11	12 019	13 159	12 589	649	617	633	2 052
Average	----	----	**12 672**	----	----	**692**	**2 600**
COV	----	----	**0.05**	----	----	**0.19**	**0.13**

5.2.4 Determination of the web torsional stiffness

The torsional stiffness of the web can be computed given that the torsional stiffness of the entire I-joist section and it flanges alone where determined experimentally. Due to limitations in specimen length, the torsional stiffness of the entire I-joist could be determined only for the 0.4m section with an average of 11.1 x 10^8 Nmm^2. On the other hand, the torsional stiffness of the flanges alone yielded an average of 7.03 x 10^8 Nmm^2. The resulting average torsional stiffness of the web (0.4m I-joist section) is 4.07 x 10^8 Nmm^2 which yields a web St-Venant shear modulus of 4390 MPa.

5.2.5 Lateral torsional buckling capacity

The lateral torsional buckling capacity was evaluated for samples #5, #6, #7, #8 and #16. Weights availability in the laboratory limited the range of spans. Measurements taken during the test considered of mid-height lateral deflection at mid-span, vertical displacement at mid-span, angular displacement at mid-span and lateral deflection of the top flange at quarter-span.

The out-of-straightness was measured at mid-span of the I-joist specimen. The average measured out-of-straightness is displayed in Table 5-6 for all specimen groups. Figure 5-1 shows the buckling motion of the I-joist specimen during the loading phase. Most of the test specimen started deflecting laterally as soon the loading was applied. Very few specimens remained straight during the loading phase until they reached their lateral torsional buckling capacity. For all test specimens, the same ultimate failure mechanism was observed, which was characterized by a rupture of the compression flange (Figure 5-2). Figures 5-3, 5-4, 5-5 and 5-6 display load-displacement curves that resulted from the test for the specimen of the sample group #6. Considering the experimental lateral torsional buckling capacity to be defined as the maximal force measurement at which inelastic deformations and collapse occurred, Table 5-7 presents the recorded LTB capacity of I-joist samples #5, #6, #7, #8 and #16.

Table 5-6 Average out-of-straightness of the top flange for each tested sample group

Sample #	**Average initial out-of-straightness (mm)**
5	4.6
6	3.8
7	3.0
8	3.8
16	7.3

Table 5-7 Lateral torsional buckling capacity (kN)

Specimen #	**Lateral torsional-buckling capacity (kN)**				
	Sample #5	**Sample #6**	**Sample #7**	**Sample #8**	**Sample #16**
1	5.03	4.33	3.58	2.57	5.67
2	5.53	4.24	3.49	2.66	5.35
3	5.39	4.41	3.40	2.75	5.53
4	5.30	4.06	3.28	2.48	5.76
5	5.44	4.15	2.95	2.75	5.58
6	5.06	----	----	2.75	5.50
7	5.48	----	----	2.66	5.67
8	5.66	----	----	2.57	5.58
9	5.30	----	----	2.57	5.85
10	5.44	----	----	2.66	5.50
11	----	----	----	2.48	5.85
Average	**5.36**	**4.24**	**3.34**	**2.63**	**5.62**
COV	**0.03**	**0.03**	**0.06**	**0.03**	**0.03**

Figure 5-1 Lateral torsional buckling test deformations in the elastic and inelastic range

Figure 5-2 Characteristic failure mechanism at collapse load

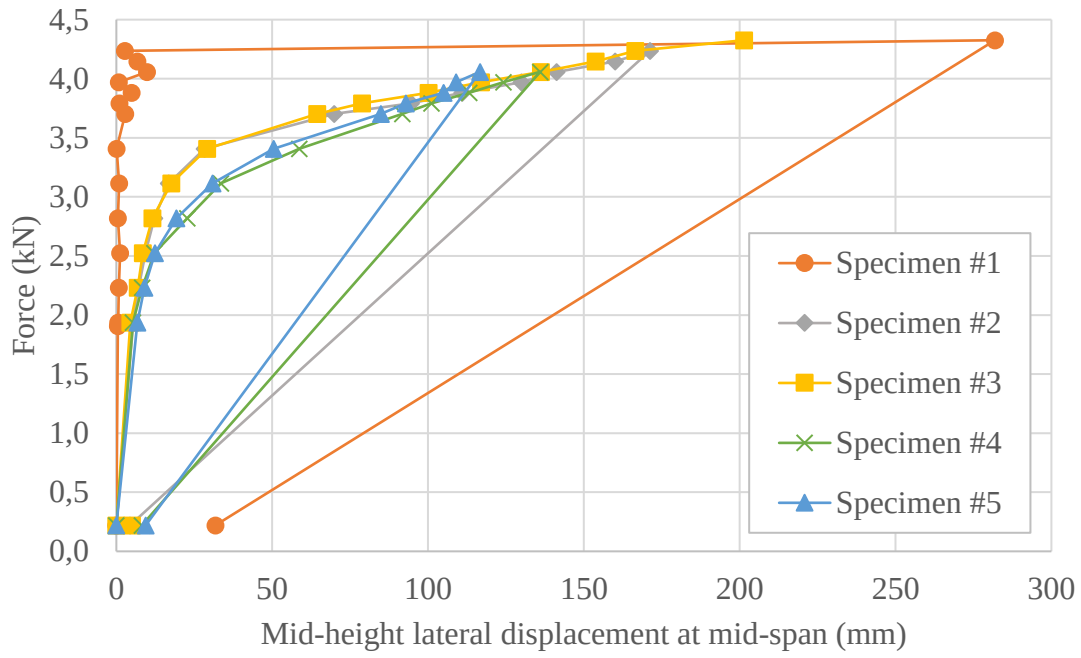

Figure 5-3 Force-lateral displacement curve of specimens in sample group #6

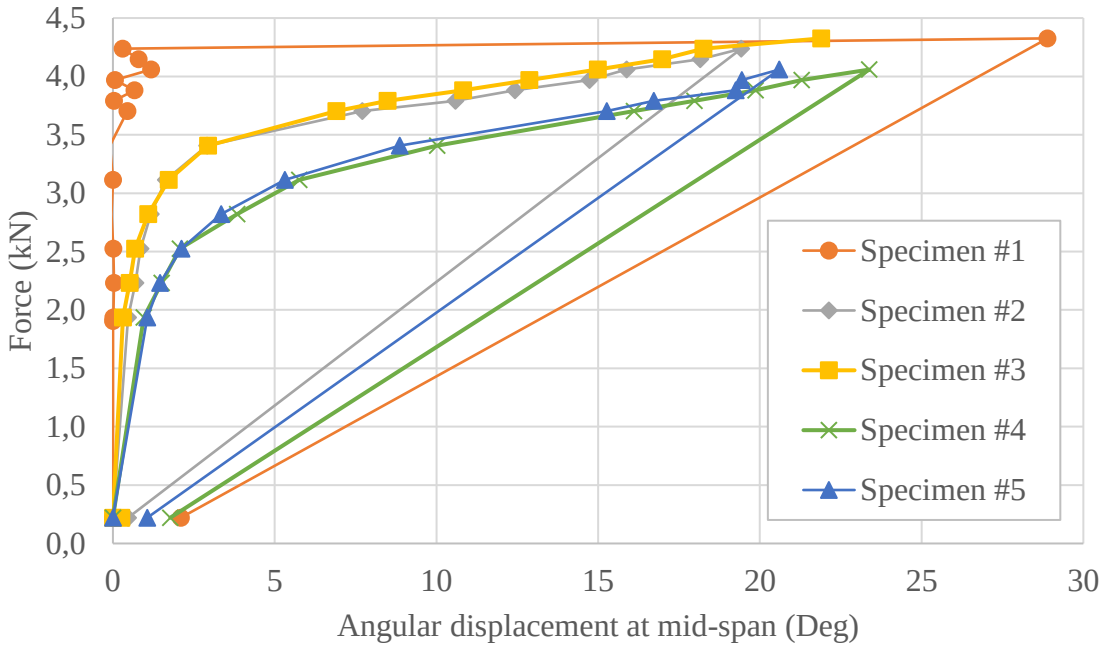

Figure 5-4 Force-angular displacement curve of specimens in sample group #6

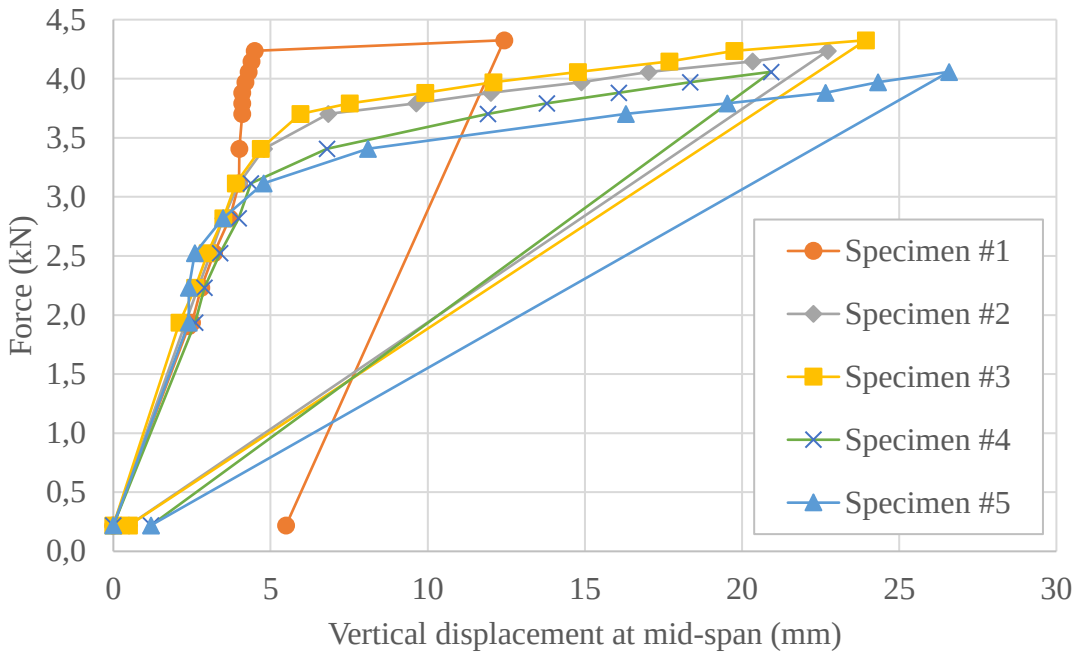

Figure 5-5 Force-vertical displacement curve of specimens in sample group #6

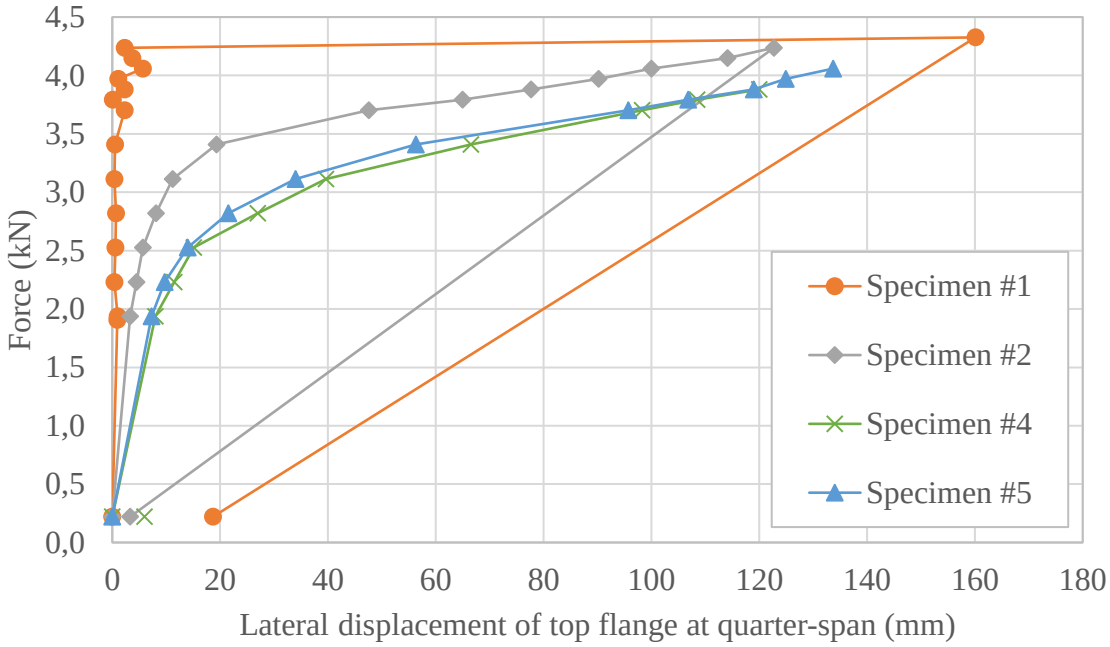

Figure 5-6 Force-lateral displacement curve of specimens in sample group #6

5.2.6 Ultimate flexural capacity

The ultimate flexural capacity test was conducted on 15 I-joist specimens of the sample group #8. The flexural capacity was governed by the failure of either the compression or tension flange. Eight compression and seven tension failures resulted from this test series. It was observed that rupture had a tendency to take place in regions with inclined grain orientation and defects such as knots and splits.

A typical load-deflection curve for tension and compression failure is displayed in Figure 5-7. Table 5-8 displays the maximum load and deflection data recorded for all specimen tested. Failures that occurred in the tension flange are denoted with (T) and those that occurred in the compression flange are denoted with (C). The ultimate mean flexural capacity was found to be 29.9 kNm with a COV of 0.19. Figure 5-8 reports the ultimate moment capacity of each test specimen and illustrates the spread of each failure types with respect to the ultimate mean flexural capacity. Figure 5-9 shows typical tension and compression failures. The 0.6 m I-joist specimens were not able to fail in bending, due to their high span-depth ratio which promoted buckling of the web in a region of high shear force, despite web stiffeners were used at proper locations (Figure 5-10).

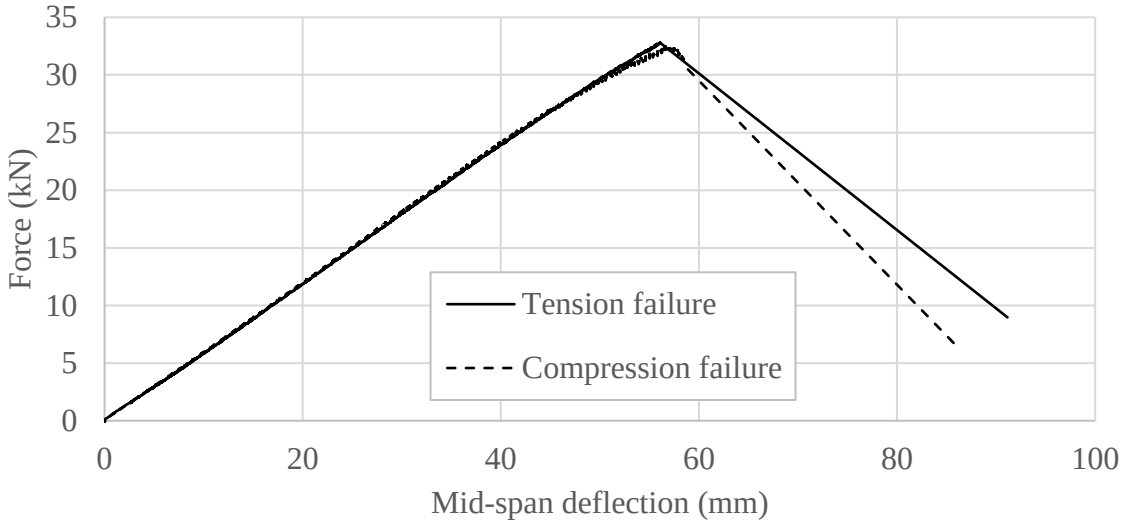

Figure 5-7 Load-deflection curves for ultimate flexural capacity

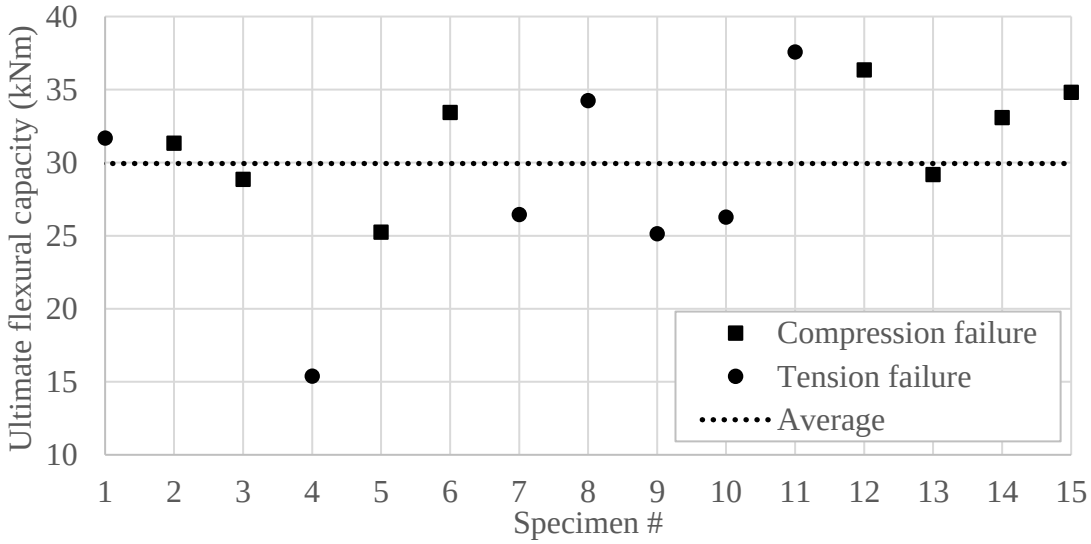

Figure 5-8 Ultimate flexural capacity of I-joist sample #8

Table 5-8 Ultimate flexural capacity, corresponding deflections and failure modes

Specimen #	**Ultimate flexural capacity (kNm)**	**Deflection at ultimate (mm)**	**Failure type[1]**
1	31.7	56.0	T
2	31.3	57.8	C
3	28.9	54.0	C
4	15.4	28.1	T
5	25.3	46.0	C
6	33.4	58.2	C
7	26.5	46.0	T
8	34.2	57.2	T
9	25.1	45.0	T
10	26.3	44.0	T
11	37.6	66.3	T
12	36.4	68.0	C
13	29.2	52.0	C
14	33.1	56.5	C
15	34.8	64.0	C
Average	**29.9**	**53.3**	----
COV	**0.19**	**0.19**	----

Figure 5-9 Failure modes of the 0.4m I-joists, Tension (left) and compression (right)

Figure 5-10 Failure mode of the 0.6m I-joists (Web distortion)

CHAPTER 6

FINITE ELEMENT MODELLING

6.1 General

This chapter presents the finite element modelling of the 42 wood I-joist specimens that were tested for lateral torsional buckling. The finite element analysis approach is described in section 6.2, after which the model is described in section 6.3. Analysis procedures and results are presented in sections 6.4 and 6.5.

6.2 Linear and nonlinear analysis

A linear analysis denotes a linear relationship between the applied load and the displacement of a given system. Although most physical structures may exhibit nonlinear behaviour at some point, linear analysis undoubtedly remains a preferred approach for design purpose due to its simplicity in solving typical structural problems. The first step in a finite element analysis for lateral torsional buckling of a perfect wood I-joist is a pre-buckling analysis involving an in-plane stiffness matrix $[K_{IP}]$ subjected to a reference load $\{P_{ref}\}$ that can be described with Equation 6-1:

$$[K_{IP}]\lambda\{v_i\} = \lambda\{P_{ref}\} \qquad (6\text{-}1)$$

where $\{v_i\}$ is the in-plane nodal displacement and λ the load multiplier. The wood I-joist remains in-plane during the loading and the system's response is assumed to be linear, until the structure reaches a tendency to undergo lateral torsional buckling.

The next step involves an eigenvalue solver that is used to obtain the critical buckling load, where the smallest eigenvalue λ_i is sought for which Equation 6-2 has a non-trivial solution:

$$([K_{OP}] + \lambda_i[K_G])\{v_i\} = 0 \qquad (6\text{-}2)$$

where $[K_{OP}]$ denotes the out-of-plane stiffness matrix, $[K_G]$ is the geometric matrix and $\{v_i\}$ is the nodal displacement vector of the mode shape i.

Nonlinear analysis, on the other hand, is characterized by a nonlinear response of a given system where the structure's stiffness varies with respect to the displacement. When the structure's stiffness depends on the displacement, the initial stiffness can no longer be multiplied by the applied load to find the displacement and can be expressed as:

$$[K(v)]\{v\} = \{P\} \qquad (6\text{-}3)$$

where $[K(v)]$ denotes the stiffness matrix that is dependent on the nodal displacement $\{v\}$ under loading $\{P\}$. In Abaqus Standard, a nonlinear problem is solved incrementally by using the Newton-Raphson method (Simulia, 2012). This method solves for the single equilibrium path of a nonlinear problem in a load-displacement space using iterations. Equation 6-3 best describes the behavior that resulted in most specimens from the lateral torsional buckling experiments (Figure 6-1).

Different factors can lead to non-linearity in the system's response. The finite strength of a material can lead to non-linearity, where high strains lead to yielding and thus, a significant change in the stiffness is observed. Another factor includes boundary non-linearity that can result from a change in the boundary conditions during the loading, affecting subsequently the structure's behaviour. The nonlinear relationship observed for most wood I-joist specimens can be attributed to geometric non-linearity. The latter occurs when the structure's stiffness changes as it undergoes large rotations and displacements. In lateral torsional buckling, this non-linearity is a function of the strong axis bending stiffness, the weak axis bending stiffness, the warping stiffness and the St-Venant torsional stiffness.

A critical aspect that triggers a nonlinear response from the system, rather than a linear behaviour, remains the initial imperfections present in the structure. Realistic wood I-joists

usually contain initial imperfections, such as out-of-straightness, that promotes lateral and angular displacement of the cross-section as soon as the loading takes place, leading to non-linearity in the system's response.

In this context, an eigenvalue buckling analysis is to be carried out to provide an estimate of the critical buckling load, followed by a nonlinear analysis to reproduce the lateral instability behavior of the wood I-joists observed during the experiments. In order to investigate the nonlinear response, the out-of-straightness of each wood I-joist compression flange were measured at mid-span to determine the amount of initial imperfections.

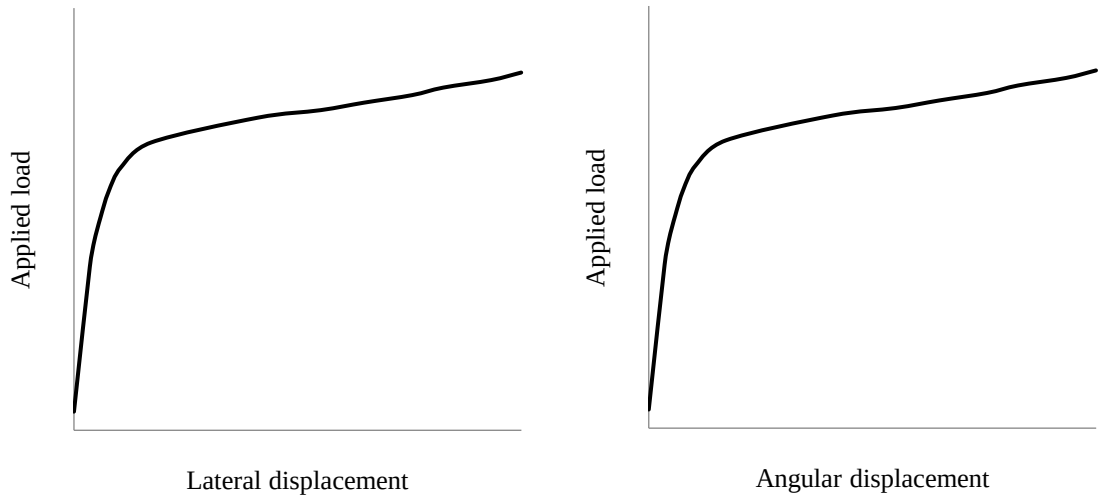

Figure 6-1 Typical load-displacement curves from wood I-joist LTB test

6.3 Model description

6.3.1 Elements details

Similar to the FE model used in the sensitivity analysis (Chapter 3), the S4R shell element is used to model the web, while the flanges use solid brick elements C3D8R. This element assembly allow to effectively discretize the wood I-joist structure while reducing the computational cost.

6.3.2 Material parameters

The finite element model accounts for the composite nature of the wood I-joist using the mechanical properties determined from the experimental program. Only the flange MOE will vary with each specimen while all the other mechanical properties use average mechanical values taken from the component testing. These include an average flange St-Venant shear modulus of 966 MPa, a web modulus of elasticity of 3392 MPa. The web shear modulus is assumed to be 100 MPa, based on average values in the literature (Grandmont et al. 2008). Table 6-1 presents the flange modulus of elasticity used for each specimen, obtained from the flexural stiffness test.

Table 6-1 Specimen flange modulus of elasticity input parameters

Sample group #	**Specimen #**	**Flange MOE Side A (MPa)**	**Flange MOE Side B (MPa)**	**Flange MOE average (MPa)**
5	1	12 923	12 623	12 773
	2	14 363	12 727	13 545
	3	14 212	12 623	13 417
	4	12 321	12 146	12 233
	5	13 468	13 233	13 351
	6	13 755	12 988	13 372
	7	13 362	13 619	13 490
	8	13 184	14 328	13 756
	9	12 213	12 796	12 504
	10	13 500	13 509	13 505
6	1	12 523	11 886	12 205
	2	13 348	13 253	13 301
	3	11 806	12 094	11 950
	4	11 594	13 193	12 394
	5	13 095	13 095	13 095
7	1	11 363	11 307	11 335
	2	13 247	13 506	13 377
	3	12 865	12 761	12 813
	4	13 261	14 429	13 845
	5	10 045	12 277	11 161
8	1	13 808	13 605	13 706
	2	15 555	13 066	14 310
	3	13 212	15 234	14 223

	4	12 810	15 326	14 068
	5	15 035	12 357	13 696
	6	20 082	18 482	19 282
	7	14 733	14 341	14 537
	8	13 041	14 443	13 742
	9	13 089	15 043	14 066
	10	14 335	13 720	14 028
	11	13 356	13 383	13 370
16	1	13 785	13 194	13 490
	2	11 681	11 106	11 393
	3	12 490	11 829	12 160
	4	11 872	11 597	11 735
	5	11 374	11 341	11 357
	6	11 327	12 365	11 846
	7	11 378	11 816	11 597
	8	12 208	12 364	12 286
	9	12 765	12 740	12 753
	10	12 010	13 177	12 593
	11	13 053	13 355	13 204

6.3.3 Mesh detail

The details regarding the mesh of each I-joist specimen size is provided in Table 6-2. An ideal element aspect ratio of 1.0 was targeted, however, a mesh study showed convergence of the critical load when the flanges contained 8 elements along the flange's width, 5 elements along its thickness and 232 elements along its length. The web contains 16 elements along the height and 232 elements along its length.

Table 6-2 Wood I-joist FE models mesh details

Sample group #	Span (mm)	# Elements		Element Size		Aspect ratio	
		Flange	Web	Flange (mm)	Web (mm)	Flange	Web
5	3970	9280	3712	8 x 7.6 x 18	25 x 18	2.3	1.4
6	4580	9280	3712	8 x 7.6 x 21	25 x 21	2.6	1.2
7	5190	9280	3712	8 x 7.6 x 24	25 x 24	3.0	1.1
8	5800	9280	3712	8 x 7.6 x 26	25 x 26	3.3	1.0
16	5800	9280	3712	11 x 7.6 x 26	38 x 26	2.4	1.5

6.3.4 Boundary conditions and load application

The restrained degree of freedom that best describe the experimental support configuration involves the vertical and lateral displacement of the upper and lower flange (Figure 6-2 & 6-3). In order to mimic the experimental configuration, the lower nodes of the bottom flange are restrained from moving vertically, while the nodes located on each side of the top and bottom flanges are restrained from moving laterally.

At the junction of the web and flange elements, the degrees of freedom of the shell and solid elements are coupled using the ABAQUS feature ‘’SHELL TO SOLID COUPLING’’. This feature enables to transfer the translational degrees of freedom of the web shell elements to the solid elements located in the flanges. Furthermore, a concentrated load was symmetrically positioned at mid-span.

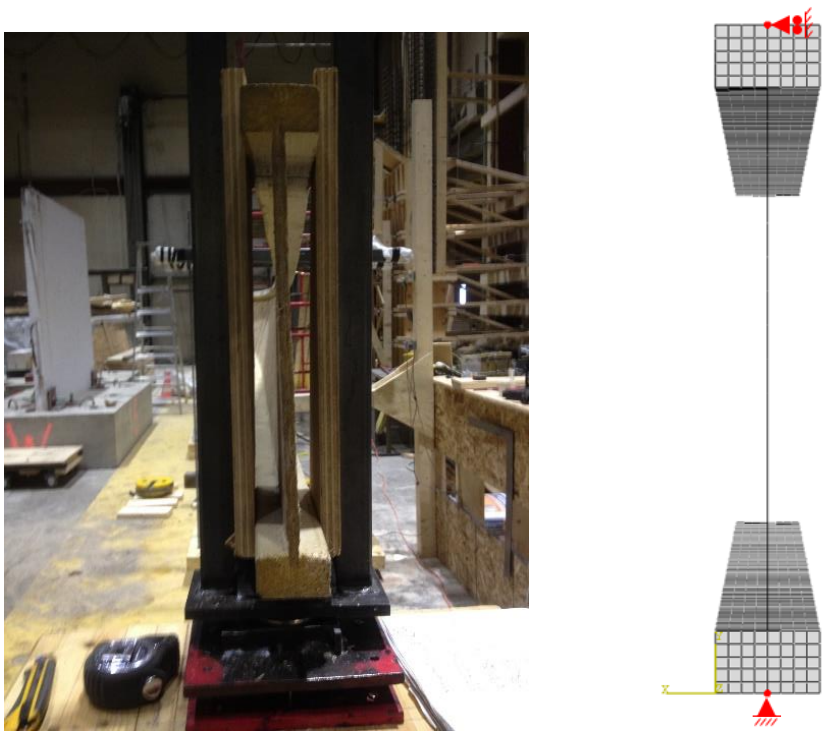

Figure 6-2 Modeling of the boundary conditions

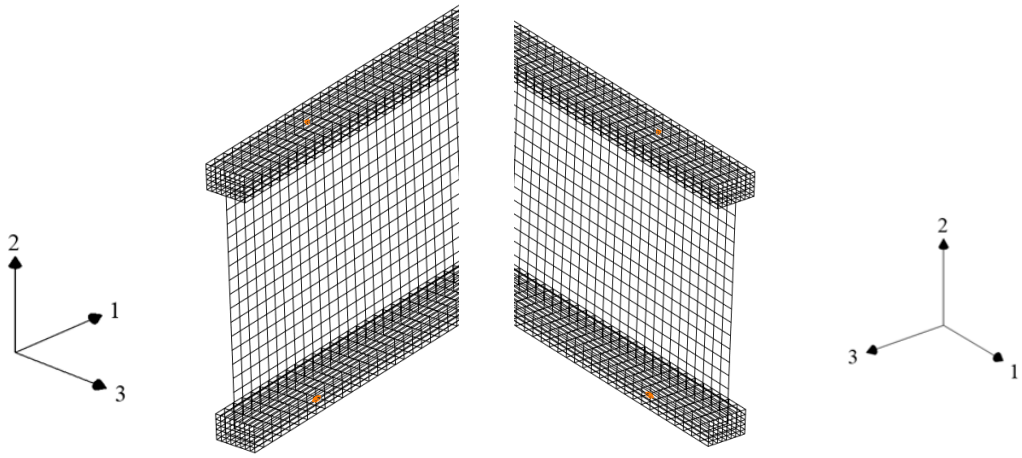

Figure 6-3 Location of the boundary conditions along the I-joist FE model

6.4 Eigenvalue analysis procedure

An Eigenvalue buckling analysis is first conducted to estimate the buckling capacity for the wood I-joist specimens. Table 6-3 presents the Eigenvalue buckling analysis results for each tested wood I-joist specimens. The retained buckling mode shape for each sample group is shown in Figure 6-4.

Table 6-3 Eigenvalue buckling analysis results

Sample group #	**Specimen #**	**Critical buckling load (kN)**	**Sample group #**	**Specimen #**	**Critical buckling load (kN)**
5	1	4.40	8	1	2.23
	2	4.54		2	2.28
	3	4.52		3	2.27
	4	4.30		4	2.26
	5	4.50		5	2.23
	6	4.51		6	2.63
	7	4.53		7	2.30
	8	4.58		8	2.23
	9	4.35		9	2.26
	10	4.53		10	2.26
	AVG	4.48		11	2.21
6	1	3.31		AVG	2.29
	2	3.45	16	1	4.65
	3	3.27		2	4.21
	4	3.33		3	4.37
	5	3.42		4	4.28
	AVG	3.36		5	4.20
7	1	2.52		6	4.31
	2	2.73		7	4.25
	3	2.67		8	4.40
	4	2.77		9	4.50
	5	2.50		10	4.46
	AVG	2.64		11	4.59
				AVG	4.38

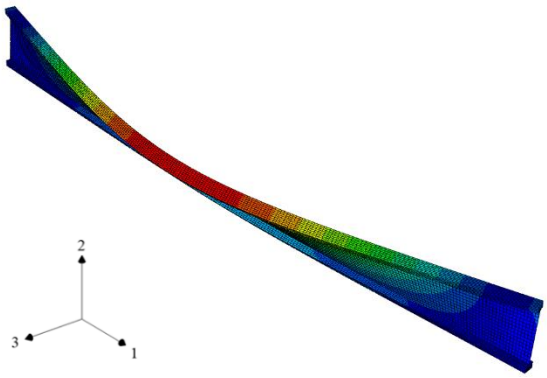

Specimen sample group #5

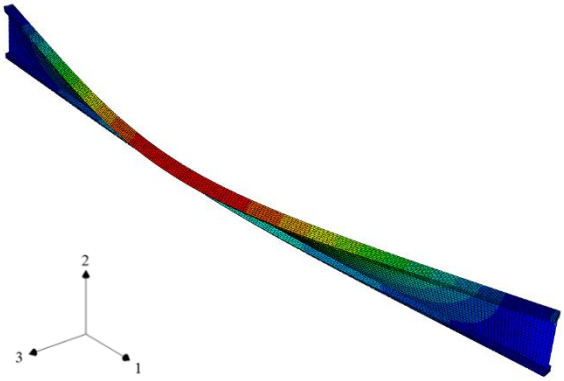

Specimen sample group #6

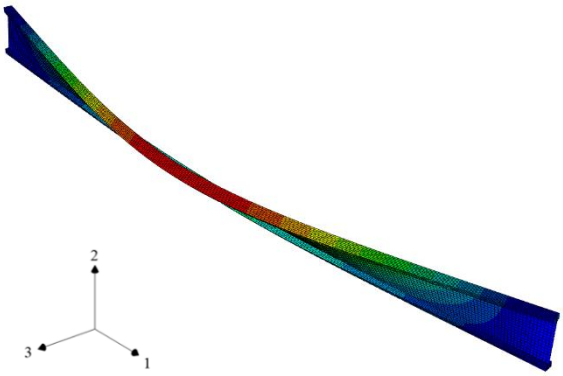

Specimen sample group #7

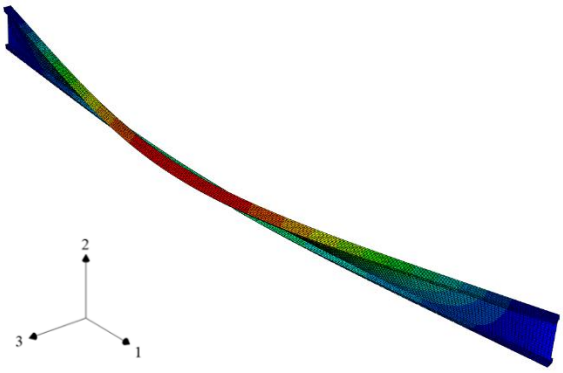

Specimen sample group #8

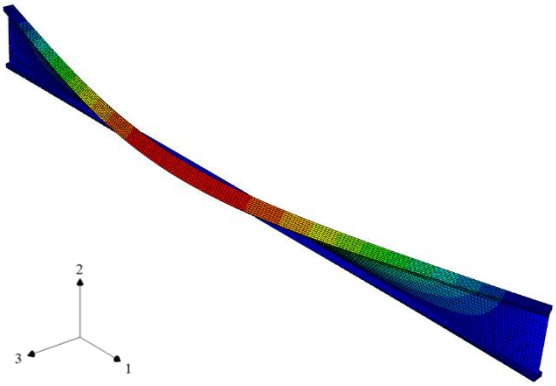

Specimen sample group #16

Figure 6-4 First buckling mode shape of the wood I-joist FE models

6.5 Nonlinear analysis procedure

The modified Riks method is used to conduct a geometric nonlinear analysis on the wood I-joist models. This iterative procedure incorporates initial imperfections on the wood I-joist using the preceding Eigen modes shape which are scaled to match the out-of-straightness of the top flange of each test specimens. Figure 6-5 displays the initial imperfection that is incorporated into the model before running the nonlinear analysis. Moreover, Table 6-4 presents the out-of-straightness that was measured during the LTB experiment for each wood I-joist specimens. Most models required 30-40 load increments and on average 125 iterations to converge to a mid-height lateral displacement at mid-span of 200 mm. Figure 6-6 displays the buckling deformation pattern of Specimen # 4 (sample group #8). Figure 6-7 plot the nonlinear response of the FE model for the (a) Force-lateral displacement plot and (b) Force-angular displacement plot.

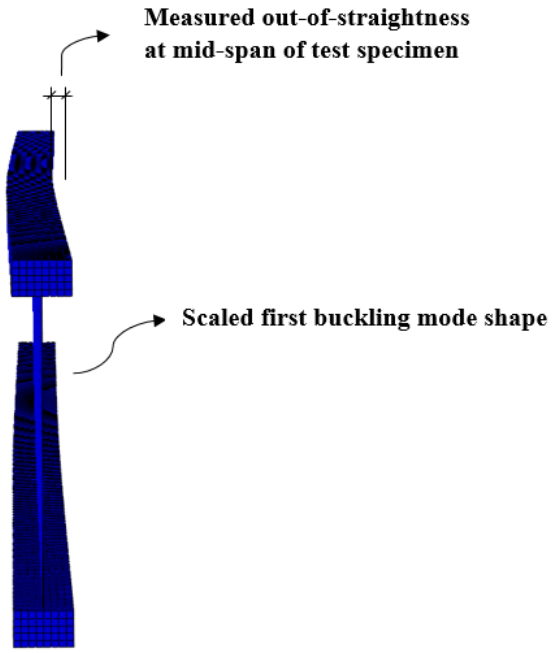

Figure 6-5 Initial imperfection geometry incorporated in the wood I-joist FE models

Table 6-4 Out-of-straightness of specimen compression flange

Sample group #	**Specimen #**	**Length (mm)**	**Sample group #**	**Specimen #**	**Length (mm)**
5	1	3	8	1	2
	2	7		2	0
	3	2		3	12
	4	4		4	12
	5	6		5	0
	6	7		6	0
	7	4		7	0
	8	1		8	3
	9	9		9	3
	10	3		10	5
6	1	2		11	5
	2	2	16	1	6
	3	6		2	6
	4	7		3	8
	5	2		4	1
7	1	6		5	20
	2	4		6	7
	3	0		7	5
	4	3		8	6
	5	2		9	15
----	----	----		10	6
----	----	----		11	0

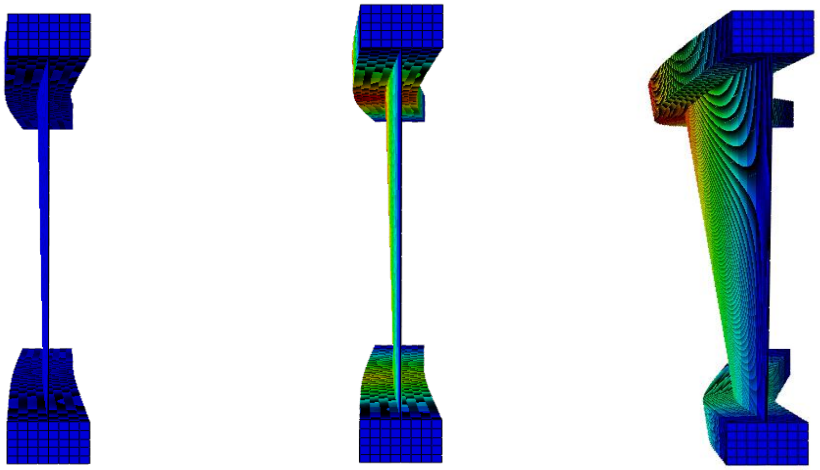

Load increment	1	16	22
Applied force (kN)	0.00	0.75	2.17
Mid-height lateral displ. @ mid-span (mm)	0.00	3.00	48.6
Angular displ. @ mid-span (Deg)	0.00	0.04	7.72

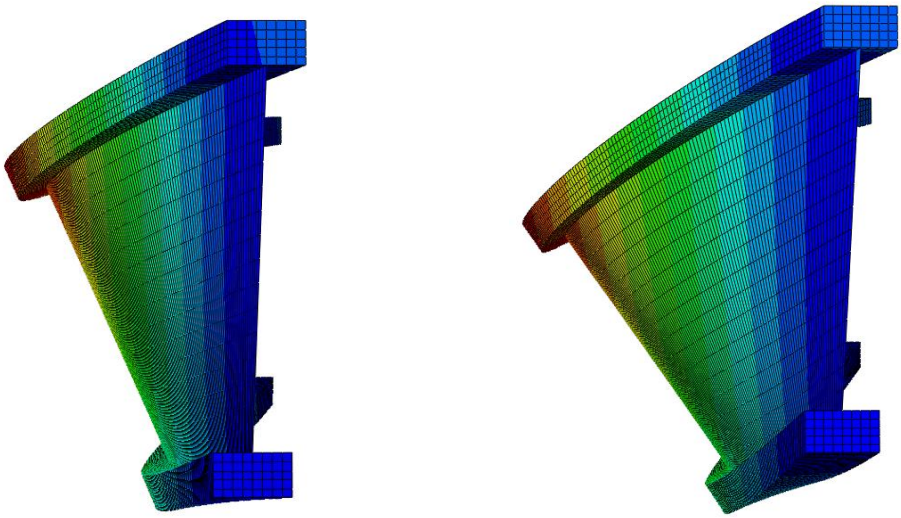

Load increment	26	32
Applied force (kN)	2.55	2.87
Mid-height lateral displ. @ mid-span (mm)	138	201
Angular displ. @ mid-span (Deg)	22.0	32.7

Figure 6-6 FE nonlinear geometric analysis

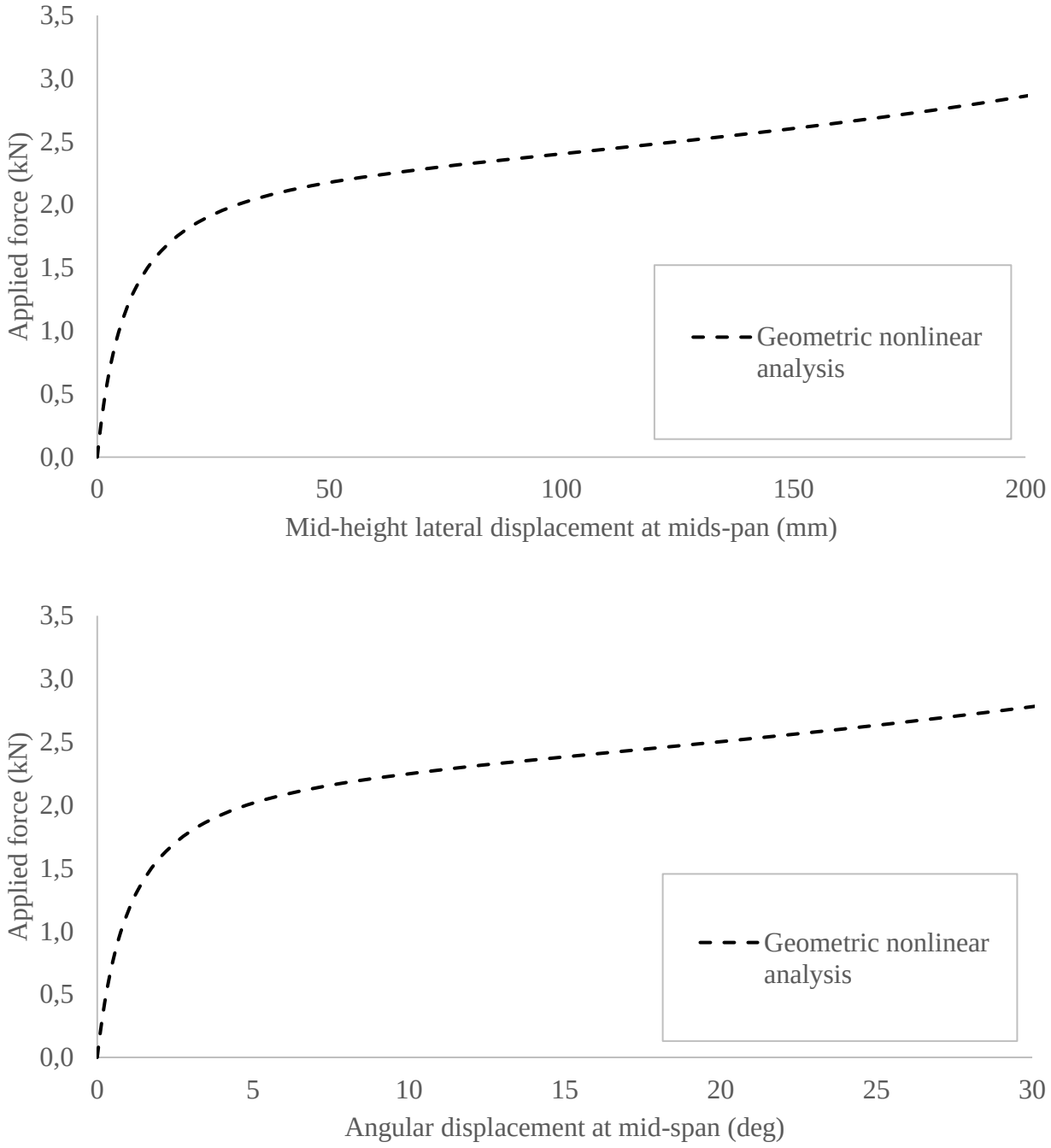

Figure 6-7 Linear and geometric nonlinear analysis of wood I-joist specimen #4 of sample group 8

6.5.1 Imperfection sensitivity analysis

The amount of initial imperfections has an impact on the nonlinear response. To assess this effect, a sensitivity analysis was conducted using various out-of-straightness magnitudes of the top flange. The imperfection sensitivity model used the geometry definition for sample #8 along with the material parameters presented in Table 6-5. These material properties are found to be the average longitudinal modulus of elasticity of the flange, the St-Venant shear modulus of the flange and the web modulus of elasticity that were experimentally determined. Furthermore, it was reasonable to assume the flange and web as isotropic materials, based on the sensitivity analysis results. As shown in Figure 6-8, minor out-of-straightness of the top flange at mid-span lead to an abrupt change in the stiffness whereas more significant imperfections produce a smoother curve with a smaller rate in the variation of the stiffness.

Table 6-5: Imperfection sensitivity FE model material parameters

Part	**E_1 (MPa)**	**E_2 (MPa)**	**E_3 (MPa)**	**μ_{12}**	**μ_{13}**	**μ_{23}**	**G_{12} (MPa)**	**G_{13} (MPa)**	**G_{23} (MPa)**
Flanges	12754	12754	12754	0	0	0	966	966	966
Web	3392	3392	3392	0	0	0	100	100	100

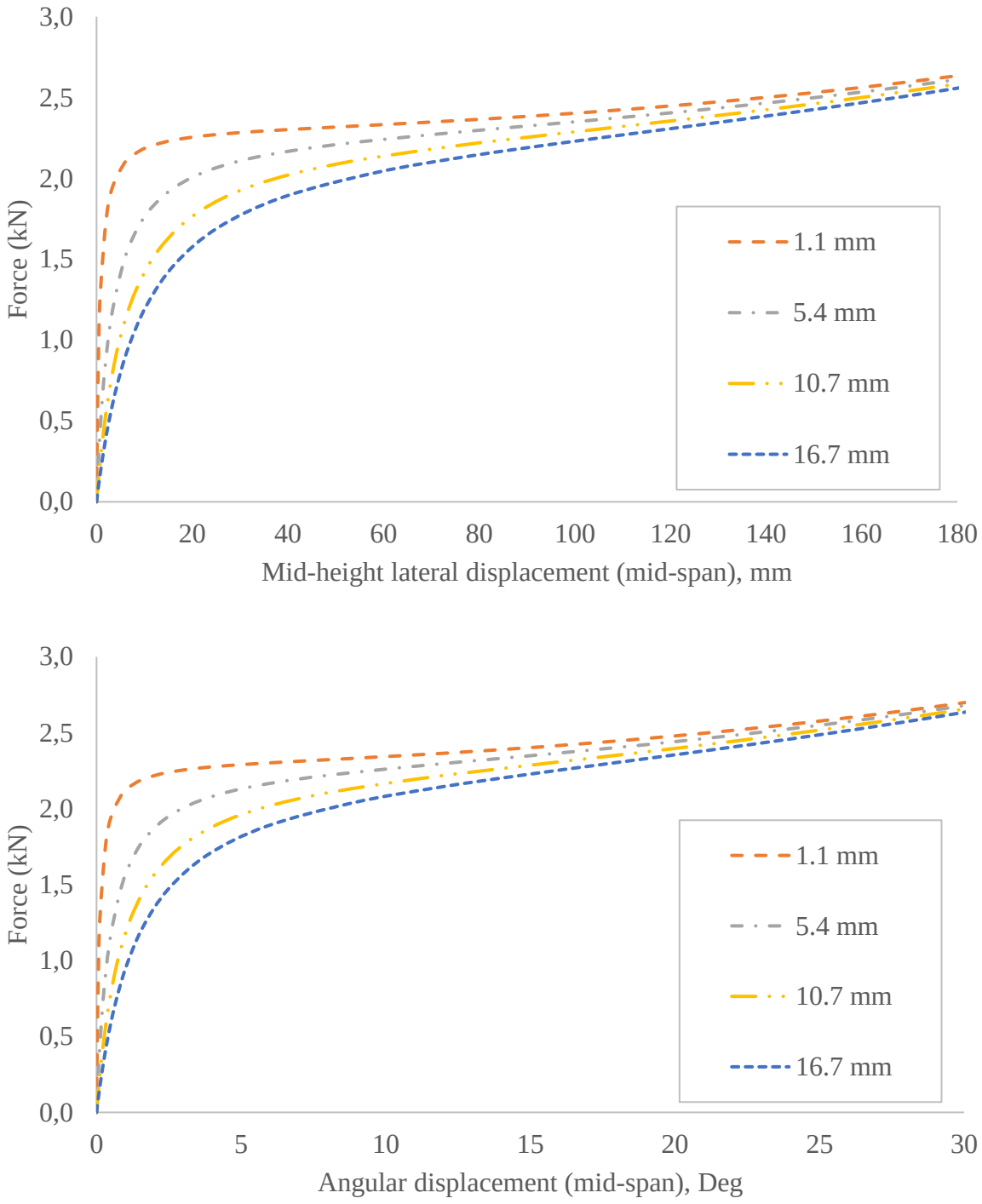

Figure 6-8 Effect of initial imperfections on the non-linearity of a typical Wood I-joist model

CHAPTER 7

DISCUSSION

7.1 General

This chapter discusses the results of both the experimental investigation conducted on the wood I-joist specimens and the numerical model that predict the capacity in lateral torsional buckling. Section 7.2 summarizes the findings of the mechanical properties from the sensitivity analysis. Section 7.3 presents findings from the experimental investigation on the lateral torsional buckling capacity of the wood I-joist and also compares the experimental buckling load data with the model prediction results that involve the finite element analysis, the analytical solution and the American timber design standard model. Ultimately, Section 7.4 discusses the results of the experimental investigation on the ultimate flexural capacity of the wood I-joist.

7.2 Experimental investigation of the wood I-joist mechanical properties

7.2.1 Sensitivity analysis

The sensitivity study conducted on the mechanical properties showed that the most sensitive parameter is the modulus of elasticity of the flanges in the longitudinal direction. The sensitivity analysis also showed that the material properties in the compression flange influence the most the critical buckling moment. An increase of 50% on the MOE of the compression flange resulted in an increase in the buckling capacity by 20% while the same rate MOE increase in the tension flange improved the buckling capacity by only 4%. The shear modulus of the flanges also plays a role in the lateral buckling response. More

specifically, a 50% increase in the shear modulus that follows the longitudinal-transverse (1-2) and longitudinal-lateral (1-3) planes induced an increase on the buckling capacity of 2% and 5%, respectively. Both the compression and tension flange exhibited the same sensitivity with regards to these shear moduli.

Moreover, the modulus of elasticity of the web also displayed a slight influence on the buckling capacity. In the case where the web is allowed to distort, the modulus of elasticity in the transverse direction increased the buckling capacity by 2% with an increase of 50% on the MOE. Additionally, the MOE and shear modulus in the remaining planes as well as the Poisson's ratio had no effect on the buckling capacity. It can be concluded that the results obtained from the sensitivity study corroborate the stiffness parameters involved in the energy expression for lateral torsional buckling (Equation 1-1). More specifically, the weak axis bending stiffness (EI_1) and the warping stiffness (E_w) are associated with strains along the fiber's direction in the flanges and the St-Venant torsional stiffness (GJ) is associated with shear stresses of the flanges and web in the 1-2 and 1-3 planes.

7.2.2 Longitudinal modulus of elasticity determination

The lateral flexural stiffness tests on entire I-joist sections provided an average lateral bending stiffness of 2.10 x 10^{10} Nmm^2 for the 0.4m I-joist section with a COV of 0.087. The 0.6m I-joist section yielded an average lateral bending stiffness of 5.27 x 10^{10} Nmm^2 with a COV of 0.072. These levels of COV were expected given the defects present in the flanges such as sloped grain, checks and knots.

The web contribution to the lateral flexural stiffness of the entire I-joist seems to be negligible. For instance, for the 0.4m I-joist cross-section, assuming a longitudinal modulus of elasticity of 12 500 and 3000 N/mm^2 for the flanges and the web, respectively one obtains a transformed section ratio of $n_1 = 0.24$. The transformed weak axis moment of inertia can then be calculated to be 1.67x10^6 N/mm^2, which when compared to the moment of inertia of the flanges alone (1.66x10^6 N/mm^2), provides a difference of only 0.4%.

The MOE resulting from the lateral flexural tests were compared to the MOE obtained from the same wood I-joist specimen for the flange component flexural tests, as shown in Table 7-1. The comparison in Table 7-1 yielded a percentage difference in the range of 3 to 11%. This difference is likely due to the fact that the component testing approach used only half of the flange length, while the lateral flexural test used the whole flange length. Both methods denoted similar variability in the resulting MOE values. Nevertheless, the MOE results from the lateral flexural test, involving the entire I-joist, is expected to provide more reliable data for the analytical models for the following reasons;

1) It involves the entire wood I-joist specimen length, thus accounts for the strength variations along the flanges;
2) The bending deformations took place in the same critical section as for the lateral torsional buckling tests. Considering the flanges are made of small lumber pieces of various species jointed at their ends, variations in strength can be considerable along the length of a wood flange and thus would alter the bending stiffness results if those tests were not conducted at the specimen mid-span.

Testing was also conducted to determine whether the MOE obtained from specimens cut from wood I-joists tested for full-scale LTB were affected by the loading history. These specimens were therefore compared to similar specimens cut from untested I-joist members. The results shown in Table 7-2 suggest, by comparing flange 1 and 2 from the respective groups, that the specimens obtained from previously tested I-joists did not show any significant decrease in stiffness compared to those obtained from untested I-joists. This indicates that in general the I-joist components were in the elastic region and any damage or inelastic deformations occurred locally at the flange mid-span.

Table 7-1 MOE comparison for uncut wood I-joist and component testing (Sample group #5)

Specimen #	Lateral flexural tests	Component testing	% difference
	AVG Flange MOE (MPa)	AVG Flange MOE (MPa)	
1	12 773	12 445	2.57
2	13 545	12 385	8.56
3	13 417	12 471	7.05
4	12 233	12 791	4.56
5	13 351	12 700	4.88
6	13 372	12 777	4.45
7	13 490	12 466	7.59
8	13 756	12 340	10.29
9	12 504	12 206	2.38
10	13 505	14 960	10.77
Average	**13 194**	**12 754**	----
COV	**0.04**	**0.06**	----

Table 7-2 Effect of the inelastic deformations on the MOE

Specimen #	Modulus of elasticity (N/mm^2)			
	Sample group #5		Sample group #1	
	Flange 1	Flange 2	Flange 1	Flange 2
1	13 445	11 445	----	----
2	11 824	12 946	----	----
3	12 330	12 611	13 533	13 580
4	13 806	11 775	14 077	12 008
5	12 439	12 961	12 871	15 042
6	12 705	12 848	10 625	12 550
7	11 841	13 092	----	----
8	11 706	12 974	13 756	14 790
9	12 210	12 202	11 925	13 029
10	15 477	14 444	----	----
Average	**12 778**	**12 730**	**12 798**	**13 500**
COV	**0.09**	**0.06**	**0.09**	**0.08**

7.2.3 Determination of the flange shear modulus

Similar to the flange MOE tests, determining the flange shear modulus involved two approaches, one where the whole I-joist was subjected to a torsion test and one where only the flanges were subjected to the same torsion test configuration.

Since no standardized procedures exist on what aspect ratio of span to depth is appropriate for testing I-joists, a study was conducted to determine the effect of the test span on the torsional stiffness (GJ). As seen in Figure 7-1, the results show that the test span had a significant effect on the resulting torsional stiffness (GJ). This effect would likely be due to warping deformations which increased as the test span decreased. The torsional rigidity was computed with Equation 5-2 for which to be valid, the specimen had to be free of warping effects. This condition was assumed to be reached as the torsional rigidity reached stable values as demonstrated in Figure 7-1. It can be observed from Figure 7-1 that, for the 0.4m I-joist, the torsional stiffness value stabilizes as the test configuration reaches a span-depth ratio around 11.5. A similar level of span-depth ratio could not be reached for the 0.6m I-joist as their length would not allow a larger span-depth ratio than 9.5. The resulting average torsional rigidity for the 0.4m I-joists was 11.1 x 10^8 Nmm^2. Because the torsional shear modulus of the web has not been determined, in this study but also in the literature, the shear modulus of the flanges cannot be derived based on composite material properties, as it was done for the flange longitudinal modulus of elasticity.

The shear modulus of the wood I-joist flanges was then determined using only half of the actual flange length. The shear modulus of the wood I-joist flanges yielded an average of 966 MPa with a COV of 0.06 for the 0.4m I-joists and 692 MPa with a COV of 0.19 for the 0.6m I-joists. The COV of the 0.4m I-joists displays an expected variability for materials made of wood, while the COV of the 0.6m I-joist presents a higher variability in the results. The torsion test configuration involving only the wood I-joist flange components was deemed more suitable to determine the shear modulus of the flange and use as input parameters for the analytical models. This method seems to be more practical

since the testing configuration allows to determine the shear modulus of the flanges regardless of the wood I-joist length, as opposed to the torsional rigidity test that involves the entire I-joist specimen.

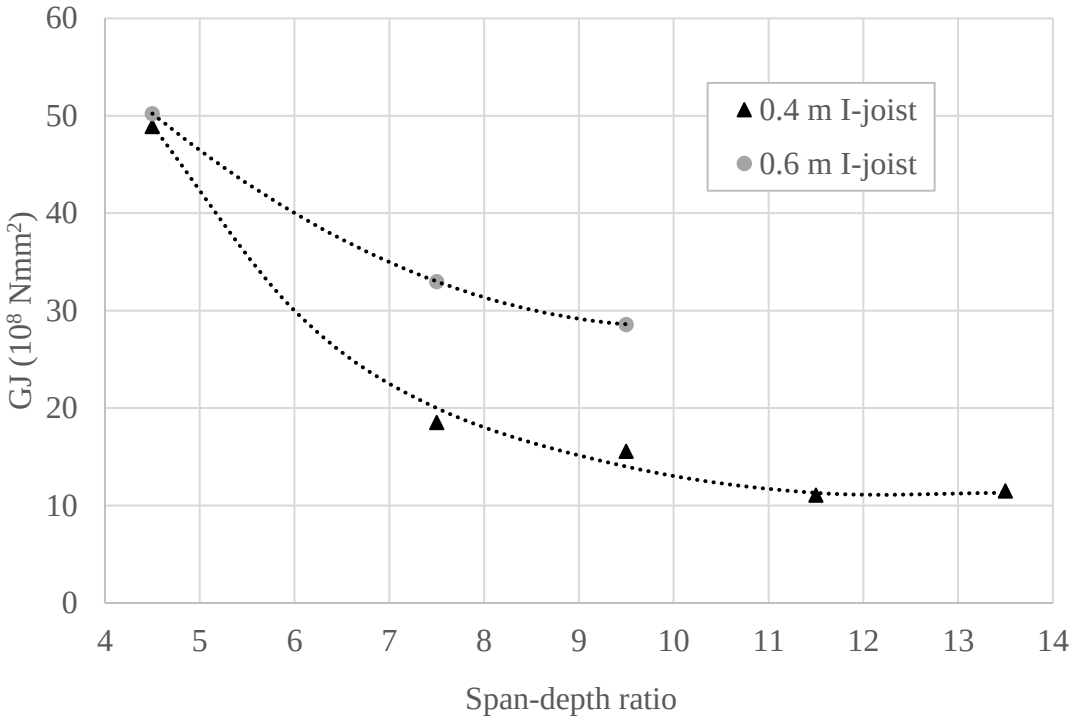

Figure 7-1 Length study on the torsional rigidity of entire wood I-joist specimens

7.3 Investigation of the lateral torsional buckling capacity

7.3.1 Experimental buckling displacements

The experimental buckling displacements captured the lateral torsional buckling deformation pattern of simply supported wood I-joist undergoing lateral torsional buckling under concentrated load applied at mid-span on the top flange. Figure 7-2 displays the buckling shape of 8 specimens from the sample group #16 which are representative of the observed force-displacement curves of the 42 wood I-joist specimens. The results reveal two lateral torsional buckling deformation behaviors: a linear curve where the I-joist

behaves as a perfectly straight beam undergoing lateral torsion buckling when reaching its critical buckling load, and another where the behavior is nonlinear due majorly to initial imperfections. It can be observed that the nonlinear buckling shapes will generally fail in the vicinity of the critical buckling load of those that exhibited a linear behavior.

Difference was documented in method of determining the critical buckling loads in the published literature. The critical buckling load point is obvious for Beam specimens #4 and #8 in Figure 7-2 as their buckling behavior is mostly linear after the bifurcation point. In the case of the other specimens (Beams specimen #1, #2, #3, #5, #6 and #7 of Figure 7-2) the force-displacement curve is nonlinear and still increases after the bifurcation point until collapse of the specimen occurred. Although the initial imperfections present in the I-joist triggered such nonlinear behavior, their effects would likely be different with other boundary conditions, lateral bracing along the span or loading below the shear center. In this study, the critical buckling load is assumed to be the last force measurement before the specimen collapsed, since an increase in the critical buckling load was observed for most specimens after the initial bifurcation point. Furthermore, the specimen that had a nonlinear behavior would fail at the material level when reaching values in the vicinity of the critical buckling load of specimens that remained straight throughout the loading history. Similar to the imperfection sensitivity analysis (Section 6.5.1), a clear bifurcation point was observed for specimens that had a smaller measured out-of-straightness of the compression flange (Beam #1 and #6) whereas the curve was smoother for specimens with a larger measured out-of-straightness (Beam #3 and #5).

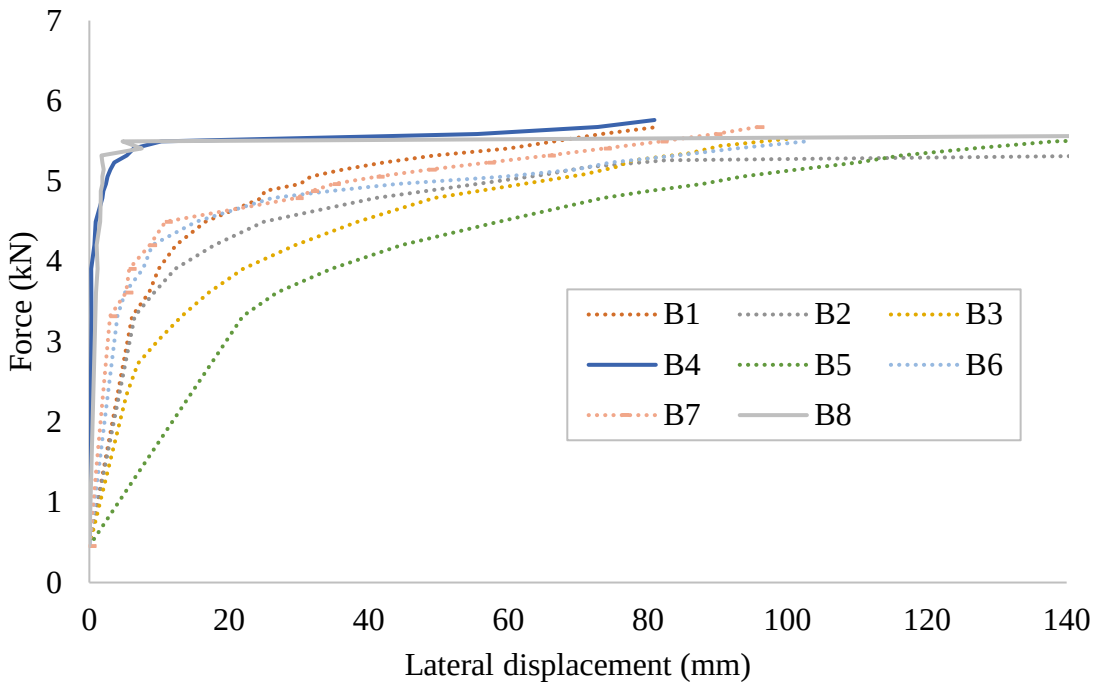

Figure 7-2 Experimental lateral buckling behavior of wood I-joist specimen from sample group #16

7.3.2 Models for predicting the critical buckling load of wood I-joist

Current provisions in the Canadian timber standard (CSA, 2014a) do not address the design of wood I-joist members. Similar to the NDS (2015), the Canadian timber design standard commentary state that "the material and geometric properties of only the compression flange should be taken into account when performing lateral stability calculations" (CWC, 2014). This statement is partially supported by the FE sensitivity analysis which showed that the most influential material parameter in lateral torsional buckling is found to be the longitudinal modulus of elasticity in the compression flange. On the other hand, the restoring action of the bottom flange is also significant and contribute to the overall lateral torsional buckling resistance.

The classical solution for lateral torsional buckling of I-sections (Equation 1-2) and the American timber design standard model (NDS, 2015) were used to predict the critical buckling load of the wood I-joist specimens. Using the finite element model outlined in

Chapter 6 and Equation 1-2, a moment gradient and load eccentricity factors were derived for a concentrated load applied at mid-span on the shear center (C_m), a concentrated load applied on the compression flange (C_e T-F) and a concentrated load applied on the tension flange (C_e B-F) as per Equation 7-1:

$$C_m, C_e = \frac{M_{cr}}{\frac{\pi}{L}\sqrt{EI_yGJ+\left(\frac{\pi E}{L}\right)^2 I_y C_w}} \qquad (7\text{-}1)$$

The moment gradient and eccentricity factors derived from Equation 7-1 along with the FE model are mutually exclusive. In other words, the moment gradient factor is not embedded in the eccentricity factor as this one was derived separately. The same factors were also derived using the AFPA approach (AFPA, 2003) and compared to the ones obtained from Equation 7-1 (Table 7-3). The AFPA factors were derived with the same values for the modulus of elasticity, the shear modulus and the geometric properties used in the FE model.

Although the AFPA procedure for the derivation of the eccentricity factors (C_e) is based on a rectangular section and neglects warping, it provides eccentricity factors that are similar to those derived with the FE model and Equation 7-1. A small divergence is observed as the span-to-depth ratio diminishes, suggesting that the warping effects are more pronounced as the model reaches smaller spans (Figure 7-3).

An analytical model is derived using the FE based load eccentricity and moment gradient factors and the classical solution for lateral torsional buckling of I-sections (Equation 1-2). This model also incorporates the transformed section properties defined in Section 1.1.6. The resulting analytical model that predict the critical buckling moment of the wood I-joist specimens is given by Equation 7-2:

$$M_{cr} = C_m C_e \frac{\pi}{L}\sqrt{EI_yGJ + \left(\frac{\pi E}{L}\right)^2 I_y C_w} \qquad (7\text{-}2)$$

The American design standard for wood construction model is outlined in Section 1.1.4 and is not modified by any factors for eccentricity nor moment gradient.

Table 7-3 FEA derived and Design Standards moment gradient and load eccentricity factors

Span to depth ratio	**Span (mm)**	**FEA C_m**	**FEA C_e T-F**	**AFPA C_e T-F**	**FEA C_e B-F**	**AFPA C_e B-F**
8.3	3 360	1.24	0.72	0.68	1.37	1.40
9.8	3 970	1.25	0.75	0.72	1.32	1.39
11.3	4 580	1.25	0.77	0.75	1.29	1.33
12.8	5 190	1.26	0.79	0.78	1.26	1.29
14.3	5 800	1.27	0.81	0.80	1.23	1.26

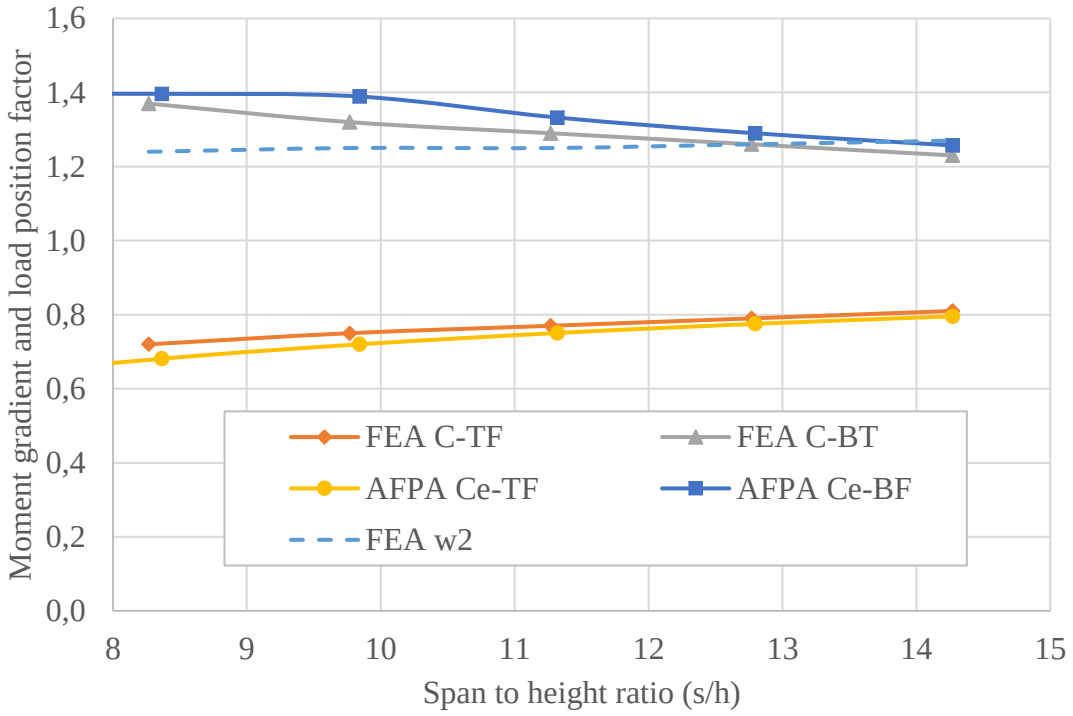

Figure 7-3 Comparison between FE and proposed moment gradient and load eccentricity factors

7.3.3 Experimental critical buckling loads and model predictions comparison

This section compares the capacity of the wood I-joist in lateral buckling observed during the experiment with buckling analysis models based on the assumption that the capacity in lateral torsional buckling of the specimens are defined as the force at which the characteristic failure mechanism developed in the compression flange. Figure 7-4 displays the experimental and predicted critical buckling loads for each model predictions. Tables 7-4, 7-5, 7-6, 7-7 and 7-8 present the experimental buckling displacement and the various model predictions for the sample group #5, #6, #7, #8 and #16. Complete results on the experimental buckling displacements and the numerical model predictions are presented in Appendix A.

The FE model buckling analysis yielded critical buckling loads that were in the range of 4-30% lower than the actual experimental capacity with a COV in the range of 3 to 7%. These results and the variability between the predictions and the experimental values showed that the FE model predicted the critical load with reasonable accuracy. The analytical solution yielded critical buckling loads that were in the range of 19 to 3% smaller than the experimental capacity with a COV between 3 and 7%. It was expected that the classical model would yield higher predictions than the FE model since it assumes a rigid section. The NDS model predictions provided critical buckling loads that were in the range of 44-70% smaller than the experimental capacity. These results expose a high conservatism from the NDS model that is also supported by previous researchers (Hindman, 2005b & Burow et al. 2006). This design standard model seems too simplistic as it idealizes the lateral buckling of the wood I-joist compression flange as the buckling of a simple column restrained in the plane of the web. The design standard clearly neglects the restoring action effect of the tension flange on the critical buckling load and the torsional resistance provided by the warping of the I-joist cross-section.

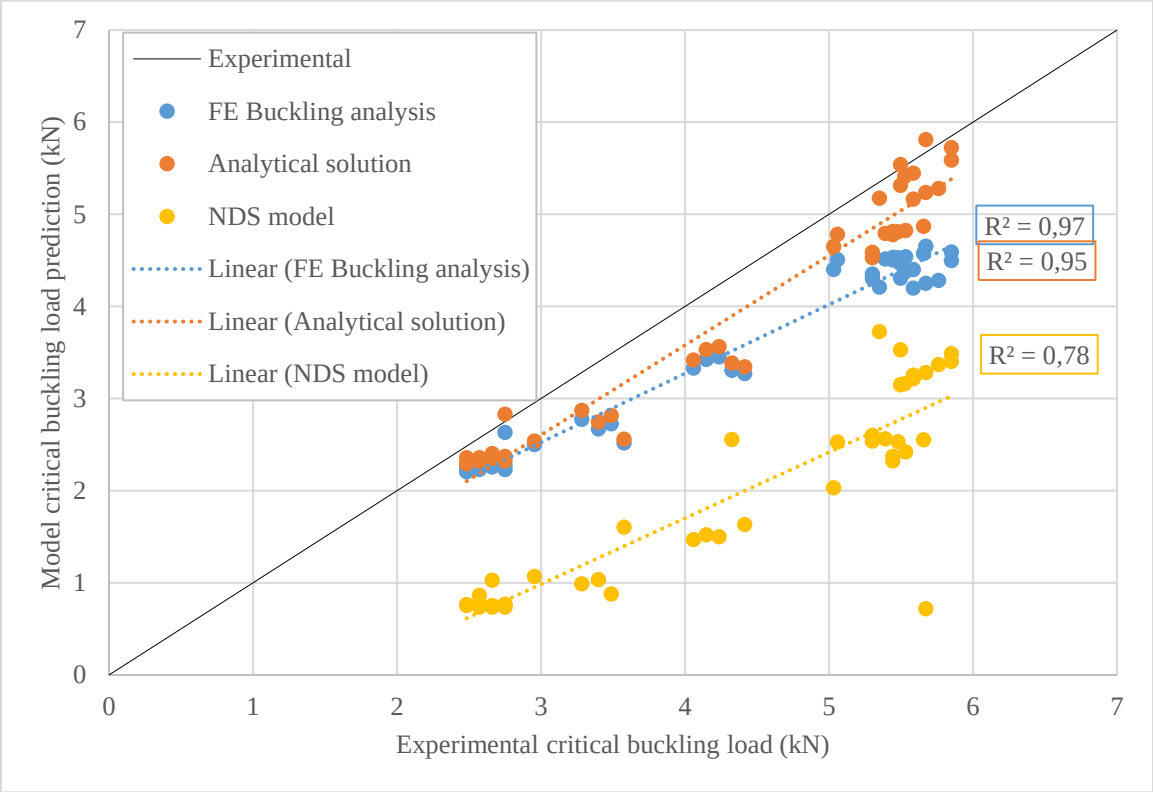

Figure 7-4 Experimental CBLs Vs. model predictions for the wood I-joist specimens

Table 7-4 Sample group #5 Experimental buckling capacity Vs. predictions

Specimen #	**CBL (kN)**				**Model / Experimental**		
	Experimental	**FEA**	**Analytical solution**	**NDS**	**FEA**	**Analytical solution**	**NDS**
1	5.03	4.40	4.65	2.03	0.87	0.92	0.40
2	5.53	4.54	4.82	2.42	0.82	0.87	0.44
3	5.39	4.52	4.79	2.56	0.84	0.89	0.48
4	5.30	4.30	4.53	2.54	0.81	0.85	0.48
5	5.44	4.50	4.78	2.32	0.83	0.88	0.43
6	5.06	4.51	4.78	2.53	0.89	0.95	0.50
7	5.48	4.53	4.81	2.53	0.83	0.88	0.46
8	5.66	4.58	4.87	2.55	0.81	0.86	0.45
9	5.30	4.35	4.59	2.60	0.82	0.87	0.49
10	5.44	4.53	4.81	2.37	0.83	0.88	0.44
Average	**5.36**	**4.48**	**4.74**	**2.45**	**0.84**	**0.89**	**0.46**
COV	**0.03**	**0.02**	**0.02**	**0.07**	**0.03**	**0.03**	**0.06**

Table 7-5 Sample group #6 Experimental buckling capacity Vs. predictions

Specimen #	CBL (kN)				Model / Experimental		
	Experimental	FEA	Analytical solution	NDS	FEA	Analytical solution	NDS
1	4.33	3.31	3.39	2.55	0.76	0.78	0.59
2	4.24	3.45	3.56	1.50	0.81	0.84	0.35
3	4.41	3.27	3.34	1.63	0.74	0.76	0.37
4	4.06	3.33	3.42	1.47	0.82	0.84	0.36
5	4.15	3.42	3.53	1.52	0.83	0.85	0.37
Average	**4.24**	**3.36**	**3.45**	**1.74**	**0.79**	**0.81**	**0.41**
COV	**0.03**	**0.02**	**0.02**	**0.24**	**0.04**	**0.05**	**0.22**

Table 7-6 Sample group #7 Experimental buckling capacity Vs. predictions

Specimen #	CBL (kN)				Model / Experimental		
	Experimental	FEA	Analytical solution	NDS	FEA	Analytical solution	NDS
1	3.58	2.52	2.56	1.61	0.70	0.72	0.45
2	3.49	2.73	2.82	0.88	0.78	0.81	0.25
3	3.40	2.67	2.75	1.03	0.79	0.81	0.30
4	3.28	2.77	2.87	0.99	0.84	0.87	0.30
5	2.95	2.50	2.54	1.07	0.85	0.86	0.36
Average	**3.34**	**2.64**	**2.71**	**1.12**	**0.79**	**0.81**	**0.33**
COV	**0.06**	**0.04**	**0.05**	**0.23**	**0.07**	**0.07**	**0.20**

Table 7-7 Sample group #8 Experimental buckling capacity Vs. predictions

Specimen #	CBL (kN)				Model / Experimental		
	Experimental	FEA	Analytical solution	NDS	FEA	Analytical solution	NDS
1	2.57	2.23	2.32	0.86	0.87	0.90	0.34
2	2.66	2.28	2.38	0.74	0.86	0.89	0.28
3	2.75	2.27	2.37	0.77	0.83	0.86	0.28
4*	2.48	2.26	2.36	0.76	0.91	0.95	0.31
5*	2.75	2.23	2.32	0.75	0.81	0.84	0.27
6	2.75	2.63	2.83	0.74	0.96	1.03	0.27
7	2.66	2.30	2.40	1.03	0.86	0.90	0.39
8	2.57	2.23	2.33	0.78	0.87	0.90	0.30
9	2.57	2.26	2.36	0.74	0.88	0.92	0.29
10	2.66	2.26	2.35	0.75	0.85	0.88	0.28
11	2.48	2.21	2.29	0.75	0.89	0.92	0.30
Average	**2.63**	**2.29**	**2.39**	**0.79**	**0.87**	**0.91**	**0.30**
COV	**0.04**	**0.05**	**0.06**	**0.11**	**0.04**	**0.05**	**0.11**

Table 7-8 Sample group #16 Experimental buckling capacity Vs. predictions

Specimen #	CBL (kN)				Model / Experimental		
	Experimental	FEA	Analytical solution	NDS	FEA	Analytical solution	NDS
1	5.67	4.65	5.81	0.72	0.82	1.02	0.13
2	5.35	4.21	5.18	3.73	0.79	0.97	0.70
3	5.53	4.37	5.41	3.16	0.79	0.98	0.57
4	5.76	4.28	5.28	3.37	0.74	0.92	0.58
5	5.58	4.20	5.17	3.25	0.75	0.92	0.58
6*	5.50	4.31	5.31	3.15	0.78	0.97	0.57
7*	5.67	4.25	5.24	3.28	0.75	0.92	0.58
8	5.58	4.40	5.45	3.22	0.79	0.98	0.58
9	5.85	4.50	5.59	3.40	0.77	0.96	0.58
10	5.50	4.46	5.54	3.53	0.81	1.01	0.64
11	5.85	4.59	5.72	3.49	0.79	0.98	0.60
Average	**5.62**	**4.38**	**5.43**	**3.12**	**0.78**	**0.97**	**0.56**
COV	**0.03**	**0.03**	**0.04**	**0.25**	**0.03**	**0.03**	**0.25**

* The wood I-joist test specimen suffered small inelastic deformations but did not collapse completely

7.3.4 Experimental buckling displacements and nonlinear FEA comparison

This section compares the experimental nonlinear buckling displacements with the predictions from the FEA geometric nonlinear buckling analysis. A representative sample of the comparison is presented in Figure 7-5. It can be observed that both the experimental angular displacement and the experimental lateral displacement have similar stiffness relationships (Figure 7-5 a) & b), respectively). The FE geometric nonlinear analyses are in good agreement with the experimental buckling displacements. The FE nonlinear model incorporated well the effect of initial imperfections of the wood I-joist specimens considering that for all models an average flange shear modulus and web modulus of elasticity inputs were used whereas a different flange MOE input was used for each specimen based on the lateral bending stiffness tests.

In some cases, the FE nonlinear analysis follows the experimental stiffness of the tested specimen only in the initial loading phase (Figure 7-6), before the bifurcation point. This difference in the upper stiffness branch of the geometric nonlinear model could be explained by an inaccurate input of the flange shear modulus in the model, considering that all the FE models used an average shear modulus of 966 MPa.

On the other hand, some specimens display a FE nonlinear response that follows the experimental specimen stiffness only after the bifurcation point (Figure 7-7). This discrepancy would likely be explained by the amount of initial imperfection in the I-joist prior to loading. As shown in the FE imperfection sensitivity (Section 6.5.1), the initial imperfections appear to affect the lower stiffness branch of the overall nonlinear behavior. The measured imperfections on the wood I-joist test specimens did not account for the initial twist at mid-span, nor the out-of-straightness of the bottom flange, which could have led to such nonlinear behavior displayed in these figures.

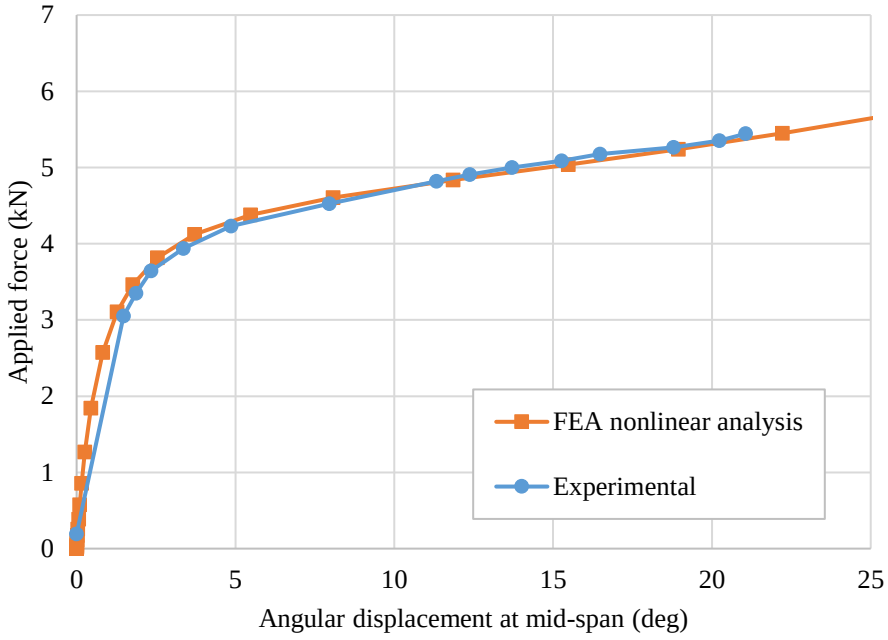

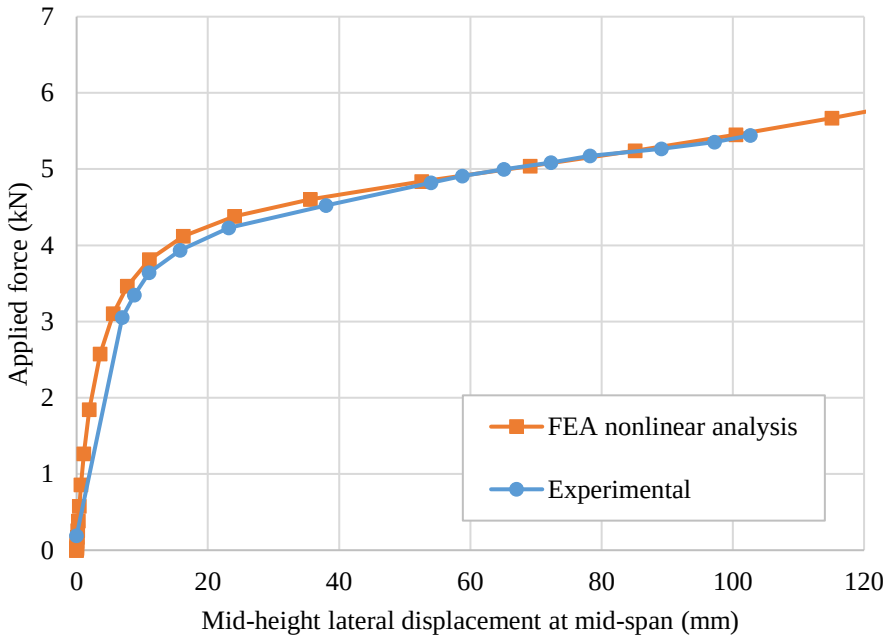

Figure 7-5 Buckling displacements of specimen 5-5, a) Angular displacement at mid-span and b) mid-height lateral displacement at mid-span

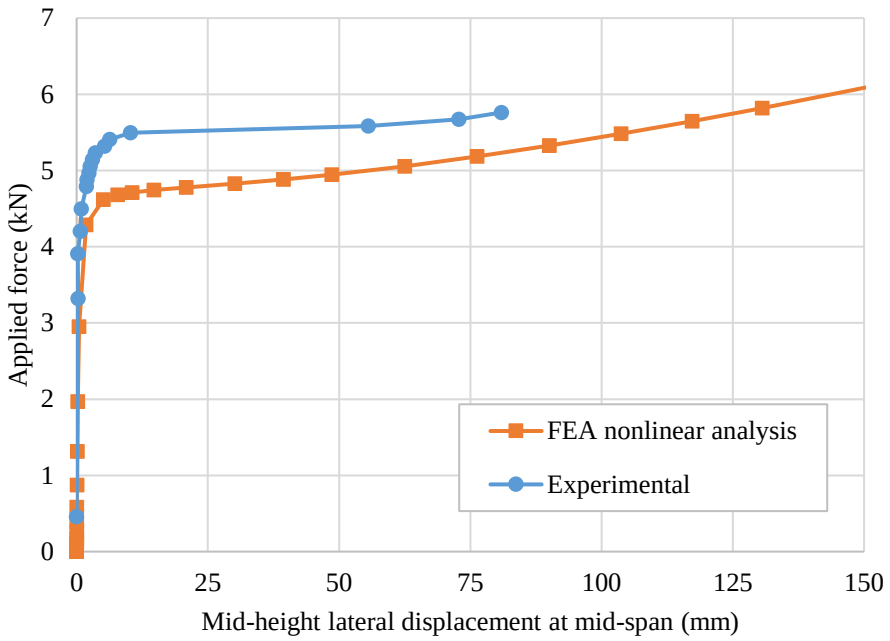

Figure 7-6 Buckling displacements of specimen 4-16

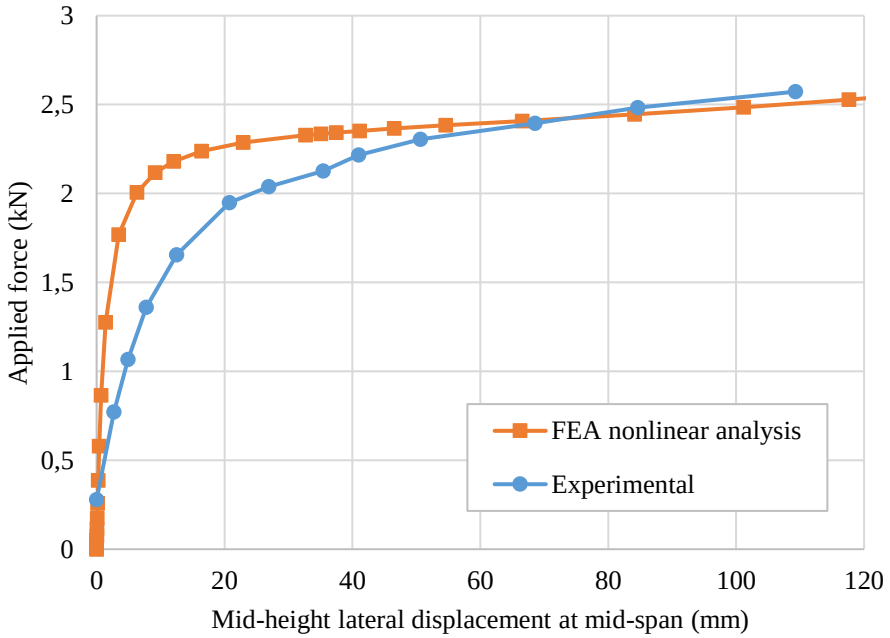

Figure 7-7 Buckling displacements of specimen 1-8

7.4 Ultimate flexural capacity

The spans of joists available allowed for the determination of the ultimate flexural resistance of the 0.4m I-joist only. The 0.6m I-joist ultimate flexural resistance could not be determined as the web failed before the flanges reached their bending capacity. An average ultimate flexural resistance of 30 kNm was determined for the 0.4m I-joist section with a COV of 19%. The average ultimate flexural capacity combined with the average experimental and FE buckling load predictions allow to draw the flexural capacity as function of the span for the 0.4m I-joist as shown in Figure 7-8. As it can be seen in Figure 7-4, the FE model that was validated using experimental result can be used to predict the lateral torsional buckling capacity of wood I-joists beyond the test spans that was practically feasible to conduct lateral torsional buckling tests. However, the capacity of shorter spans (in the range of 0-2 meters) would likely be governed by web buckling failure, which was the governing mode of failure for the 0.6m wood I-joist specimens, during the ultimate flexural resistance tests.

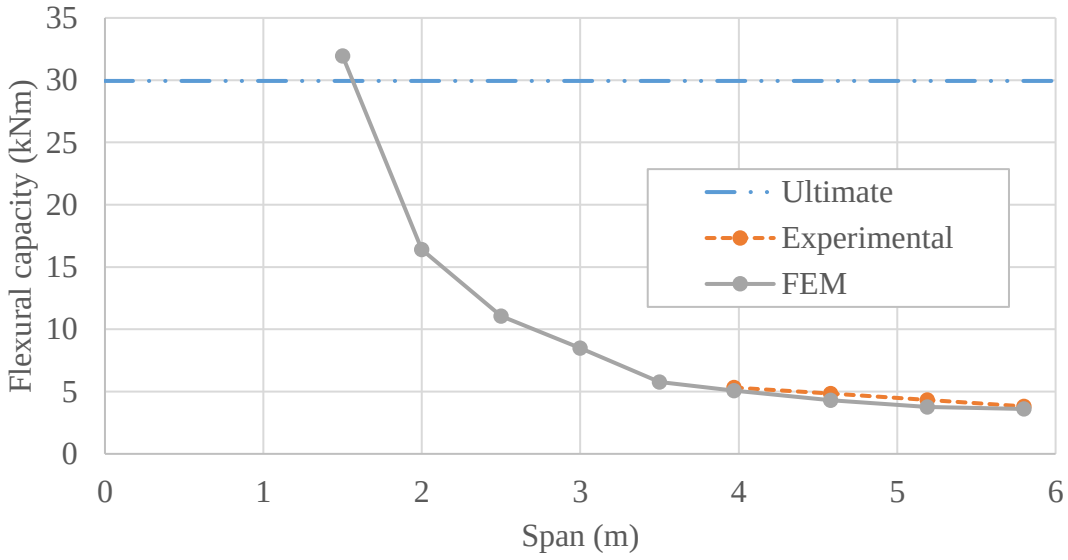

Figure 7-8 0.4m I-joist flexural capacity as a function of the span

CHAPTER 8

CONCLUSIONS AND RECOMMENDATIONS

8.1 Summary and conclusions

1) A sensitivity analysis was conducted on the mechanical properties of wood I-joist on the lateral torsional buckling capacity and it revealed that the most influential mechanical properties are the longitudinal modulus of elasticity and the torsional shear modulus of the compression flange. To a lesser extent, these same properties in the tension flange and the transverse modulus of elasticity of the web also impact the buckling response.

2) An experimental investigation was carried out on the mechanical properties that were targeted by the sensitivity analysis in order to use them as input in numerical models that would predict the critical buckling load of the wood I-joist.

3) The lateral flexural stiffness test of the entire I-joist and the torsion test on the flange alone were found to provide adequate input parameters for the analytical models.

4) An experimental investigation using a full-scale experiment subjecting wood I-joist to lateral torsional buckling was conducted on 42 I-joist test specimens with lengths ranging from 4.27m [14 ft] to 6.10m [20 ft]. The test showed that the imperfect wood I-joists reached critical buckling loads as those of perfect wood I-joists of similar geometries and mechanical properties, assuming that the critical buckling load of imperfect wood I-joists were attained at failure of the flange material.

5) The FE linear and nonlinear predictions were found to be in reasonable agreement with the experimental buckling loads and displacements. The FE buckling analysis predictions of the failure in lateral torsional buckling of wood I-joist were between 4% to 30% smaller than the experimental failure loads.

6) The FE geometric nonlinear analysis incorporated the initial imperfection into the models and was able to replicate the experimental nonlinear behavior that was observed during the test.

7) The Analytical solution for lateral torsional buckling of I-beam can provide a conservative estimate of the critical buckling load of simply supported wood I-joist providing that proper moment gradient and load eccentricity factors are used.

8) The NDS model provided predictions that were 44-70% smaller than the experimental lateral torsional buckling failure load, which shows significant conservatism in the approach, considering that the experimental capacity was reached at failure of the flange material

8.2 Recommendations for further research

1) Further experimental investigations on the lateral torsional buckling behavior of wood I-joists should be conducted given the small number of studies, especially on the effect of intermediary supports and initial imperfections in continuous span application, uniformly distributed load patterns, and partial lateral brace, which are commonly encountered in reality.

2) Further experimental study on the web instability behavior should be conducted. The web bearing capacity can be a source of instability and govern over the flexural capacity as observed in this study.

3) Experimental investigation on floor systems along with the development of a FE model would greatly contribute to the literature.

4) The developed FE model in this study has the potential to model other load and boundary configurations and realistically model wood I-joists that had common initial imperfection using the geometric nonlinear model. It can provide actual buckling displacements and extract strains at failure.

REFERENCES

American Forest & Paper Association (2003). Designing for lateral torsional buckling in wood members, Technical report, AWC. Washington, DC, USA.

Aguilar, J. M. V. (2012). Lateral torsional Buckling Instability Caused by Individuals Walking on Wood Composite I-Joists. Doctoral thesis, Virginia Polytechnic Institute and State University, Blacksburg, Virginia, USA.

American Institute of Steel Construction. (2010). Specification for Structural Steel Buildings. Chicago, Illinois, USA

American society for testing materials. (2002). ASTM D2719 Standard test methods for Structural Panels in Shear Through-the-Thickness. <https://www.astm.org/Standards/D2719.htm> (Dec, 14, 2015)

American society for testing materials. (2003). ASTM D4761 Standard Test Methods for Mechanical Properties of Lumber and Wood-Base Structural Material. <https://www.astm.org/Standards/D4761.htm> (Aug, 18, 2015)

American society for testing materials. (2007). ASTM D7033 Standard Practice for Establishing Design Capacities for Oriented Strand Board (OSB) Wood-Based Structural-Use Panels. <https://www.astm.org/Standards/D7033.htm> (Aug, 18, 2015)

American society for testing materials. (2011). ASTM D2718 Standard Test Methods for structural panels in planar shear (rolling shear). <https://www.astm.org/Standards/D2718.htm> (Jul, 27, 2015)

American society for testing materials. (2011). ASTM D3043 Standard Test Methods for Structural Panels in Flexure. <https://www.astm.org/Standards/D3043.htm> (Jul, 27, 2015)

American society for testing materials. (2012). ASTM D198 Standard Test Methods of Static Tests of Lumber in Structural Sizes. <https://www.astm.org/Standards/D198.htm> (Jan, 14, 2015)

American society for testing materials. (2013). ASTM D5055 Standard Specification for Establishing and Monitoring Structural Capacities of Prefabricated Wood I-Joists. <https://www.astm.org/Standards/D5055.htm> (Apr, 10, 2015)

Ascione, F. (2014). Influence of initial geometric imperfections in the lateral buckling problem of thin walled pultruded GFRP I-profiles. Composite Structures, 112(1), 85–

99.

Australia Standards. (2013). Australian Standard Timber Structures. 2010 3rd edition, Sydney, Australia.

Bamberg, C. R. (2009). Lateral movement of unbraced wood composite I-joists exposed to dynamic walking loads. Master thesis, Virginia Polytechnic Institute and State University, Blacksburg, Virginia.

Bell, K., & Eggen, T. even. (2001). Stability of timber beams and columns. In Innovative wooden structures and bridges : IABSE Conference Lahti 2001 (pp. 155–161).

Buchanan, A. H. (1986). Combined Bending and Axial Loading in Lumber. Journal of Structural Engineering, 112(12), 2592–2609. (ASCE)0733-9445(1986)112:12(2592)

Burow, J. R., Manbeck, H. B., & Janowiak, J. J. (2006). Lateral stability of composite wood I-joists under concentrated load bending. American Society of Agricultural and Biological Engineers, 49(6), 1867–1880.

Canadian Standard Association. (2014a) CSA-S16-09 Engineering design in wood. Mississauga, Ontario, Canada.

Canadian Standard Association. (2014b) CSA-086-09 Design of steel structures. Mississauga, Ontario, Canada.

Cheng et al., J. et al. (1988). Lateral buckling tests on coped steel beams. Journal of Structural Engineering, 114(1), 16–30.

Canadian Wood Council, 2014. Wood Design Manual. Nepan, Ontario, Canada

Dabbas, A. (2002). Stability of laterally unsupported wide-flange structure. Master thesis, Ottawa-Carleton Institute, Ottawa, Ontario, Canada.

Du, Y. (2016). Lateral Torsional Buckling of Wooden Beam-Deck Systems. Master thesis, Ottawa-Carleton Institute, Ottawa, Ontario, Canada.

Du, Y, Mohareb M., Doudak D (2016) Lateral Torsional Buckling of Twin-beam deck assemblies under wind uplift–sway versus non-sway models, World conference in timber engineering, Vienna Austria, Aug. 22-25

Forest Laboratory Products (2010). Wood Handbook, General technical report FPL-GTR-190. United States Departement of Agriculture, Madison, Wisconsin, USA.

Gjelsvik, A. (1981). The Theory of Thin Walled Bars. Journal of Applied Mechanics 49(2).

Grandmont, J. (2011). Analyse structural du système âme-semelles de poutrelles en bois.

Doctoral thesis, Université Laval, Montréal, Québec, Canadaé

Grandmont, J.-F., Desjardins, R., Cloutier, A., & Gendron, G. (2008). Measurement of OSB properties and their variability for modeling purposes. 10th World Conference on Timber Engineering 2008, 4, 2054–2060.

Gupta, R., & Siller, T. S. (2005a). A comparison of the shear strength of structural composite lumber using torsion and shear block tests. Forest Products Journal, 55(12), 29–33.

Gupta, R., & Siller, T. S. (2005b). Stress distribution in structural composite lumber. Wood Science, 55(9753), 51–56.

Hassan, R. and Mohareb, M. (2015), Distortional lateral torsional buckling for simply supported beams with web cleats, Journal of Civil of Civil Engineering, 42, 1091–1103.

Hindman, D. P. (2003). Torsional rigidity and lateral stability of structural composite lumber and I-joists members. Doctoral thesis, Pennsylvania State University, Pennsylvania, USA.

Hindman, D. P., Bamberg, C. R., & Nussbaum, M. A. (2010). Bracing of wood composite I-joists to resist lateral buckling from walking loads. ASCE, 8(3), 1397–1403.

Hindman, D. P., Manbeck, H. B., & Janowiak, J. J. (2003). Torsional Rigidity and Lateral Stability of SCL and I-joist Beams. American Society of Agricultural and Biological Engineers, 0300(03).

Hindman, D. P., Manbeck, H. B., & Janowiak, J. J. (2005a). Measurement and Prediction of Lateral Torsional Buckling Loads of Composite Wood Materials: Rectangular Sections. Forest Products Journal, 55(9), 42-47.

Hindman, D. P., Manbeck, H. B., & Janowiak, J. J. (2005b). Measurement and Prediction of Lateral Torsional Buckling Loads of Composite Wood Materials: I-Joist Sections. Forest Products Journal, 55(10), 43-48.

Hooley, R. F. and Madsen, B. (1964). Lateral Buckling of Glued Laminated Beams, Journal of Structural Engineering Division, ASCE, Vol. 90, No. ST3, pp. 201-303.

Kala, Z. (2013). Elastic lateral torsional buckling of simply supported hot-rolled steel I-beams with random imperfections. In Procedia Engineering (Vol. 57, pp. 504–514). Elsevier B.V.

Kirby, P. A. and Nethercot, D. A. (1979). Design for Structural stability. Constrado Monographs, Granada Publishing, Suffolk, UK.

Liang, K., Ruess, M., & Abdalla, M. (2014). The Koiter-Newton approach using von Karman kinematics for buckling analyses of imperfection sensitive structures. Computer Methods in Applied Mechanics and Engineering, 279, 440–468.

Link, R., Link, R., Gupta, R., Heck, L., & Miller, T. (2002). Experimental Evaluation of the Torsion Test for Determining Shear Strength of Structural Lumber. Journal of Testing and Evaluation, 30(4), 283.

Machado, S. P. (2010). Non-linear stability analysis of imperfect thin-walled composite beams. International Journal of Non-Linear Mechanics, 45(2), 100–110.

Mandal, P., & Calladine, C. R. (2002). Lateral torsional buckling of beams and the Southwell plot. International Journal of Mechanical Sciences, 44(12), 2557–2571.

Markiz, N. (2011). Experimental investigation of the lateral torsional buckling of Gerber Frames. Master thesis, Ottawa-Carleton Institute, Ottawa, Ontario, Canada

Memon, B.-A., & Su, X. (2004). Arc-length technique for nonlinear finite element analysis. Journal of Zhejiang University SCIENCE. 5(5), 618–628.

National Design Standard for wood construction, NDS (2015). American Wood Council, 2015 Edition, Leesburg, Virginia.

New Steel Construction. (2006). Lateral torsional buckling and slenderness. NCS (Vol. 14).<http://www.newsteelconstruction.com/wp/wp-content/uploads/TechPaper/NSCOct06_Tech.pdf> April 1st, 2016.

Pham, P. Van, & Mohareb, M. (2014b). Thin-Walled Structures A shear deformable theory for the analysis of steel beams reinforced with GFRP plates. Thin-Walled Structures, 85, 165–182.

Simulia. (2012). ABAQUS/CAE User's Manual (Version 6.12), Dassault Systemes.

Southwell, R. (1931). On the analysis of experimental observations in problems of elastic stabililty. Proceedings of the Royal Society of London, 268, 527.

Suryoatmono B. and Tjondro A. (2008). Lateral torsional Buckling of Orthotropic Rectangular Section Beams. Department of Civil Engineering, Parahyangan Catholic University, Bandung, Indonesia.

Thomas, W. H. (2001). Mechanical properties of structural-Grade oriented strand board. Holz Als Roh- Und Werkstoff, 59(6), 405–410.

Timoshenko, S., & Gere, J. (1961). Lateral Buckling of Beams. Journal of the Structural Division, 86, 175–196.

Vensko, M. J. (2008). Lateral torsional buckling of structures with monosymmetric cross-sections. Master thesis, Pennsylvania State University, Pennsylvania, USA.

Vlasov, V. Z. (1961). Thin-walled elastic beams, 2nd edition, Israel program for scientific transanctions, Jerusalem.

Westlund, J. (2013). Lateral Torsional Buckling of I-beams. Master thesis, Chalmers University of Technology, Goteborg, Sweden, Europe.

Xiao, Q. (2014). Lateral Torsional Buckling of Wood Beams. Master thesis, Ottawa-Carleton Institute, Ottawa, Ontario, Canada

Xiao, Q., Doudak, G., & Mohareb, M. (2014). Lateral Torsional Buckling of Wood Beams: FEA-Modeling and Sensitivity Analysis, WCTE, Quebec. 1–8.

Yang, Z. (2012). Torsional shear strength and size effect in structural composite. Master thesis, University of Massachusetts, Massachusetts, USA.

Zahn, J. J. (1973). Lateral stability of wood beam-and-deck systems. Journal of Structural Division, 51(July), 1391–1409.

Zhu, E. C., Guan, Z. W., Rodd, P. D., & Pope, D. J. (2006). Buckling of Oriented Strand Board Webbed Wood I-Joists. Journal of Structural Engineering, 131(10), 1629–1636.

APPENDIX A

LATERAL TORSIONAL BUCKLING TEST RESULTS

This appendix presents the experimental results and analytical predictions for the lateral torsional buckling test. The measurements include the force at mid-span, the displacements at mid-span, the angle of twist at mid-span and the lateral displacement of the top flange at quarter span. Predictions using the FE model, the analytical solution and the NDS model are shown for the force-lateral displacement and force-angular displacement curves.

Specimen 1 Sample group 5

Table A-1: Buckling displacements of specimen 1-5

Mid-span				Quarter-span
Force (kN)	**Vertical displacement (mm)**	**Lateral displacement at mid-height (mm)**	**Angle of twist (Deg)**	**Lateral displacement at top flange (mm)**
0.19	0.0	0.0	0.0	0
3.05	3.2	8.3	1.7	8.7
3.35	3.6	11.3	2.4	12.1
3.64	4.1	14.1	2.9	14.9
3.94	4.9	20.1	4.1	21.4
4.23	7.0	35.5	7.3	39.7
4.32	7.6	39.0	8.0	43.2
4.41	8.7	44.5	9.0	49.8
4.50	10.2	51.8	10.7	57.9
4.59	11.7	58.6	12.0	66.3
4.68	13.6	65.7	13.5	74.5
4.77	15.6	72.5	14.9	82.4
4.85	17.0	78.9	16.0	89.3
4.94	19.1	85.0	17.4	96.5
5.03	----	----	----	----
0.19	0.2	19.1	2.7	17.1

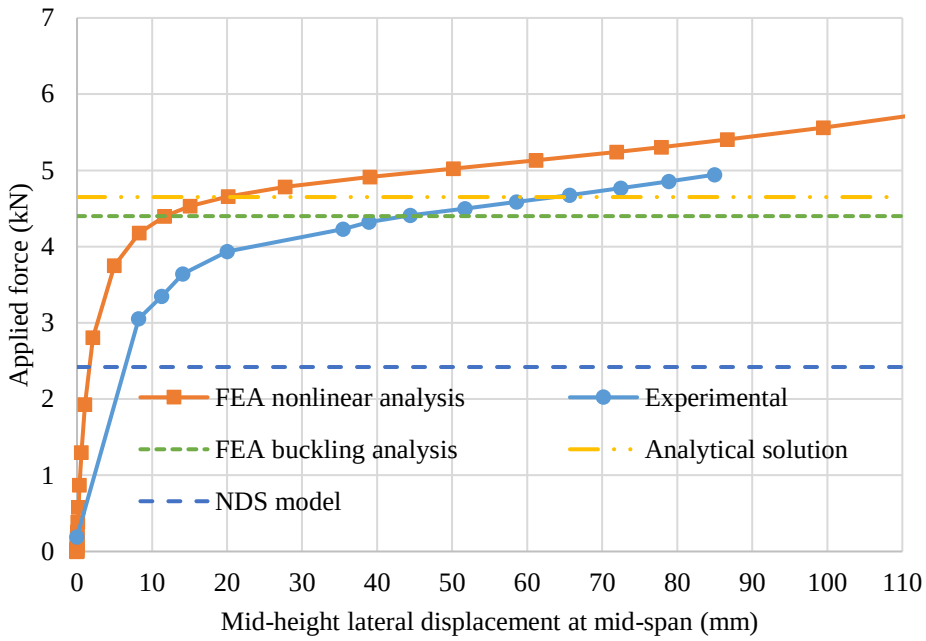

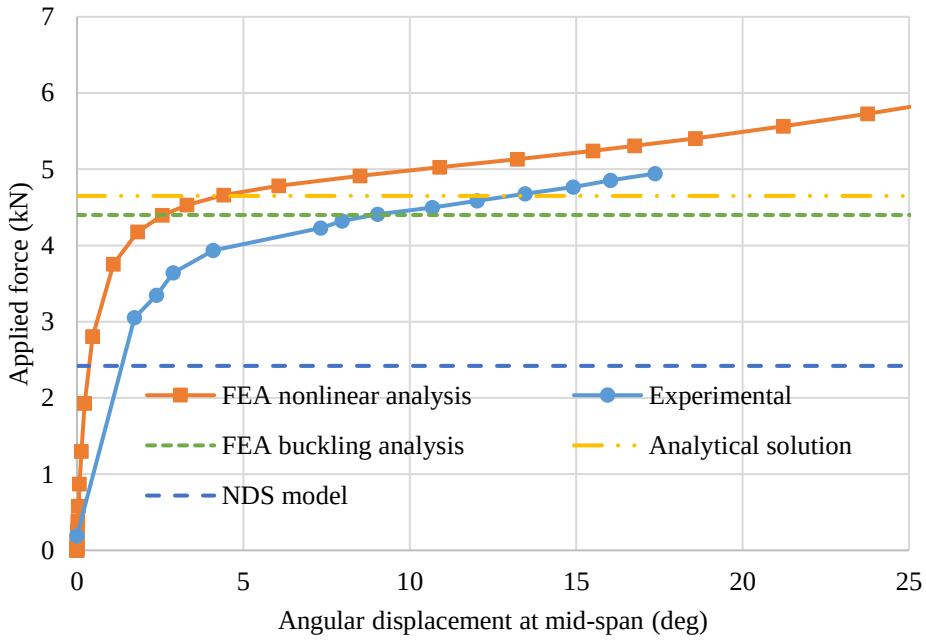

Figure A-1 Buckling displacements of specimen 1-5

Specimen 2 Sample group 5

Table A-2 Buckling displacements of specimen 2-5

Mid-span				Quarter-span
Force (kN)	**Vertical displacement (mm)**	**Lateral displacement at mid-height (mm)**	**Angle of twist (Deg)**	**Lateral displacement at top flange (mm)**
0.19	0.0	0.0	0.0	----
3.05	2.8	5.5	1.2	----
3.35	3.1	7.2	1.5	----
3.64	3.5	8.6	1.8	----
3.94	3.8	11.2	2.4	----
4.23	4.1	14.0	2.8	----
4.53	4.8	20.2	4.2	----
4.82	6.3	35.0	7.2	----
4.91	6.8	38.3	8.0	----
5.00	7.7	44.1	9.2	----
5.09	8.5	48.9	10.1	----
5.18	9.9	56.3	11.6	----
5.27	11.5	64.5	13.4	----
5.35	13.1	71.7	14.9	----
5.44	15.0	78.8	16.4	----
5.53	16.1	82.5	17.1	----
0.19	1.2	3.7	0.7	----

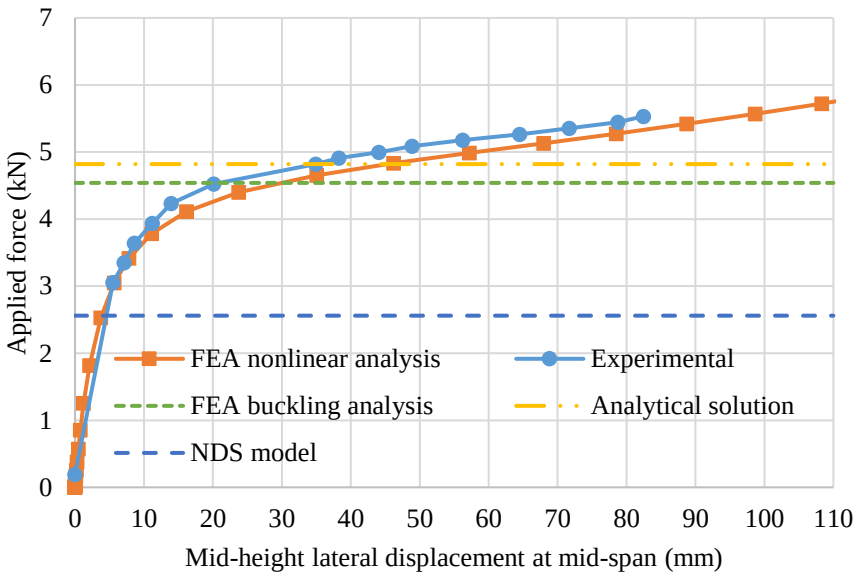

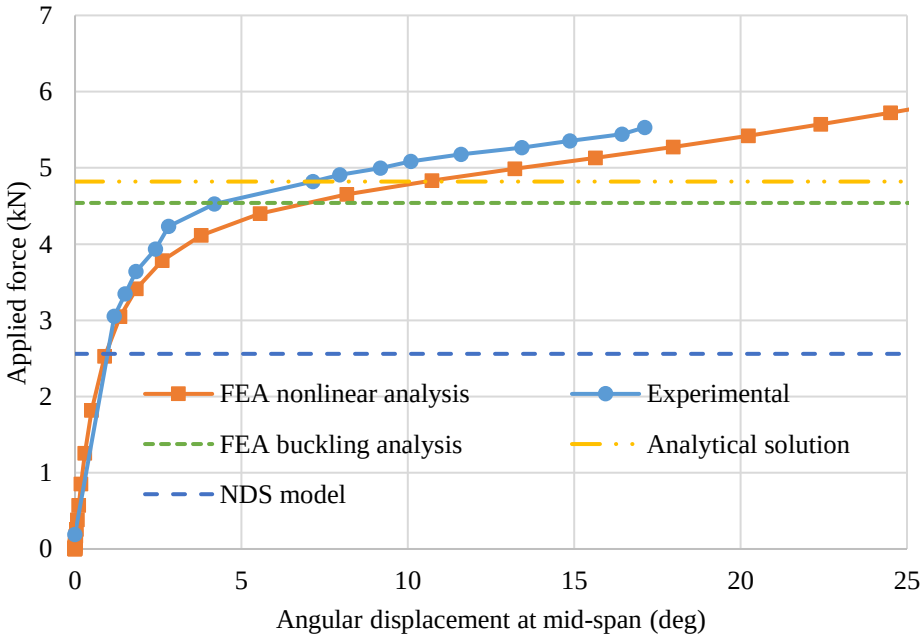

Figure A-2 Buckling displacements of specimen 2-5

Specimen 3 Sample group 5

Table A-3 Buckling displacements of specimen 3-5

Mid-span				Quarter span
Force (kN)	**Vertical displacement (mm)**	**Lateral displacement at mid-height (mm)**	**Angle of twist (Deg)**	**Lateral displacement at top flange (mm)**
0.19	0.0	0.0	0.0	0
3.05	2.6	0.4	0.0	0.8
3.35	2.8	0.2	0.0	0.5
3.64	3.1	0.4	0.0	0.7
3.94	3.3	0.2	0.0	0.6
4.23	3.5	1.1	0.2	0.5
4.32	3.7	0.8	0.2	1.8
4.41	3.8	3.3	0.9	5.1
4.50	4.0	4.5	1.1	6.6
4.59	4.0	2.7	0.7	3.7
4.68	4.0	0.3	0.0	1.3
4.77	4.2	4.3	1.0	5.9
4.85	5.1	22.0	4.3	28.6
4.94	6.2	34.9	6.9	43.7
5.03	7.7	46.5	9.1	57.4
5.12	9.9	60.4	12.0	73.8
5.21	12.0	70.7	13.9	84.9
5.30	14.6	82.8	16.3	98.5
5.39	18.6	100.2	19.3	----
0.19	1.0	25.4	3.3	18.3

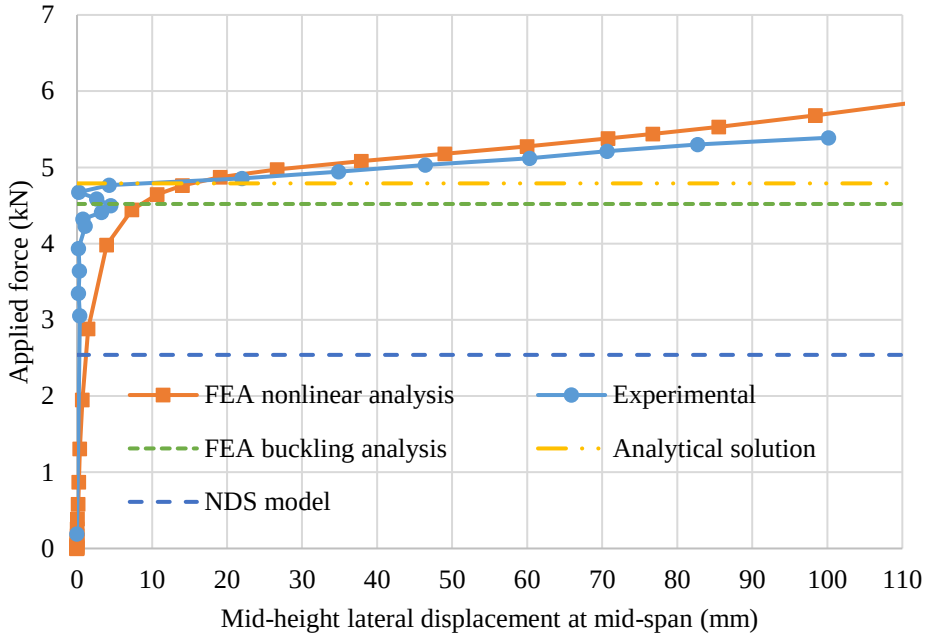

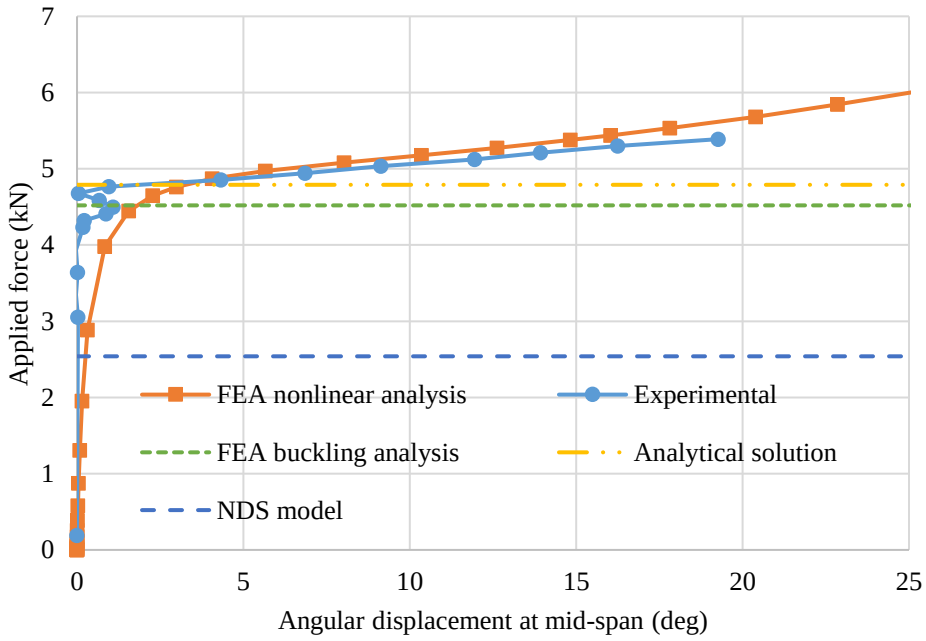

Figure A-3 Buckling displacements of specimen 3-5

Specimen 4 Sample group 5

Table A-4 Buckling displacements of specimen 4-5

Mid-span				Quarter span
Force (kN)	**Vertical displacement (mm)**	**Lateral displacement at mid-height (mm)**	**Angle of twist (Deg)**	**Lateral displacement at top flange (mm)**
0.19	0.0	0.0	0.0	----
3.05	3.4	3.4	0.7	----
3.35	3.8	5.5	1.2	----
3.64	4.1	9.4	1.9	----
3.94	4.4	11.3	2.2	----
4.23	5.0	20.2	4.0	----
4.32	6.0	31.9	6.4	----
4.41	7.2	43.2	8.7	----
4.50	9.3	57.2	11.5	----
4.59	11.2	68.8	13.8	----
4.68	12.0	72.3	14.5	----
4.77	14.3	82.9	16.5	----
4.85	16.0	91.8	18.1	----
4.94	18.8	104.4	20.3	----
5.03	20.3	110.1	21.4	----
5.12	21.8	117.3	22.5	----
5.21	23.5	124.1	23.5	----
5.30	24.8	132.3	24.9	----
0.19	1.3	1.8	0.0	----

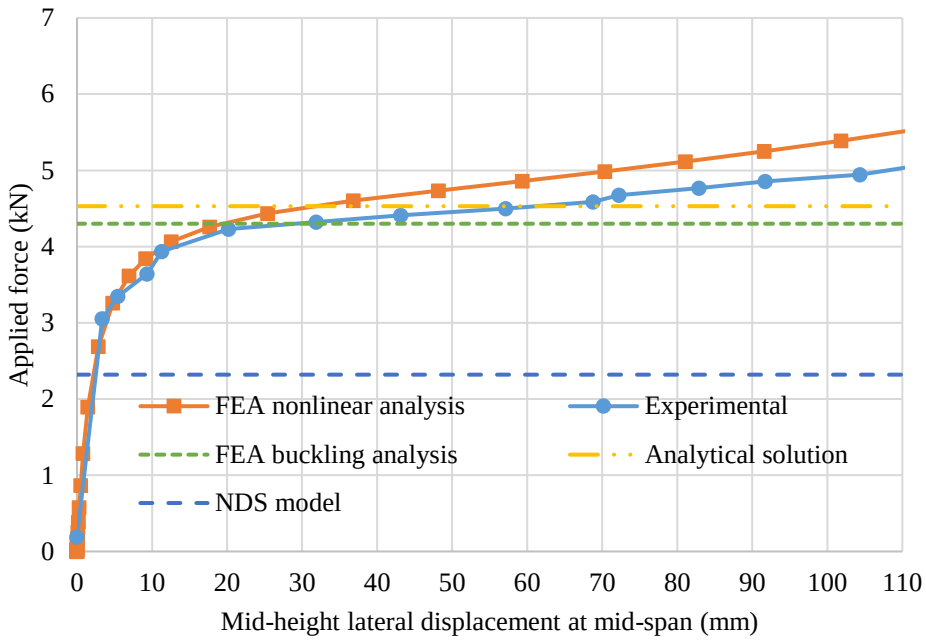

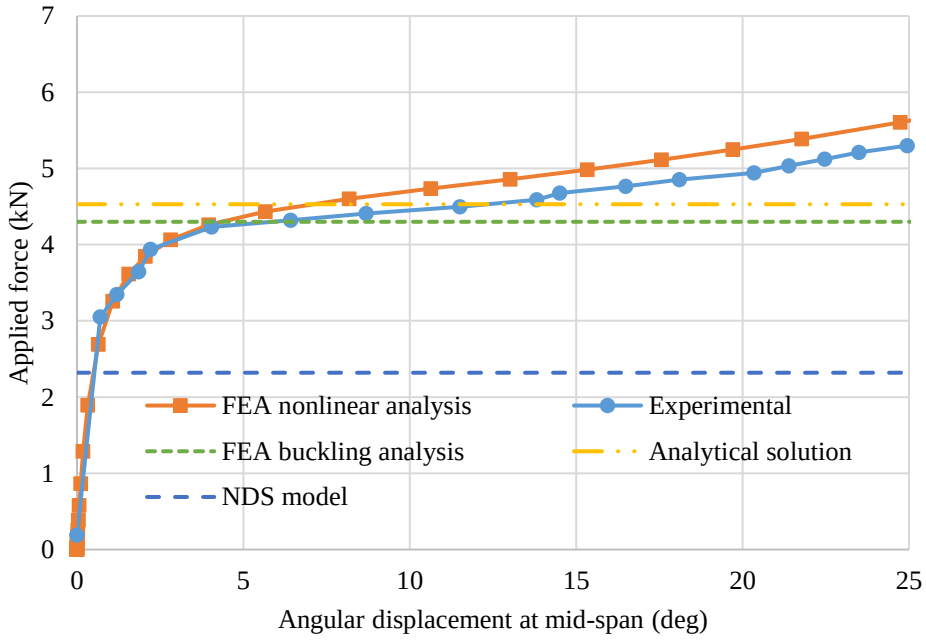

Figure A-4 Buckling displacements of specimen 4-5

Specimen 5 Sample group 5

Table A-5 Buckling displacements of specimen 5-5

Mid-span				Quarter span
Force (kN)	**Vertical displacement (mm)**	**Lateral displacement at mid-height (mm)**	**Angle of twist (Deg)**	**Lateral displacement at top flange (mm)**
0.19	0.0	0.0	0.0	0
3.05	3.3	7.0	1.5	7.6
3.35	3.7	8.8	1.9	10.0
3.64	4.0	11.1	2.3	12.1
3.94	4.6	15.8	3.4	17.5
4.23	5.4	23.2	4.9	25.6
4.53	7.3	38.0	8.0	42.6
4.82	10.1	54.0	11.3	60.9
4.91	11.1	58.8	12.4	66.4
5.00	12.7	65.2	13.7	74.4
5.09	14.6	72.3	15.3	82.4
5.18	16.2	78.3	16.5	89.5
5.27	19.5	89.2	18.8	101.9
5.35	21.7	97.2	20.2	110.5
5.44	23.2	102.7	21.1	116.3
0.19	2.7	32.9	5.3	21.4

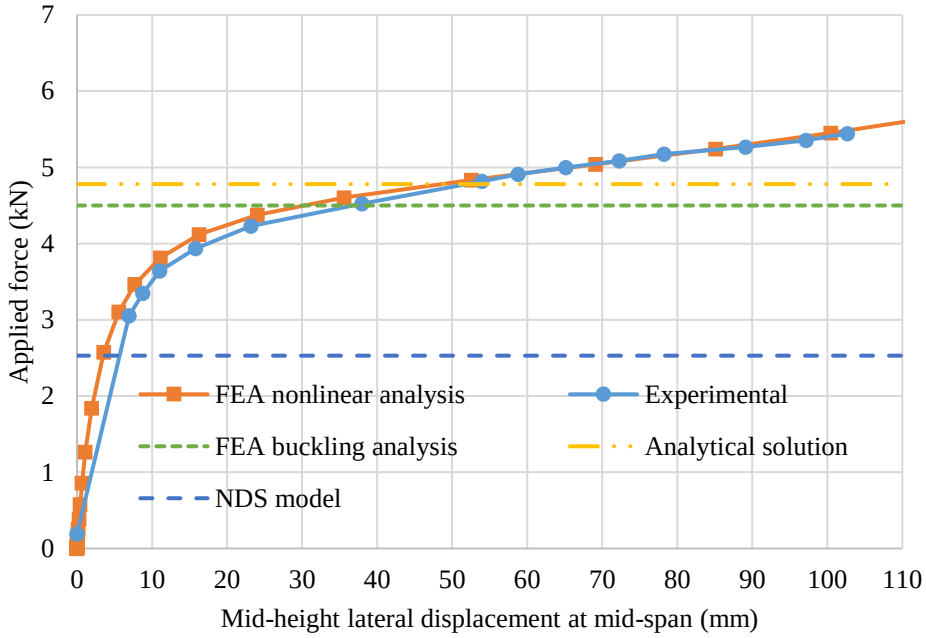

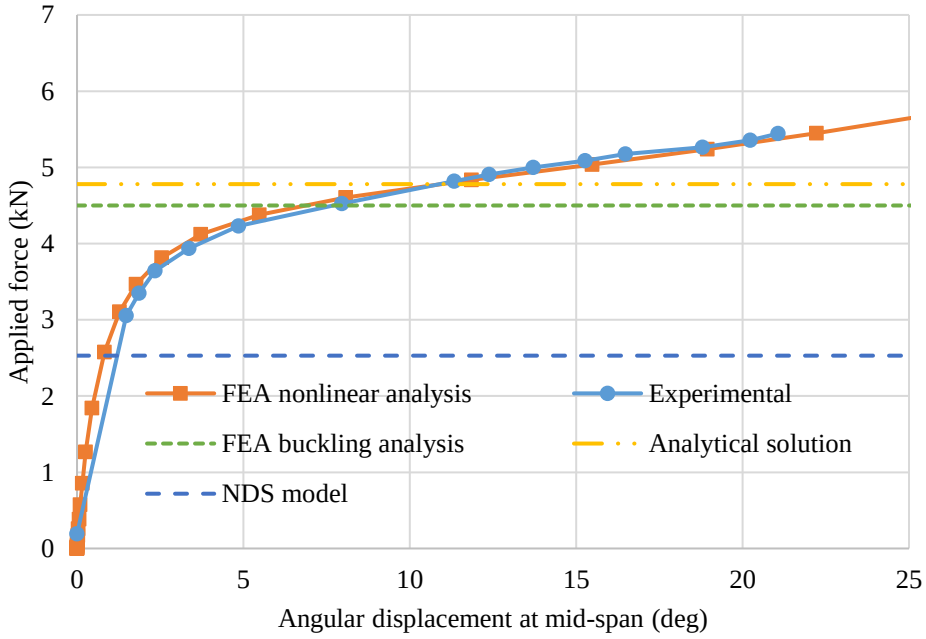

Figure A-5 Buckling displacements of specimen 5-5

Specimen 6 Sample group 5

Table A-6 Buckling displacements of specimen 6-5

Mid-span				Quarter-span
Force (kN)	**Vertical displacement (mm)**	**Lateral displacement at mid-height (mm)**	**Angle of twist (Deg)**	**Lateral displacement at top flange (mm)**
0.19	0.0	0.0	0.0	0
3.05	2.9	4.0	0.9	6.0
3.35	3.2	6.3	1.4	9.1
3.64	3.5	7.3	1.5	10.3
3.94	3.9	10.0	2.1	13.7
4.23	4.3	13.7	2.8	17.6
4.53	5.6	27.9	5.7	34.3
4.61	6.1	31.6	6.5	38.5
4.70	6.6	37.1	7.6	44.9
4.79	8.0	46.1	9.5	55.6
4.88	9.1	53.1	10.9	63.6
4.97	10.7	62.2	12.7	73.8
5.06	13.2	74.5	15.1	88.0
0.19	1.4	6.0	0.8	3.9

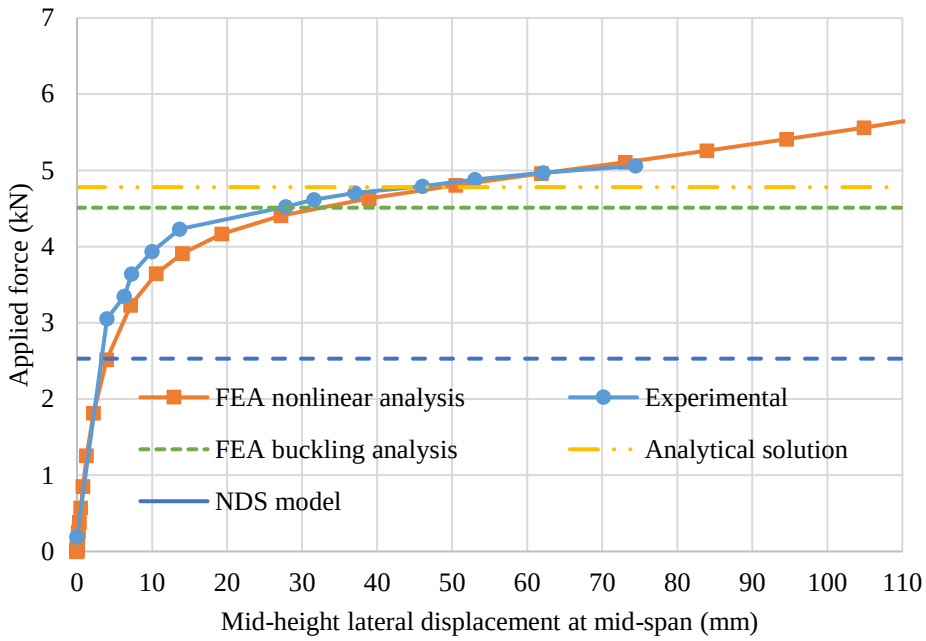

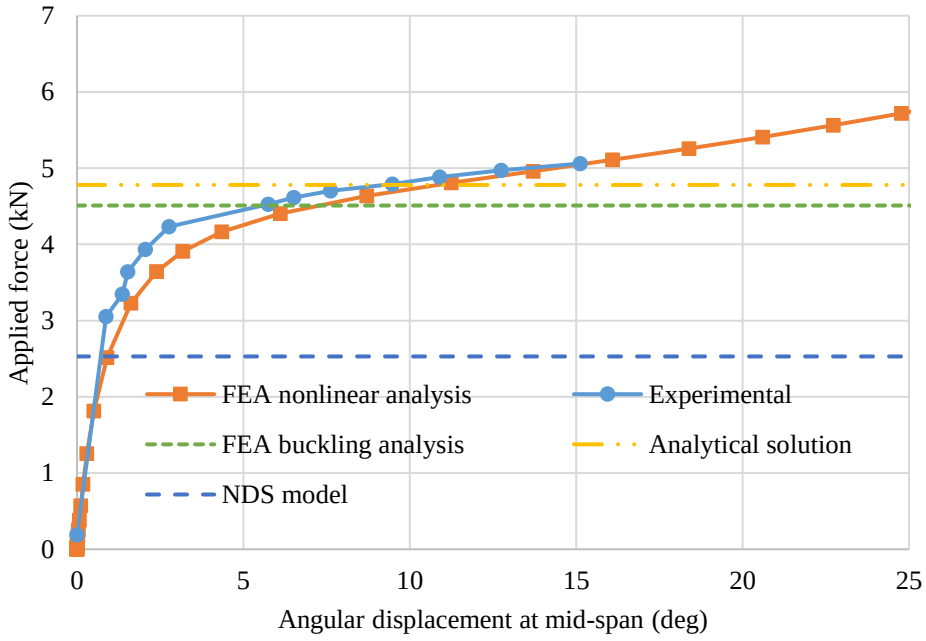

Figure A-6 Buckling displacements of specimen 6-5

Specimen 7 Sample group 5

Table A-7 Force and displacements of specimen 7-5

Mid-span				Quarter-span
Force (kN)	**Vertical displacement (mm)**	**Lateral displacement at mid-height (mm)**	**Angle of twist (Deg)**	**Lateral displacement at top flange (mm)**
0.19	0.0	0.0	0.0	0
3.05	2.9	3.5	0.7	5.2
3.35	3.2	5.0	1.0	7.2
3.64	3.4	5.7	1.1	8.6
3.94	3.7	8.7	1.6	11.0
4.23	3.9	15.4	2.9	19.1
4.32	3.9	16.5	3.2	20.5
4.41	4.1	19.2	3.7	23.6
4.50	4.2	20.6	4.0	24.9
4.59	4.4	23.8	4.6	28.7
4.68	4.6	27.2	5.3	32.4
4.77	5.0	33.2	6.6	39.3
4.85	5.7	41.3	8.3	48.5
4.94	6.6	49.2	9.8	57.4
5.03	8.0	59.1	11.9	69
5.12	9.7	69.5	14.0	81.3
5.21	11.0	76.7	15.4	88.9
5.30	12.1	85.4	16.9	98.7
5.39	13.3	93.4	18.5	107.1
5.48	16.4	102.8	20.4	118.9
0.19	1.7	25.8	3.3	17.7

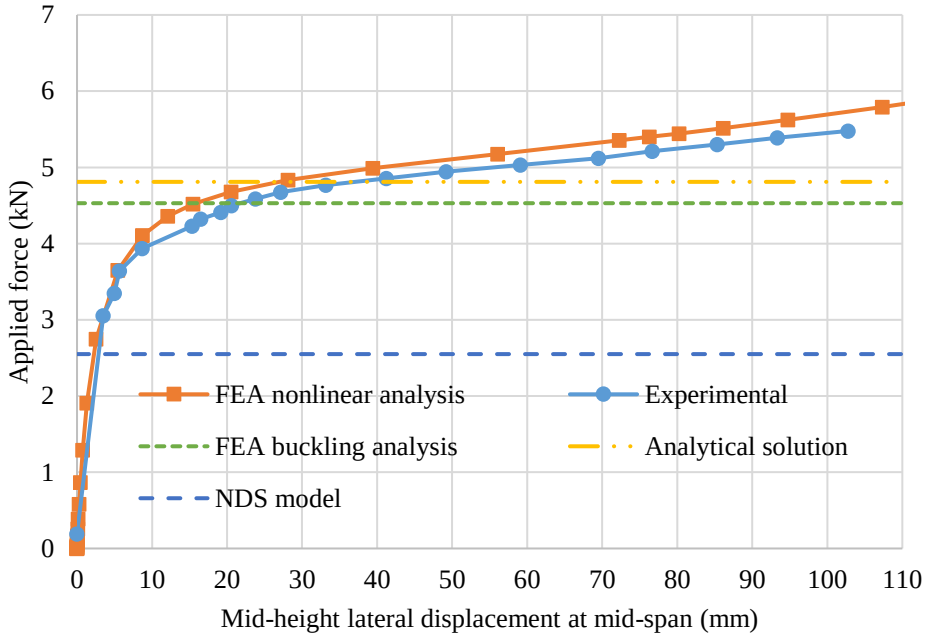

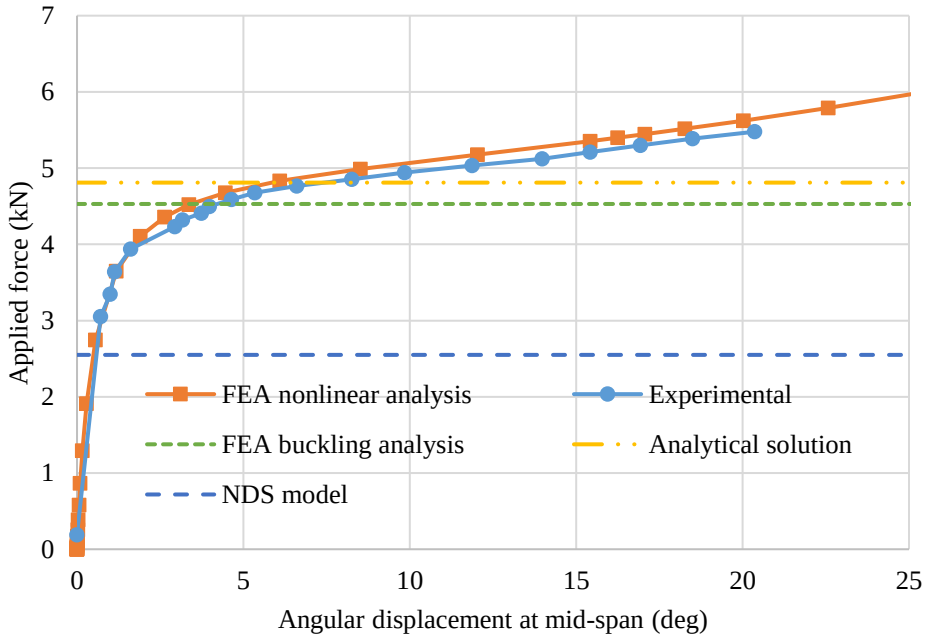

Figure A-7 Buckling displacements of specimen 7-5

Specimen 8 Sample group 5

Table A-8 Buckling displacements of specimen 8-5

Mid-span				Quarter-span
Force (kN)	**Vertical displacement (mm)**	**Lateral displacement at mid-height (mm)**	**Angle of twist (Deg)**	**Lateral displacement at top flange (mm)**
0.19	0.0	0.0	0.0	0.0
3.05	2.8	3.1	0.6	4.6
3.35	3.1	3.9	0.8	5.6
3.64	3.3	4.7	0.8	6.5
3.94	3.5	7.2	1.3	9.1
4.23	3.8	9.7	1.9	12.4
4.32	3.9	10.4	2.0	13.1
4.41	4.0	11.4	2.2	14.2
4.50	4.0	12.3	2.4	15.1
4.59	4.1	13.6	2.6	16.7
4.68	4.2	15.2	2.9	18.5
4.77	4.3	16.4	3.1	19.6
4.85	4.4	19.1	3.7	22.5
4.94	4.5	21.7	4.3	25.5
5.03	4.9	27.5	5.5	32.5
5.12	5.3	32.2	6.5	37.9
5.21	6.2	40.0	8.3	47.2
5.30	7.1	46.7	9.7	55.3
5.39	8.2	54.7	11.5	64.8
5.48	9.6	62.5	13.2	74.6
5.57	11.9	72.9	15.5	86.7
5.66	13.4	79.6	16.9	94.5
0.19	0.5	1.6	0.5	2.4

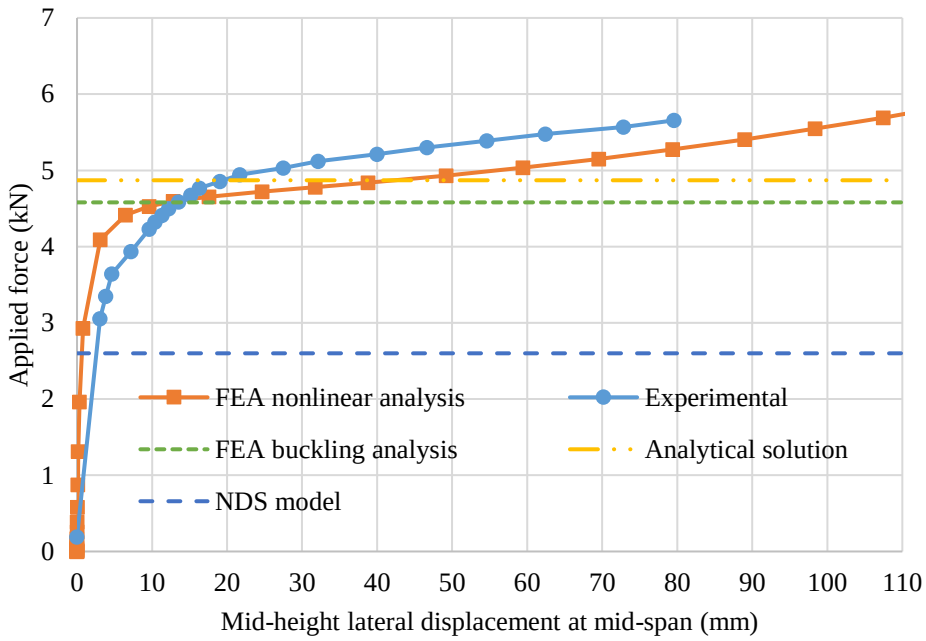

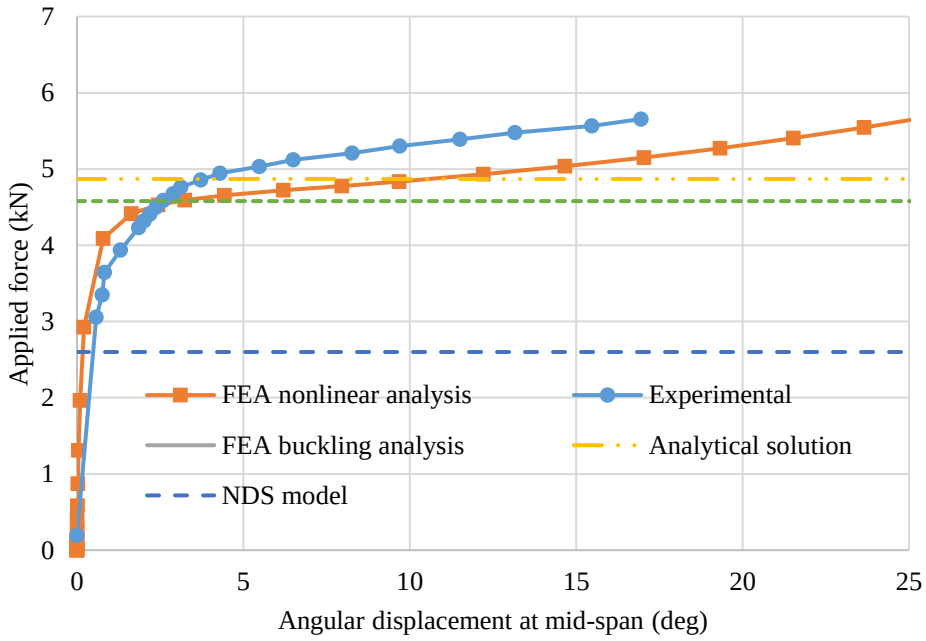

Figure A-8 Buckling displacements of specimen 8-5

Specimen 9 Sample group 5

Table A-9 Buckling displacements of specimen 9-5

Mid-span				Quarter-span
Force (kN)	**Vertical displacement (mm)**	**Lateral displacement at mid-height (mm)**	**Angle of twist (Deg)**	**Lateral displacement at top flange (mm)**
0.19	0.0	0.0	0.0	0.0
3.05	3.0	5.8	1.2	6.7
3.35	3.3	7.2	1.4	8.3
3.64	3.7	8.7	1.7	9.9
3.94	4.1	11.7	2.3	13.2
4.23	4.7	18.2	3.7	21.1
4.32	5.0	21.0	4.3	24.4
4.41	5.5	25.7	5.4	30.4
4.50	5.9	28.8	5.9	33.9
4.59	6.3	32.7	6.7	38.6
4.68	6.8	37.9	7.8	44.6
4.77	7.3	40.6	8.3	47.5
4.85	8.3	47.2	9.6	55.2
4.94	9.5	55.1	11.2	64.4
5.03	10.8	62.4	12.6	72.3
5.12	12.6	70.9	14.3	81.7
5.21	14.2	79.6	16.0	91.0
5.30	17.9	93.1	18.5	106.6
0.19	0.3	26.9	3.0	19.10

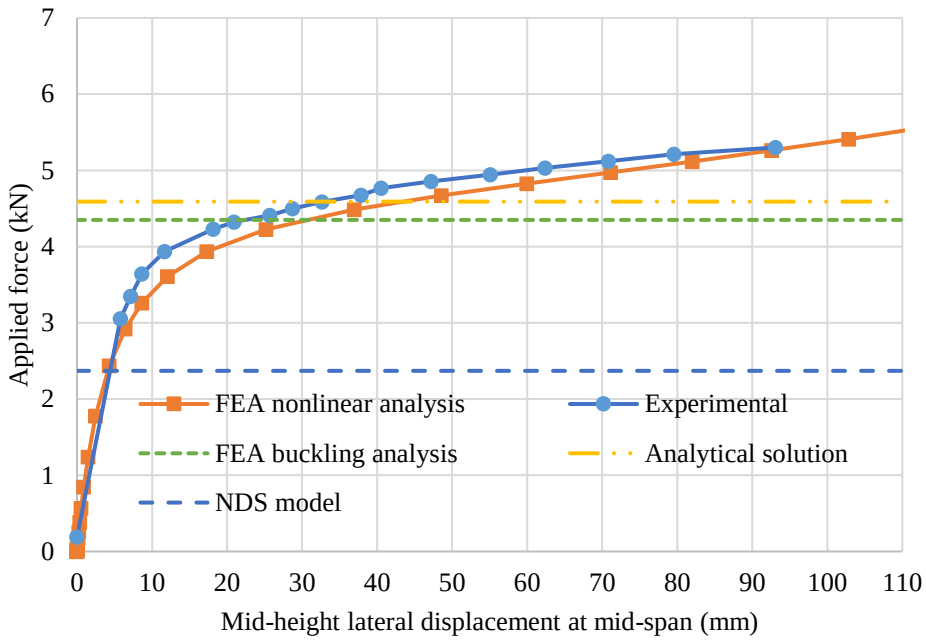

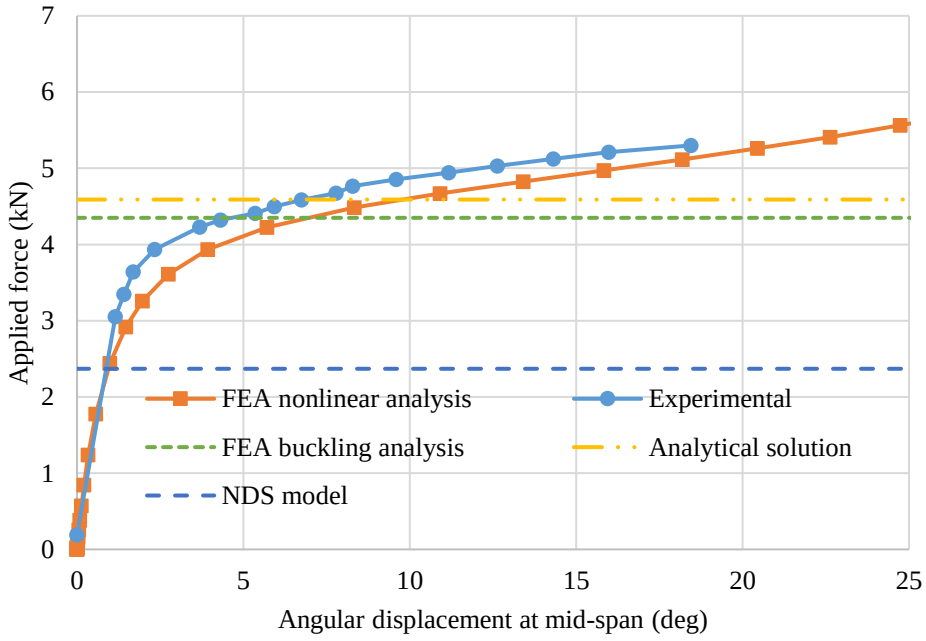

Figure A-9 Buckling displacements of specimen 9-5

Specimen 10 Sample group 5

Table A-10 Buckling displacements of specimen 10-5

Mid-span				Quarter-span
Force (kN)	**Vertical displacement (mm)**	**Lateral displacement at mid-height (mm)**	**Angle of twist (Deg)**	**Lateral displacement at top flange (mm)**
0.19	0.0	0.0	0.0	0.0
3.05	3.0	7.4	1.0	7.1
3.35	3.3	8.8	1.3	8.9
3.64	3.6	10.5	1.6	10.5
3.94	4.0	13.7	2.2	14.1
4.23	4.4	17.1	2.8	17.7
4.53	5.5	29.0	5.1	31.2
4.82	7.1	43.0	7.9	46.9
4.91	7.6	45.1	8.5	49.7
5.00	8.8	52.2	10.0	58.2
5.09	10.3	58.9	11.3	66.5
5.18	11.4	64.2	12.4	72.7
5.27	13.6	72.9	14.3	83.2
5.35	16.1	81.4	15.8	93.8
5.44	17.6	86.9	17.0	100.0
0.19	0.6	2.2	0.5	2.30

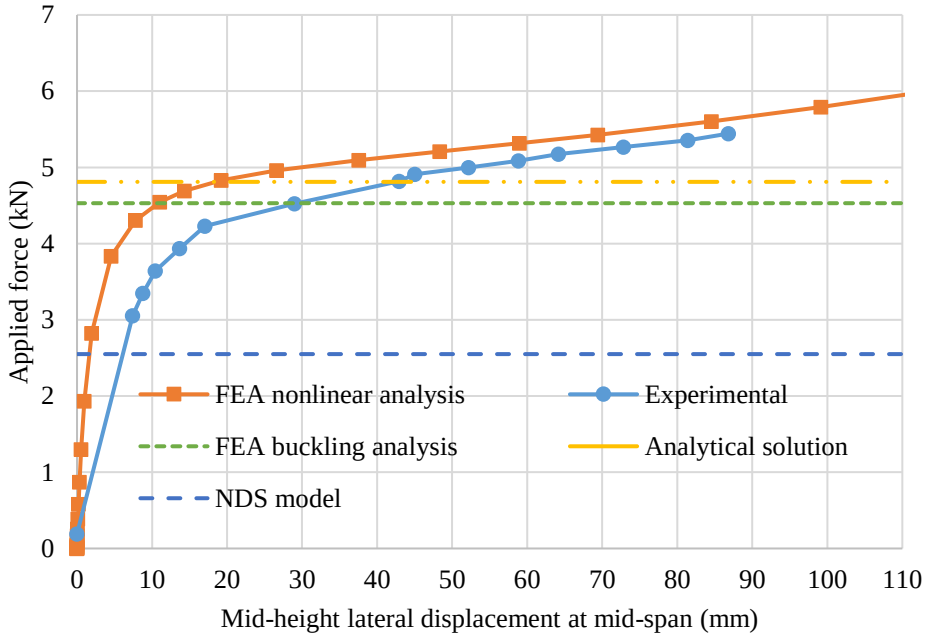

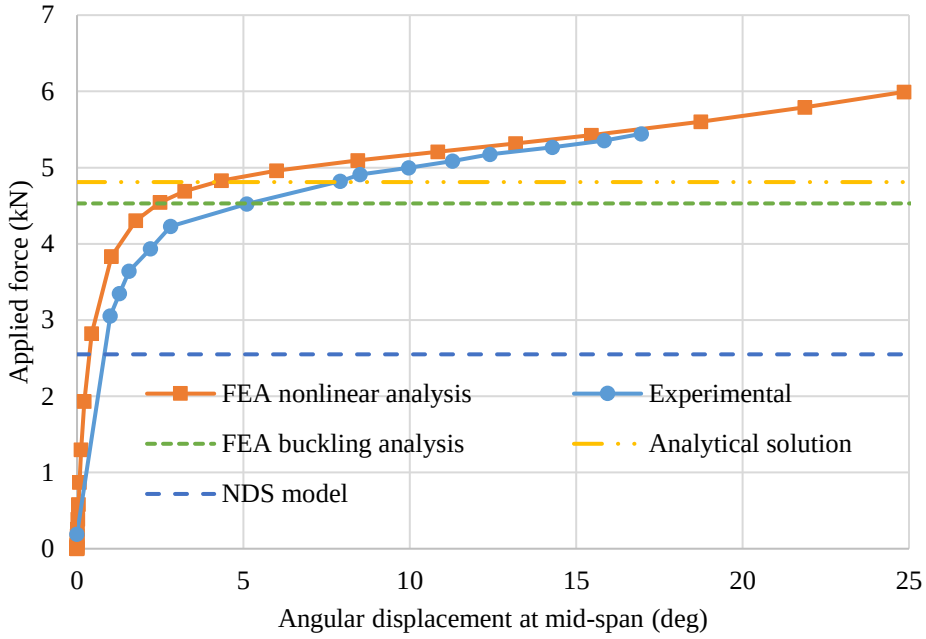

Figure A-10 Buckling displacements of specimen 10-5

Specimen 1 Sample group 6

Table A-11 Buckling displacements of specimen 1-6

Mid-span				Quarter-span
Force (kN)	**Vertical displacement (mm)**	**Lateral displacement at mid-height (mm)**	**Angle of twist (Deg)**	**Lateral displacement at top flange (mm)**
0.22	0.0	0.0	0.0	0.0
1.91	2.4	0.5	0.0	0.9
1.94	2.5	0.6	0.0	1.0
2.23	2.8	0.7	0.0	0.4
2.53	3.2	1.2	0.0	0.6
2.82	3.7	0.7	0.0	0.7
3.11	4.0	0.9	0.0	0.4
3.41	4.0	0.4	0.1	0.5
3.70	4.1	1.5	0.5	2.3
3.79	4.1	0.9	0.0	0.1
3.88	4.1	2.8	0.7	2.3
3.97	4.2	0.6	0.1	1.1
4.06	4.3	6.0	1.2	5.7
4.15	4.4	4.2	0.8	3.7
4.24	4.5	1.8	0.3	2.3
4.33	12.4	192.9	28.9	160.1
0.22	5.5	25.1	2.1	18.7

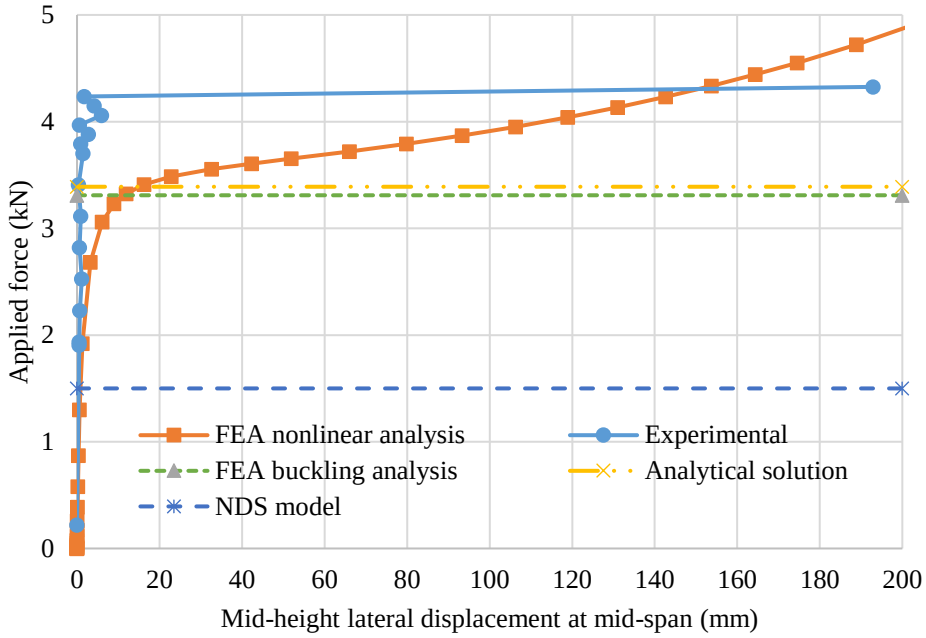

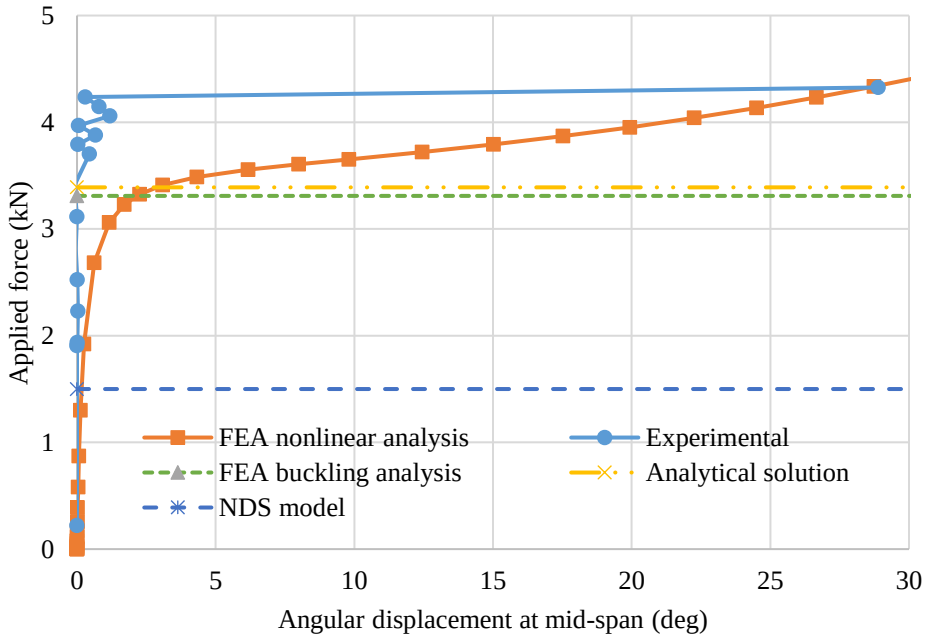

Figure A-11 Buckling displacement of specimen 1-6

Specimen 2 Sample group 6

Table A-12 Buckling displacements of specimen 2-6

Mid-span				Quarter-span
Force (kN)	**Vertical displacement (mm)**	**Lateral displacement at mid-height (mm)**	**Angle of twist (Deg)**	**Lateral displacement at top flange (mm)**
0.22	0.0	0.0	0.0	0.0
1.94	2.3	3.9	0.5	3.3
2.23	2.7	5.0	0.7	4.5
2.53	3.1	6.6	0.9	5.7
2.82	3.5	8.5	1.2	8.1
3.11	4.0	11.6	1.6	11.2
3.41	4.8	19.0	2.9	19.3
3.70	6.8	45.2	7.7	47.6
3.79	9.6	60.7	10.6	65.0
3.88	12.0	71.4	12.4	77.7
3.97	14.9	83.2	14.7	90.2
4.06	17.0	90.8	15.9	100.0
4.15	20.3	102.6	18.2	114.1
4.24	22.7	110.0	19.4	122.7
0.22	0.5	2.9	0.5	3.3

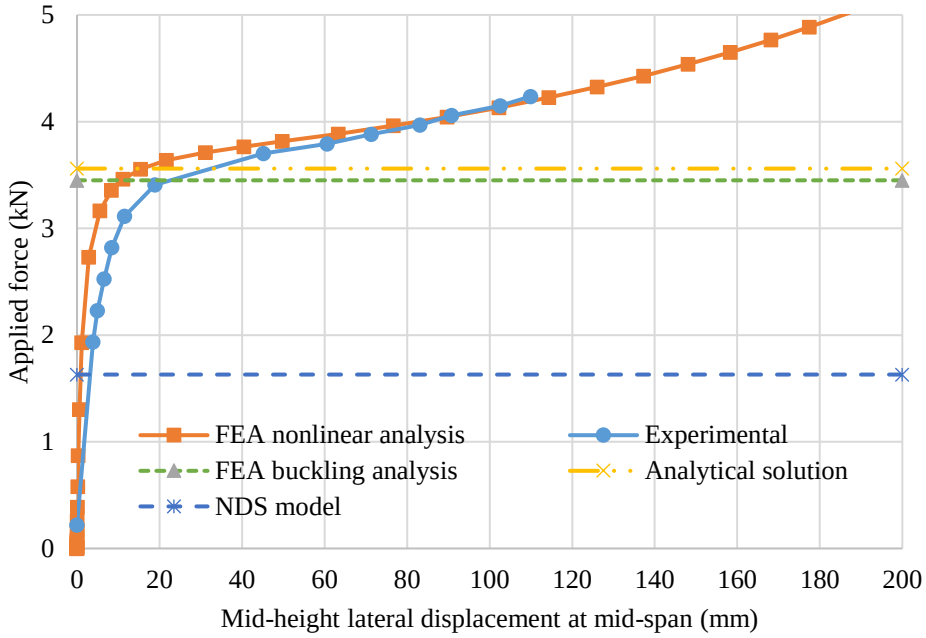

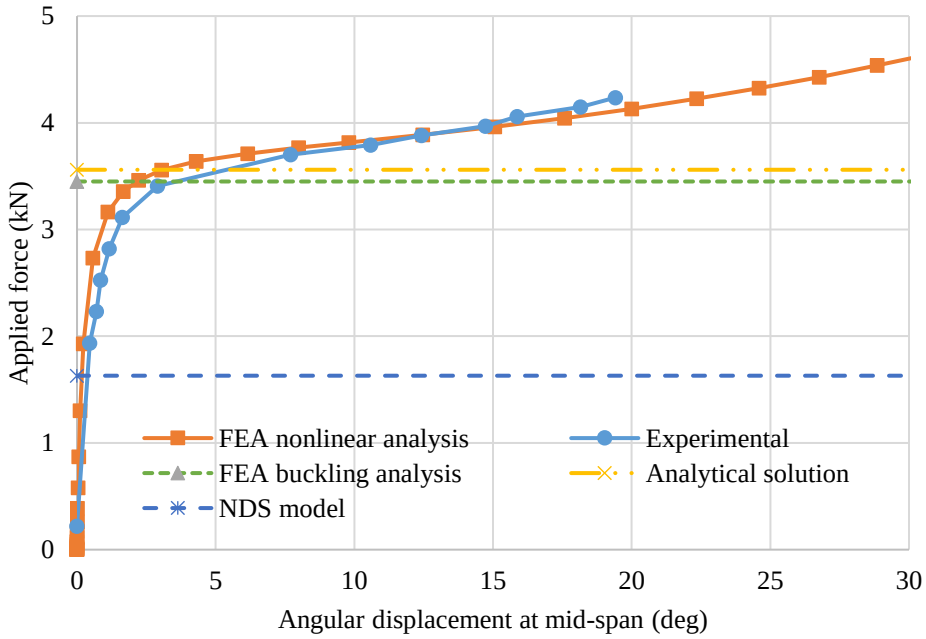

Figure A-12 Buckling displacements of specimen 2-6

Specimen 3 Sample group 6

Table A-13 Buckling displacements of specimen 3-6

Mid-span				Quarter-span
Force (kN)	**Vertical displacement (mm)**	**Lateral displacement at mid-height (mm)**	**Angle of twist (Deg)**	**Lateral displacement at top flange (mm)**
0.22	0.0	0.0	0.0	----
1.94	2.1	3.5	0.3	----
2.23	2.6	5.3	0.5	----
2.53	3.0	6.3	0.7	----
2.82	3.5	8.1	1.1	----
3.11	3.9	12.1	1.7	----
3.41	4.7	19.7	2.9	----
3.70	6.0	42.3	6.9	----
3.79	7.5	51.6	8.5	----
3.88	9.9	65.6	10.8	----
3.97	12.1	76.0	12.9	----
4.06	14.8	88.6	15.0	----
4.15	17.7	100.0	17.0	----
4.24	19.8	108.8	18.3	----
4.33	23.9	132.7	21.9	----
4.41	0.0	0.0	0.0	----
0.22	0.5	4.1	0.3	----

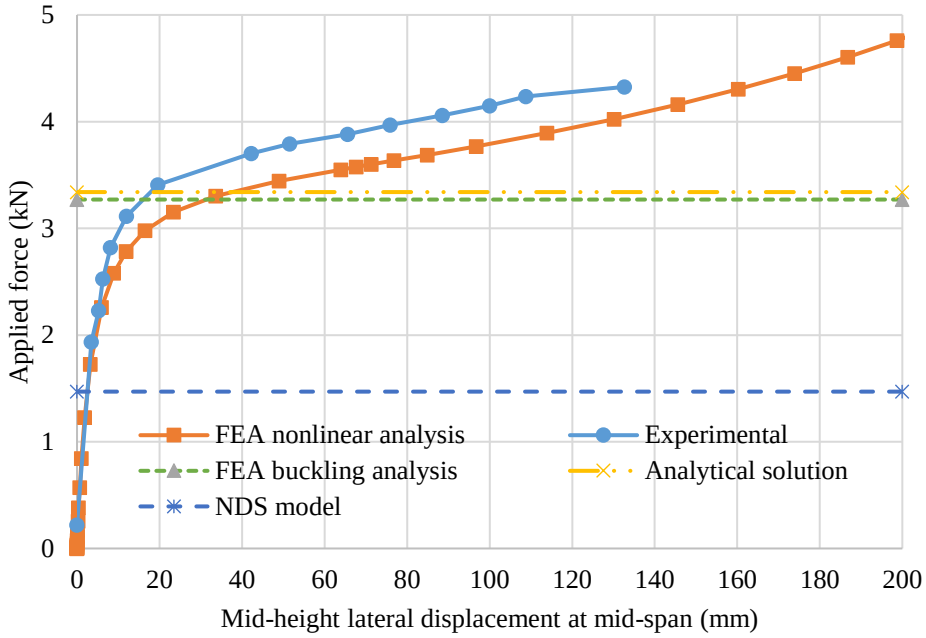

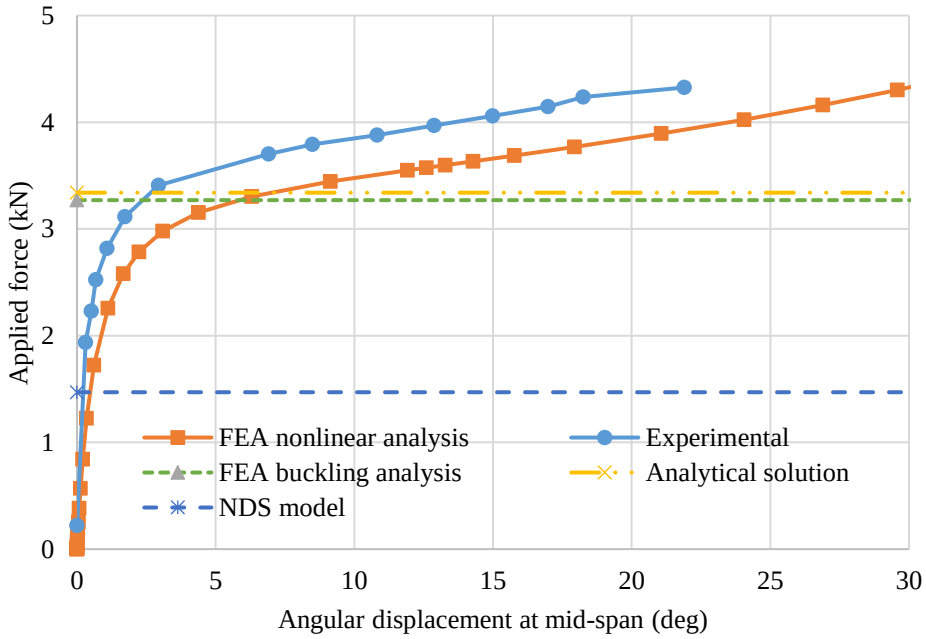

Figure A-13 Buckling displacements of specimen 3-6

Specimen 4 Sample group 6

Table A-14 Buckling displacements of specimen 4-6

Mid-span				Quarter-span
Force (kN)	**Vertical displacement (mm)**	**Lateral displacement at mid-height (mm)**	**Angle of twist (Deg)**	**Lateral displacement at top flange (mm)**
0.22	0.0	0.0	0.0	0
1.94	2.6	5.4	0.9	8.0
2.23	2.9	8.3	1.5	11.5
2.53	3.4	12.2	2.1	15.1
2.82	4.0	22.8	3.8	27.0
3.11	4.4	33.5	5.8	39.6
3.41	6.8	58.8	10.0	66.5
3.70	11.9	91.8	16.1	98.3
3.79	13.8	101.2	18.0	108.5
3.88	16.1	113.2	19.9	120.0
3.97	18.4	124.2	21.3	----
4.06	20.9	136.0	23.4	----
0.22	1.2	8.2	1.8	6.0

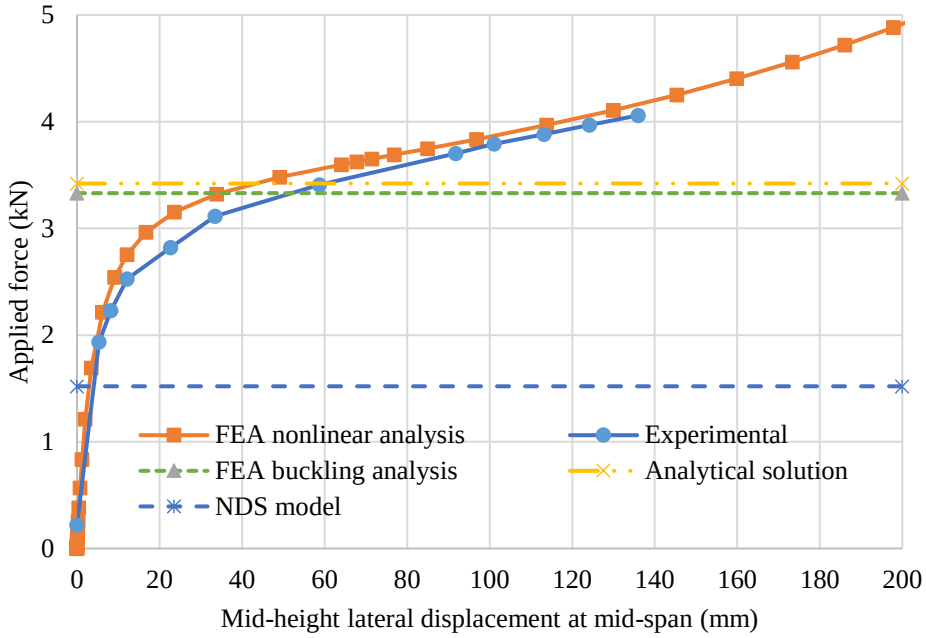

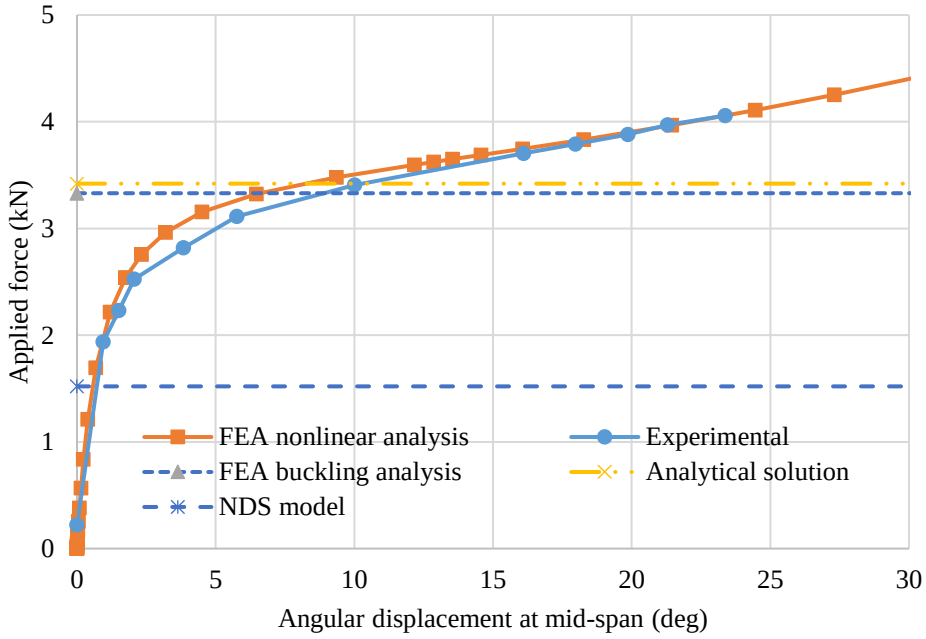

Figure A-14 Buckling displacements of specimen 4-6

Specimen 5 Sample group 6

Table A-15 Buckling displacements of specimen 5-6

Mid-span				Quarter-span
Force (kN)	**Vertical displacement (mm)**	**Lateral displacement at mid-height (mm)**	**Angle of twist (Deg)**	**Lateral displacement at top flange (mm)**
0.22	0.0	0.0	0.0	0
1.94	2.4	6.7	1.1	7.3
2.23	2.4	9.0	1.5	9.7
2.53	2.6	12.4	2.1	14.0
2.82	3.5	19.3	3.3	21.5
3.11	4.8	30.9	5.3	34.0
3.41	8.1	50.5	8.9	56.3
3.70	16.3	84.9	15.3	95.7
3.79	19.5	92.9	16.7	106.8
3.88	22.7	105.1	19.3	119.0
3.97	24.3	109.0	19.4	124.9
4.06	26.6	116.7	20.6	133.7
4.15	0.0	0.0	0.0	----
0.22	1.2	9.4	1.1	165.6

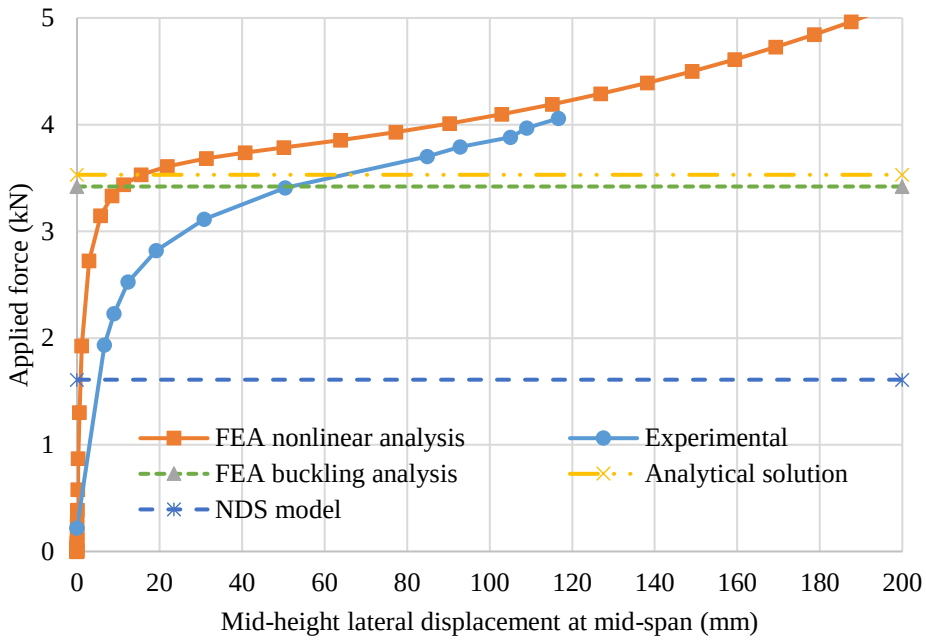

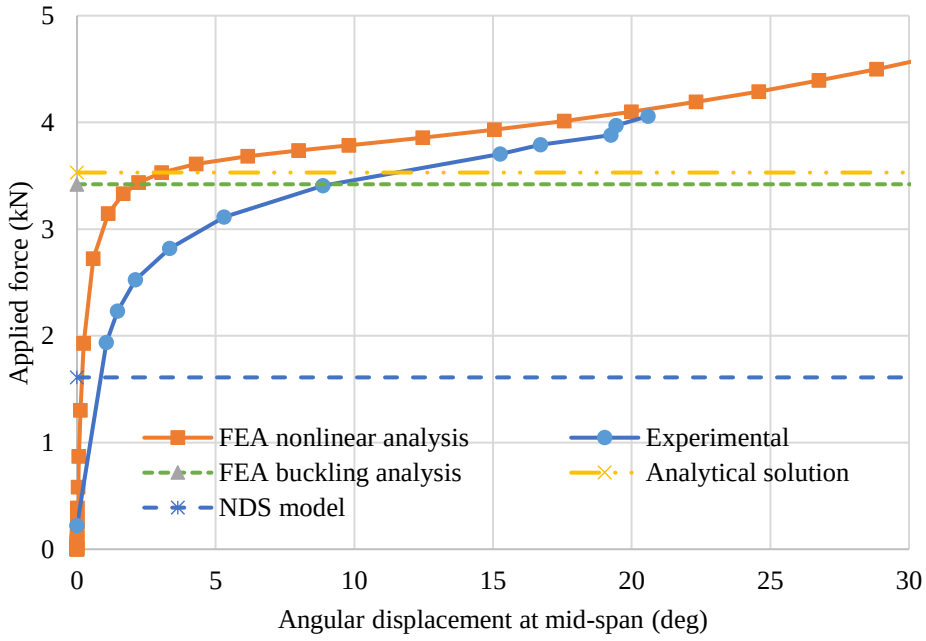

Figure A-15 Buckling displacements of specimen 5-6

Specimen 1 Sample group 7

Table A-16 Buckling displacements of specimen 1-7

Mid-span				Quarter-span
Force (kN)	**Vertical displacement (mm)**	**Lateral displacement at mid-height (mm)**	**Angle of twist (Deg)**	**Lateral displacement at top flange (mm)**
0.25	0.0	0.0	0.0	0.0
0.74	1.0	2.2	0.1	1.2
1.04	1.7	4.1	0.3	1.5
1.33	2.4	5.9	0.5	2.9
1.63	3.0	8.1	0.7	4.5
1.92	3.7	11.1	1.0	7.4
2.21	4.3	16.1	2.2	14.0
2.51	4.6	25.4	3.4	22.0
2.60	5.3	31.5	4.3	28.3
2.69	6.0	38.1	5.4	34.6
2.78	7.3	49.1	7.2	45.9
2.86	9.0	58.9	8.9	56.9
2.95	11.7	73.9	11.3	72.7
3.04	14.8	89.4	13.9	88.6
3.13	17.7	101.0	16.0	102.3
3.22	21.5	115.1	18.1	118.8
3.31	22.4	121.6	19.1	124.7
3.40	23.9	130.1	20.1	133.7
3.49	23.6	135.3	20.6	138.3
3.58	23.0	140.1	20.9	142.3
0.25	0.4	21.0	2.6	9.8

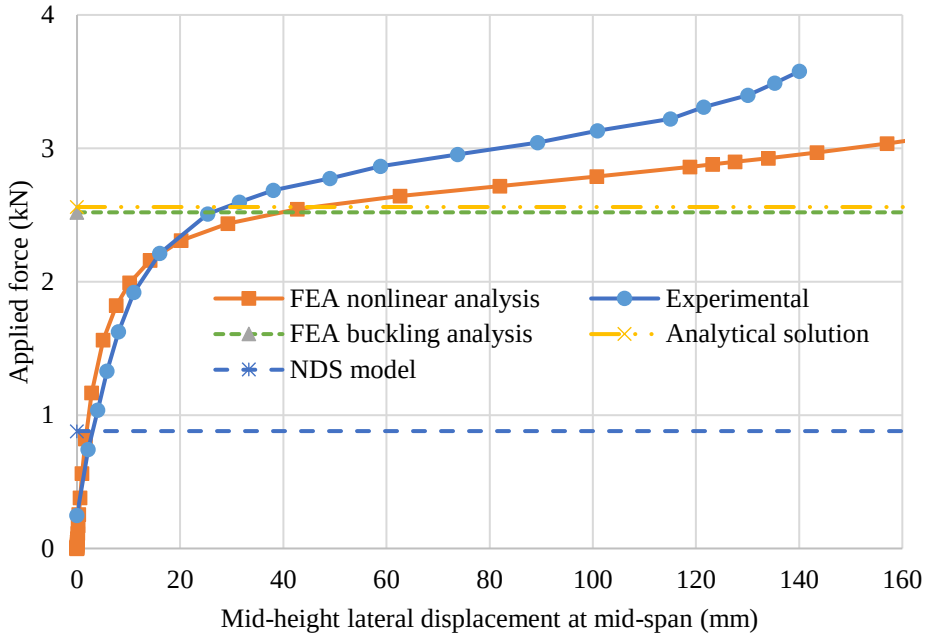

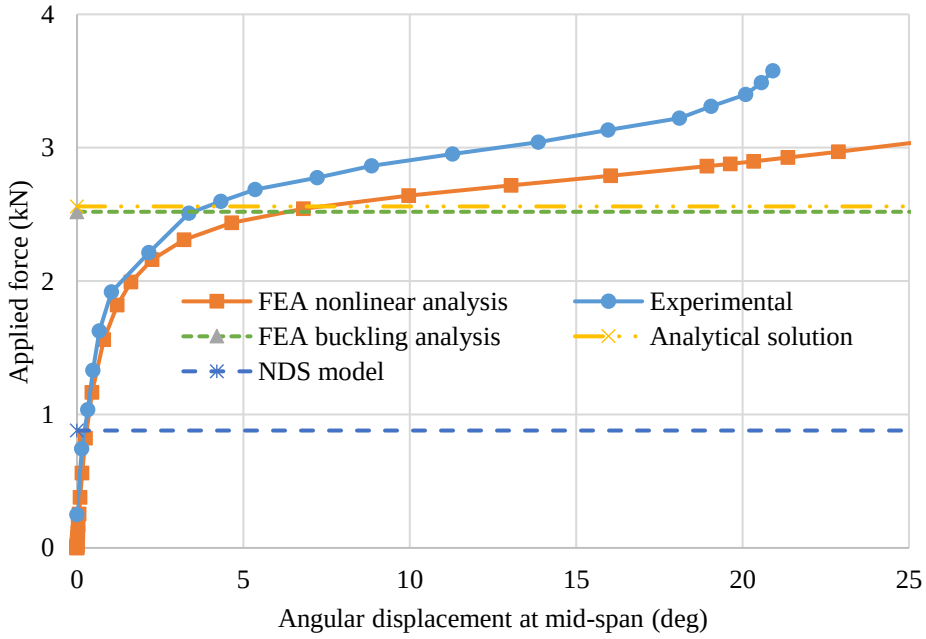

Figure A-16 Buckling displacements of specimen 1-7

Specimen 2 Sample group 7

Table A-17 Buckling displacements of specimen 2-7

Mid-span				Quarter-span
Force (kN)	**Vertical displacement (mm)**	**Lateral displacement at mid-height (mm)**	**Angle of twist (Deg)**	**Lateral displacement at top flange (mm)**
0.25	0.0	0.0	0.0	0.0
0.74	0.9	0.4	0.1	0.2
1.04	1.4	0.5	0.1	0.4
1.33	1.8	0.7	0.1	0.5
1.63	1.8	1.5	0.3	1.9
1.92	1.9	2.8	0.5	3.7
2.21	2.3	4.8	0.7	5.4
2.51	2.8	6.1	1.0	7.0
2.60	2.9	8.2	1.3	9.8
2.69	3.2	11.2	1.7	14.1
2.78	3.4	21.7	3.4	26.0
2.86	3.7	27.5	4.3	31.8
2.95	4.4	38.6	6.0	42.9
3.04	5.9	56.4	9.1	61.5
3.13	7.5	74.0	11.6	78.3
3.22	11.0	99.4	16.1	103.0
3.31	13.7	117.0	18.6	120.6
3.40	15.4	131.7	20.7	----
3.49	17.8	151.2	23.5	----
0.25	0.4	4.8	0.8	6.2

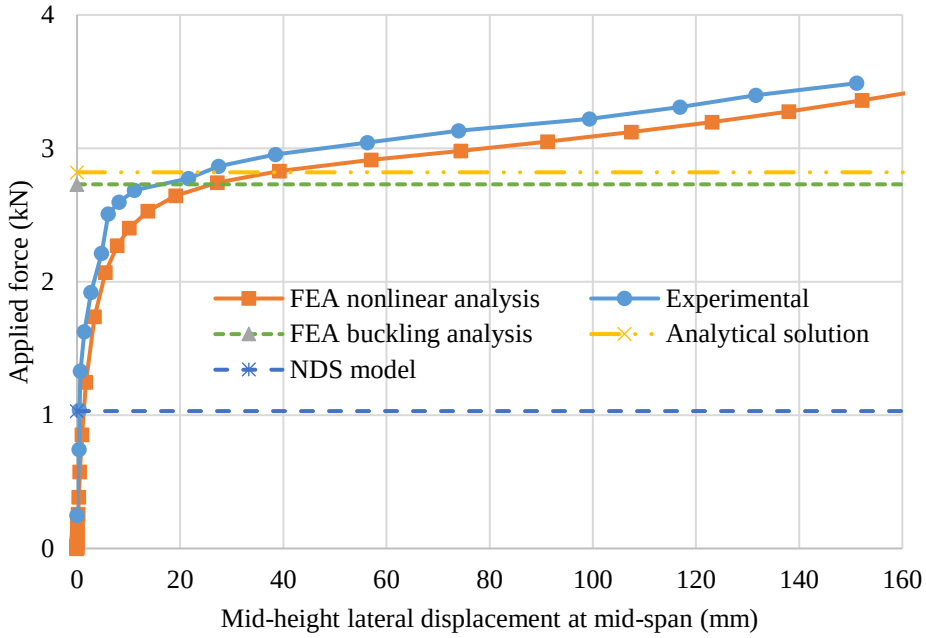

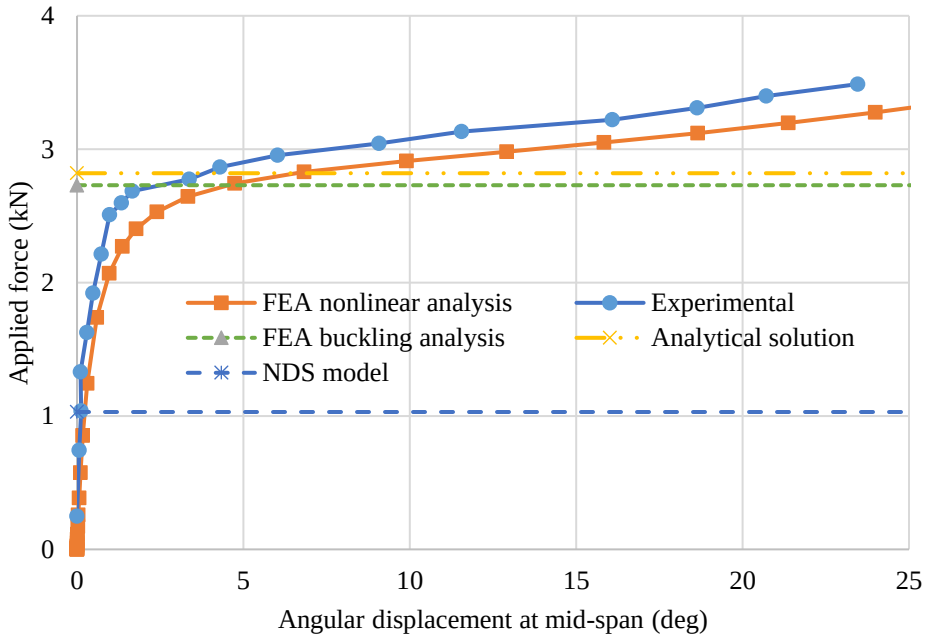

Figure A-17 Buckling displacements of specimen 2-7

Specimen 3 Sample group 7

Table A-18 Buckling displacements of specimen 3-7

Mid-span				Quarter-span
Force (kN)	**Vertical displacement (mm)**	**Lateral displacement at mid-height (mm)**	**Angle of twist (Deg)**	**Lateral displacement at top flange (mm)**
0.25	0.0	0.0	0.0	0.0
0.74	0.9	1.1	0.0	0.8
1.04	1.5	1.6	0.0	1.2
1.33	2.0	1.9	0.2	1.6
1.63	2.6	2.8	0.2	1.8
1.92	3.1	3.4	0.3	1.8
2.21	3.7	4.3	0.4	1.8
2.51	4.3	5.7	0.5	2.9
2.60	4.7	10.0	1.2	7.8
2.69	4.9	10.8	1.3	8.5
2.78	5.1	17.9	2.3	15.6
2.86	5.1	22.7	3.0	20.5
2.95	7.7	49.5	7.2	48.2
3.04	12.1	76.9	11.6	77.2
3.13	16.8	97.9	15.1	101.2
3.22	22.2	118.0	18.5	123.2
3.31	25.7	134.2	21.1	142.5
3.40	27.3	143.1	22.3	151.7
0.25	0.5	3.9	0.8	3.2

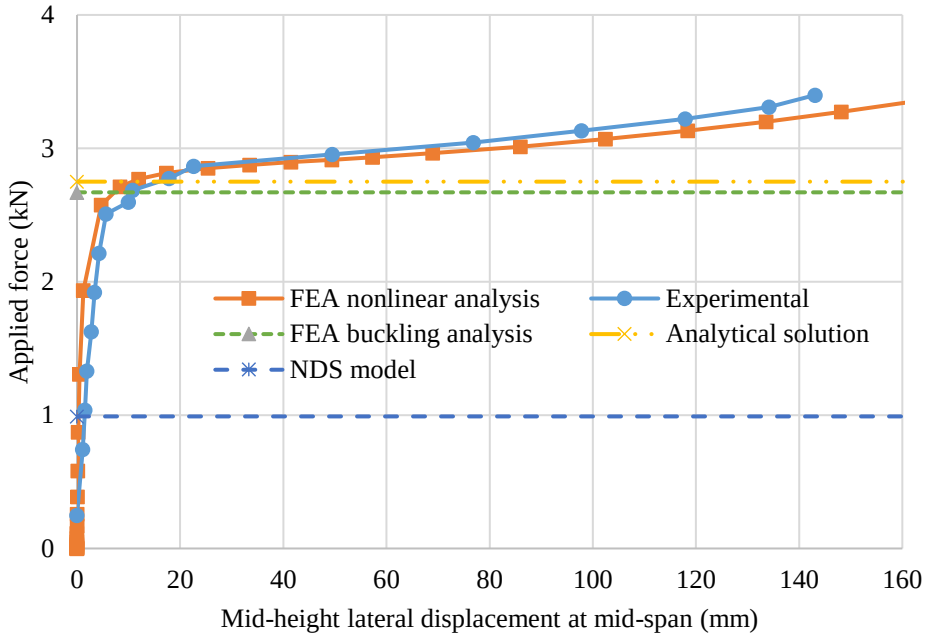

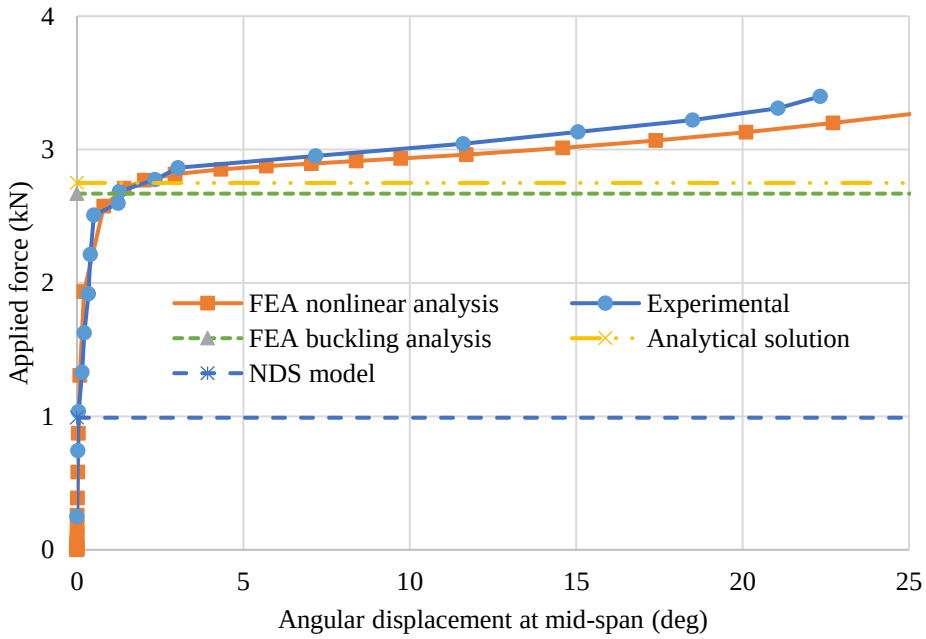

Figure A-18 Buckling displacements of specimen 3-7

Specimen 4 Sample group 7

Table A-19 Buckling displacements of specimen 4-7

Mid-span				Quarter-span
Force (kN)	**Vertical displacement (mm)**	**Lateral displacement at mid-height (mm)**	**Angle of twist (Deg)**	**Lateral displacement at top flange (mm)**
0.25	0.0	0.0	0.0	0.0
0.74	0.1	1.8	0.0	1.2
1.04	0.6	3.1	0.1	1.2
1.33	1.1	4.7	0.3	2.4
1.63	1.5	6.3	0.5	3.9
1.92	2.0	9.1	0.9	6.9
2.21	2.5	12.8	1.6	11.2
2.30	2.6	14.2	1.7	12.3
2.39	2.8	16.8	2.1	15.2
2.48	3.1	22.2	2.9	20.9
2.57	3.2	24.1	3.1	22.7
2.66	3.4	29.1	3.8	27.4
2.75	4.0	37.2	5.3	36.7
2.84	4.4	42.1	5.9	41.5
2.93	5.1	49.8	7.1	49.6
3.02	6.8	63.7	9.6	64.7
3.10	7.7	72.3	10.7	74.2
3.19	9.8	87.7	13.2	89.7
3.28	11.5	98.7	14.9	103.3
0.25	0.0	1.7	0.2	1.1

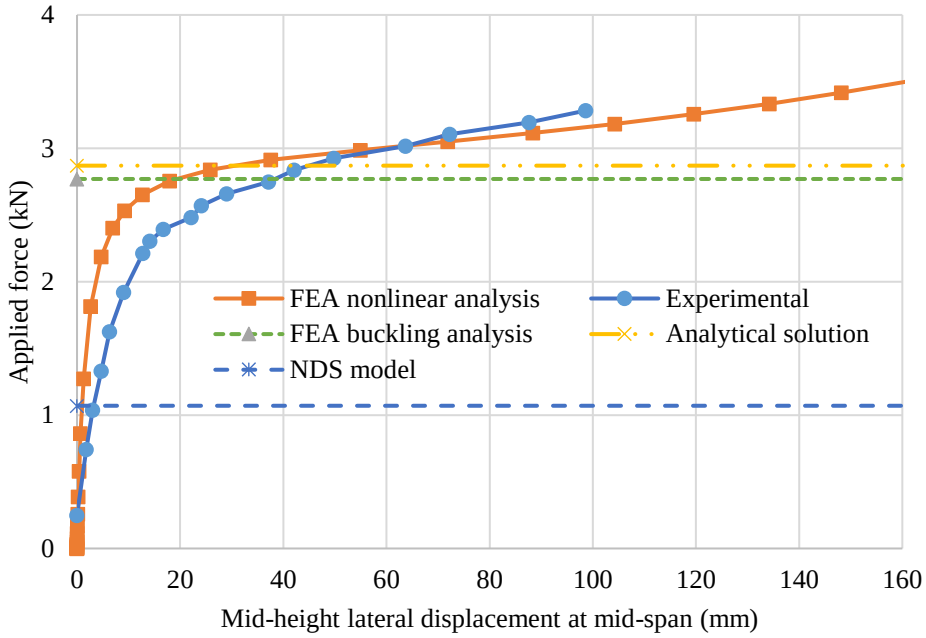

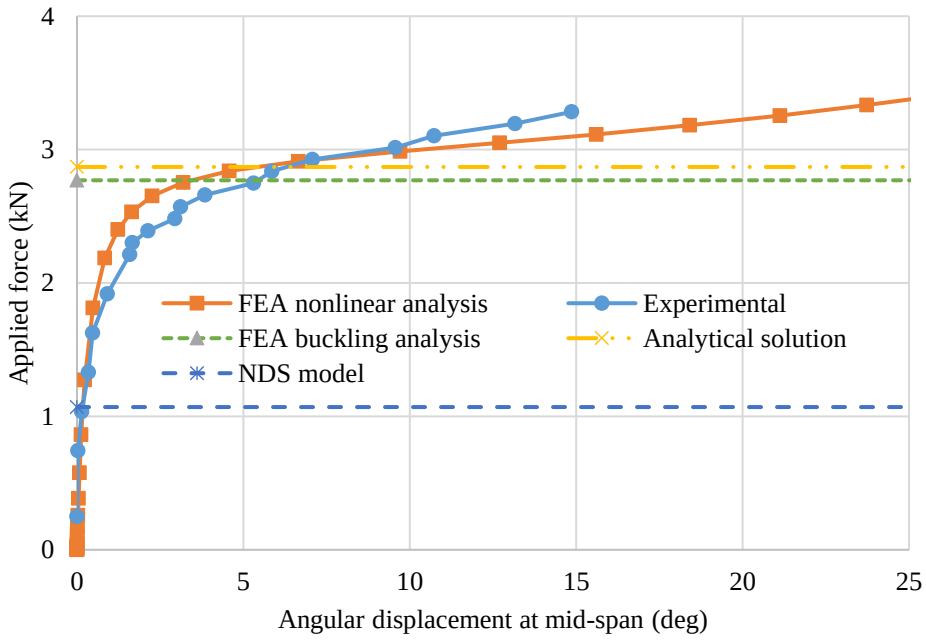

Figure A-19 Buckling displacements of specimen 4-7

Specimen 5 Sample group 7

Table A-20 Buckling displacements of specimen 5-7

Mid-span				Quarter-span
Force (kN)	**Vertical displacement (mm)**	**Lateral displacement at mid-height (mm)**	**Angle of twist (Deg)**	**Lateral displacement at top flange (mm)**
0.25	0.0	0.0	0.0	0.0
0.74	0.9	2.9	0.3	2.4
1.04	1.6	4.6	0.4	3.9
1.33	2.3	7.3	0.7	6.5
1.63	2.5	10.5	1.2	10.1
1.92	2.6	15.5	1.9	14.6
2.21	3.5	22.7	2.9	21.3
2.51	5.7	42.7	5.9	41.3
2.60	6.7	48.8	7.0	47.7
2.69	8.0	58.9	8.5	58.2
2.78	10.3	70.9	10.5	71.1
2.86	14.3	90.1	14.0	94.4
2.95	17.8	104.3	16.1	106.9
0.25	0.3	2.6	0.5	2.9

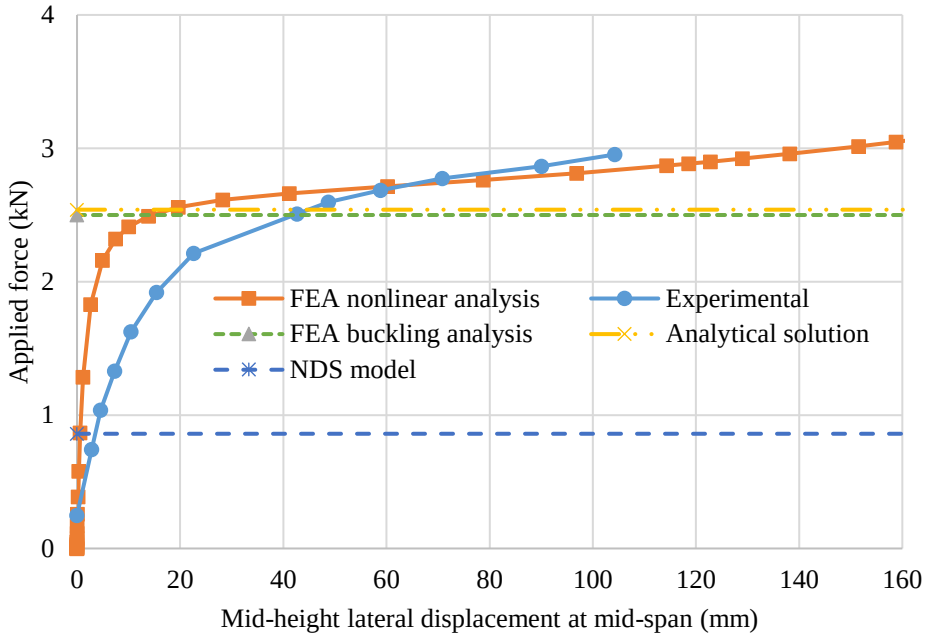

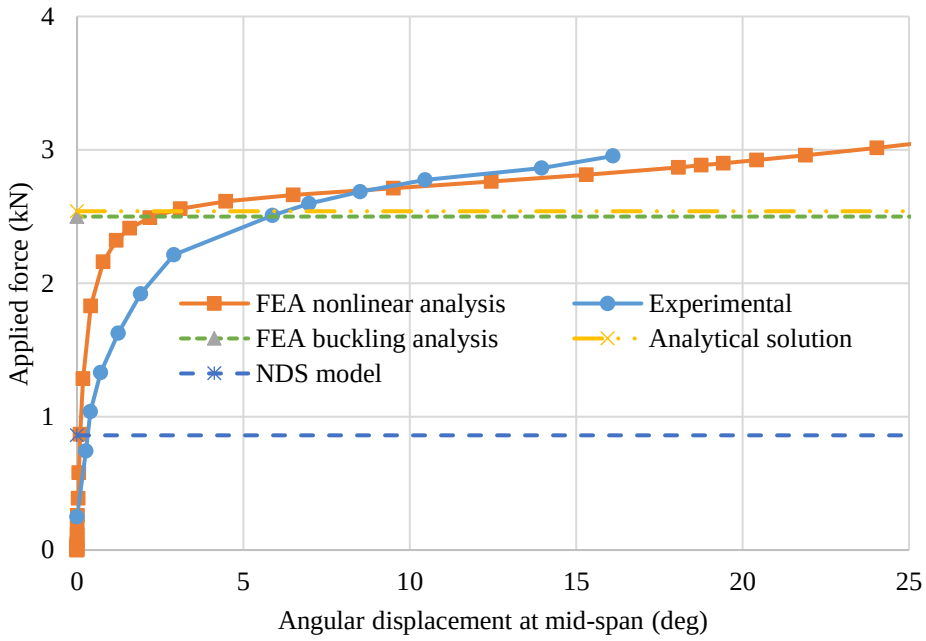

Figure A-20 Buckling displacements of specimen 5-7

Specimen 1 Sample group 8

Table A-21 Buckling displacements of specimen 1-8

Mid-span				Quarter-span
Force (kN)	**Vertical displacement (mm)**	**Lateral displacement at mid-height (mm)**	**Angle of twist (Deg)**	**Lateral displacement at top flange (mm)**
0.28	0.0	0.0	0.0	0.0
0.77	1.2	2.7	0.2	2.4
1.07	1.9	4.9	0.5	4.5
1.36	2.6	7.8	0.8	7.5
1.65	3.2	12.5	1.4	12.1
1.95	4.2	20.8	2.5	21.1
2.04	4.7	27.0	3.4	28.2
2.13	5.4	35.5	4.6	38.1
2.22	5.9	41.0	5.2	43.6
2.31	6.9	50.7	6.6	53.4
2.39	8.9	68.6	9.4	72.4
2.48	11.2	84.6	11.9	88.2
2.57	14.8	109.3	15.4	112.0

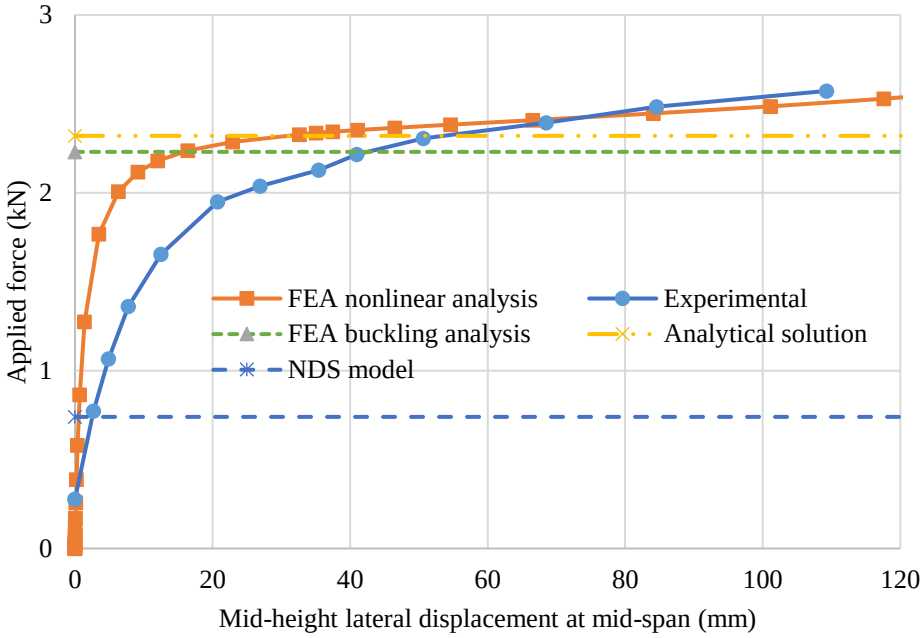

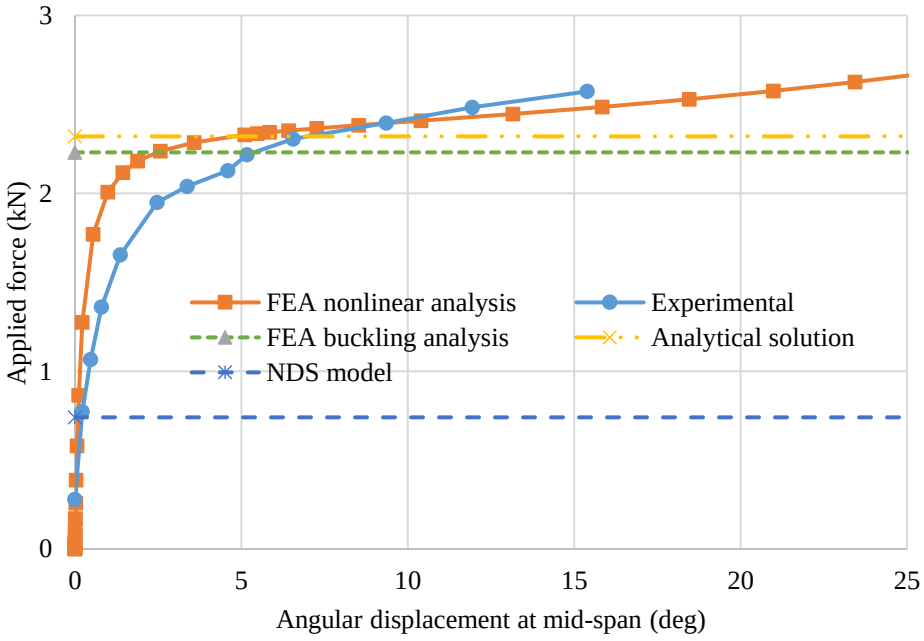

Figure A-21 Buckling displacements of specimen 1-8

Specimen 2 Sample group 8

Table A-22 Buckling displacements of specimen 2-8

Mid-span				Quarter-span
Force (kN)	**Vertical displacement (mm)**	**Lateral displacement at mid-height (mm)**	**Angle of twist (Deg)**	**Lateral displacement at top flange (mm)**
0.28	0.0	0.0	0.0	0
0.77	1.0	0.9	0.0	0.02
1.07	1.7	1.2	-0.1	0.01
1.36	2.0	1.7	-0.3	1.1
1.65	2.7	3.1	-0.2	2.9
1.95	3.2	7.1	0.5	7
2.04	3.4	8.5	0.6	8.5
2.13	3.6	11.1	1.0	11.1
2.22	3.7	16.8	1.8	16.9
2.31	3.8	24.8	2.8	25.3
2.39	4.0	31.8	3.7	33.2
2.48	4.7	49.4	6.3	50.7
2.57	7.8	89.5	12.4	90.9
2.66	10.5	114.0	15.7	115.44

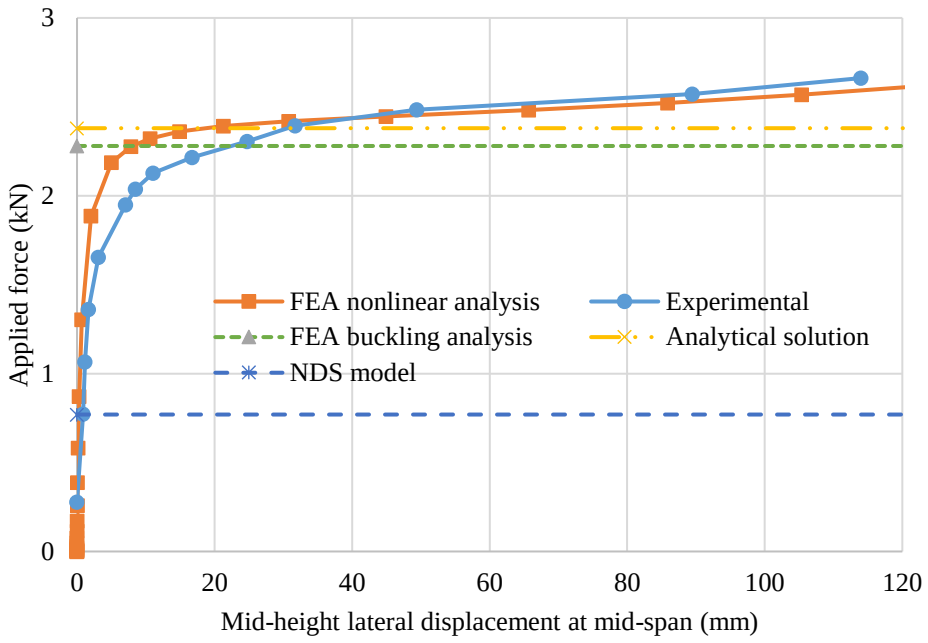

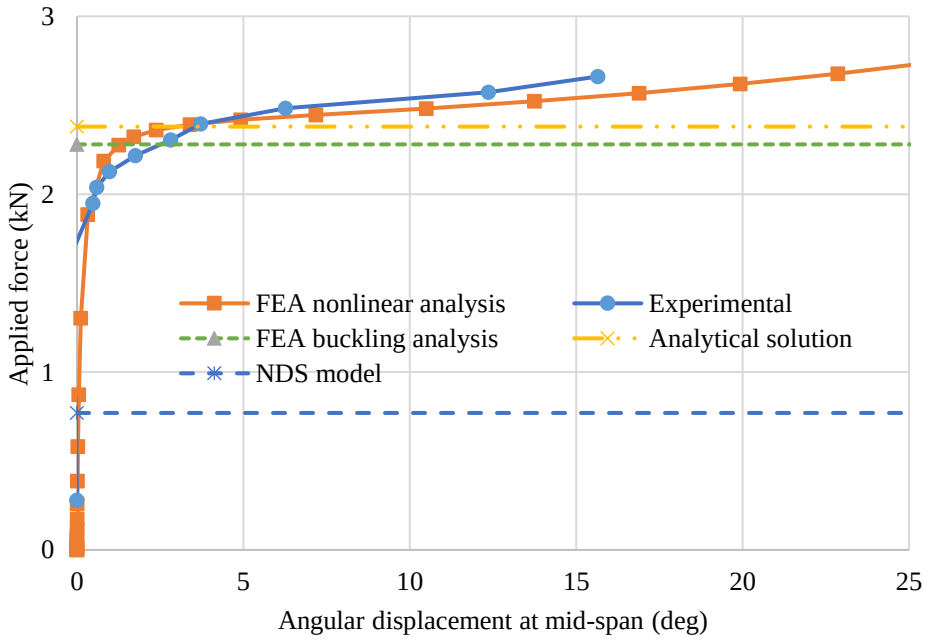

Figure A-22 Buckling displacements of specimen 2-8

Specimen 3 Sample group 8

Table A-23 Buckling displacements of specimen 3-8

Mid-span				Quarter-span
Force (kN)	**Vertical displacement (mm)**	**Lateral displacement at mid-height (mm)**	**Angle of twist (Deg)**	**Lateral displacement at top flange (mm)**
0.28	0.0	0.0	0.0	0
0.77	1.0	0.3	0.0	0.5
1.07	1.6	0.1	0.0	0
1.36	1.9	-0.3	-0.1	-0.8
1.65	2.6	0.1	0.0	-0.5
1.95	3.2	-0.2	-0.1	-0.7
2.04	3.5	3.3	0.5	3.2
2.13	3.7	3.4	0.4	3.2
2.22	3.9	2.5	0.3	2.4
2.31	4.1	0.2	-0.1	-0.2
2.39	4.4	5.8	0.8	5.7
2.48	4.5	2.2	0.2	1.9
2.57	4.8	11.6	1.6	12
2.66	11.6	84.6	12.5	83.8
2.75	17.4	119.2	17.8	121.2

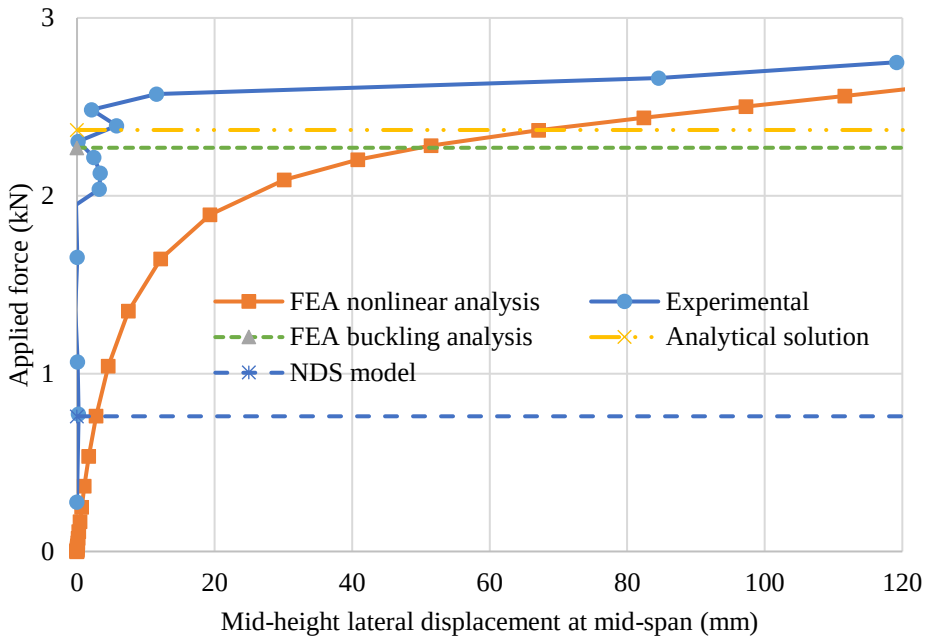

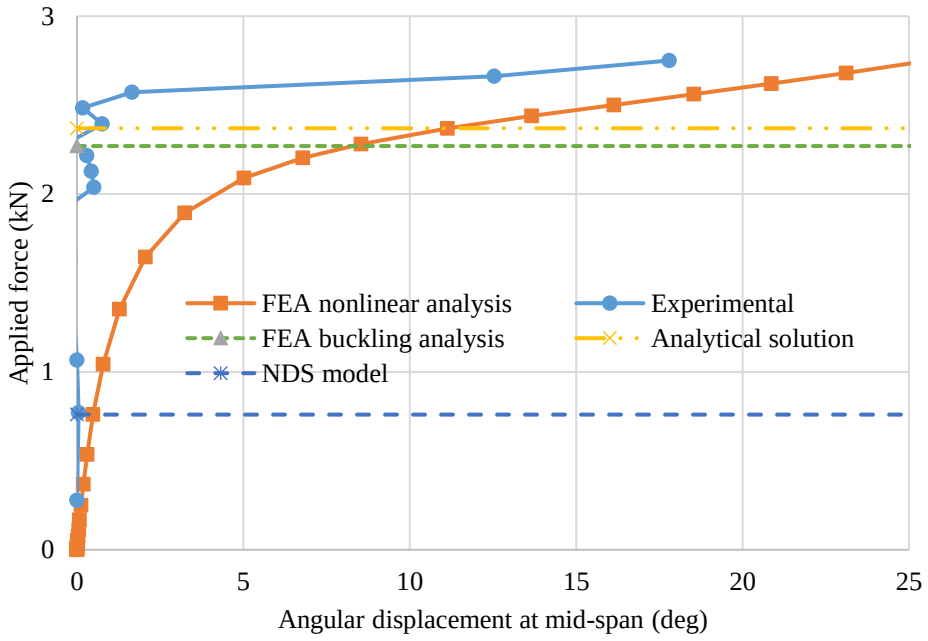

Figure A-23 Buckling displacements of specimen 3-8

Specimen 4 Sample group 8

Table A-24 Buckling displacements of specimen 4-8

Mid-span				Quarter-span
Force (kN)	**Vertical displacement (mm)**	**Lateral displacement at mid-height (mm)**	**Angle of twist (Deg)**	**Lateral displacement at top flange (mm)**
0.28	0.0	0.0	0.0	0
0.77	1.2	2.8	0.4	1.8
1.07	1.7	5.6	0.7	4.9
1.36	2.5	10.5	1.5	10.4
1.65	3.3	16.4	2.2	16.1
1.95	4.9	33.3	4.8	35.2
2.04	5.5	38.5	5.4	40.1
2.13	6.4	45.7	6.5	47.5
2.22	7.8	57.6	8.2	60
2.31	9.5	68.8	10.1	72.4
2.39	12.1	86.5	13.0	89.5
2.48	15.3	104.5	15.2	107.2

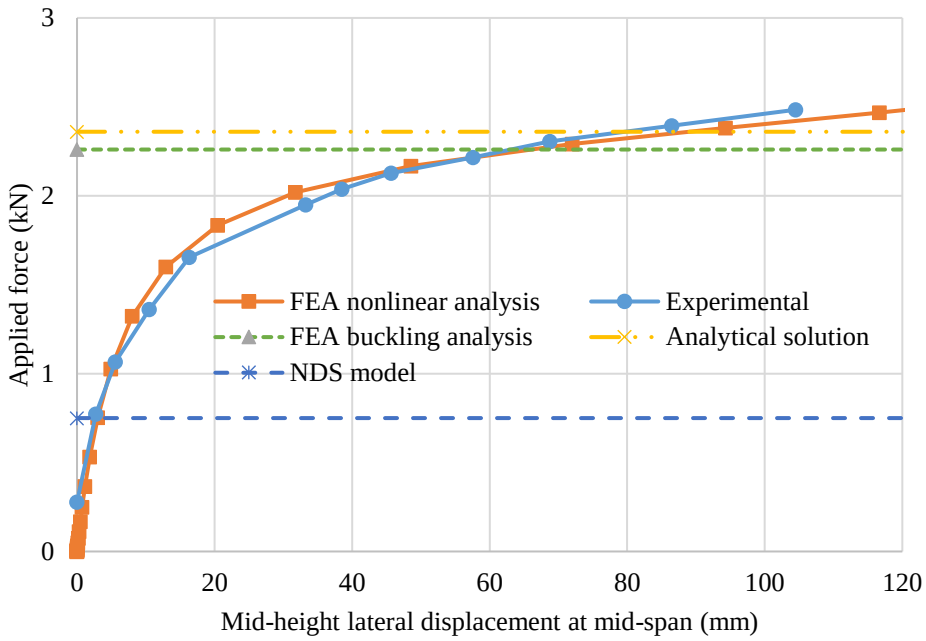

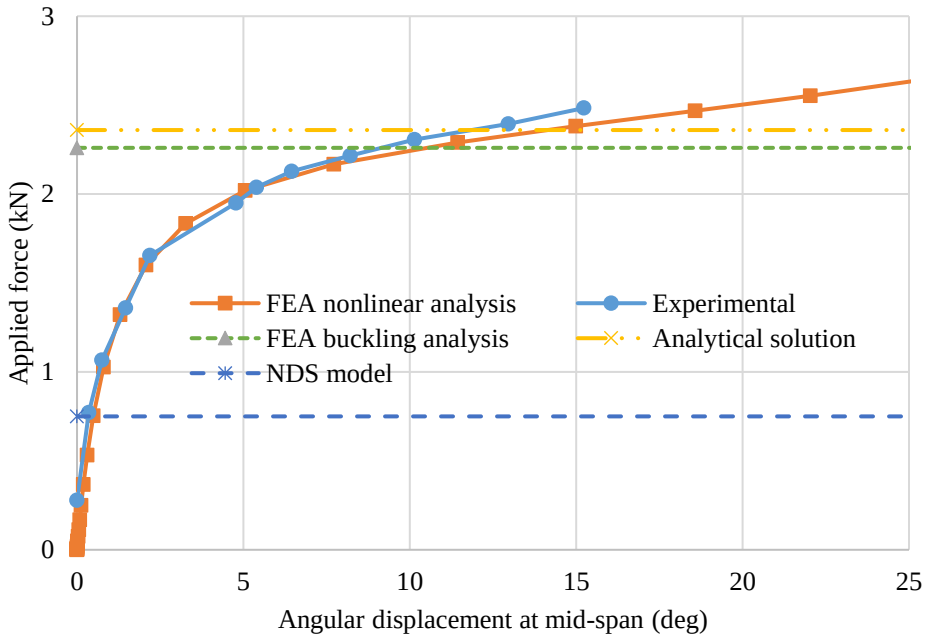

Figure A-24 Buckling displacements of specimen 4-8

Specimen 5 Sample group 8

Table A-25 Buckling displacements of specimen 5-8

Mid-span				Quarter-span
Force (kN)	**Vertical displacement (mm)**	**Lateral displacement at mid-height (mm)**	**Angle of twist (Deg)**	**Lateral displacement at top flange (mm)**
0.28	0.0	0.0	0.0	0
0.77	1.1	0.3	0.0	0.01
1.07	1.7	1.1	0.0	0.9
1.36	2.4	1.2	0.0	0.8
1.65	3.0	2.0	0.0	1.5
1.95	3.7	2.2	-0.1	2.4
2.04	3.9	2.4	-0.1	2.9
2.13	4.1	2.8	-0.1	3.4
2.22	4.3	3.8	0.1	3.5
2.31	4.5	4.9	0.2	3.9
2.39	4.6	7.1	0.5	6.1
2.48	4.8	9.3	0.8	8.2
2.57	5.0	13.7	1.3	12.8
2.66	9.1	81.1	11.4	84.7
2.75	13.6	118.1	16.3	121.8

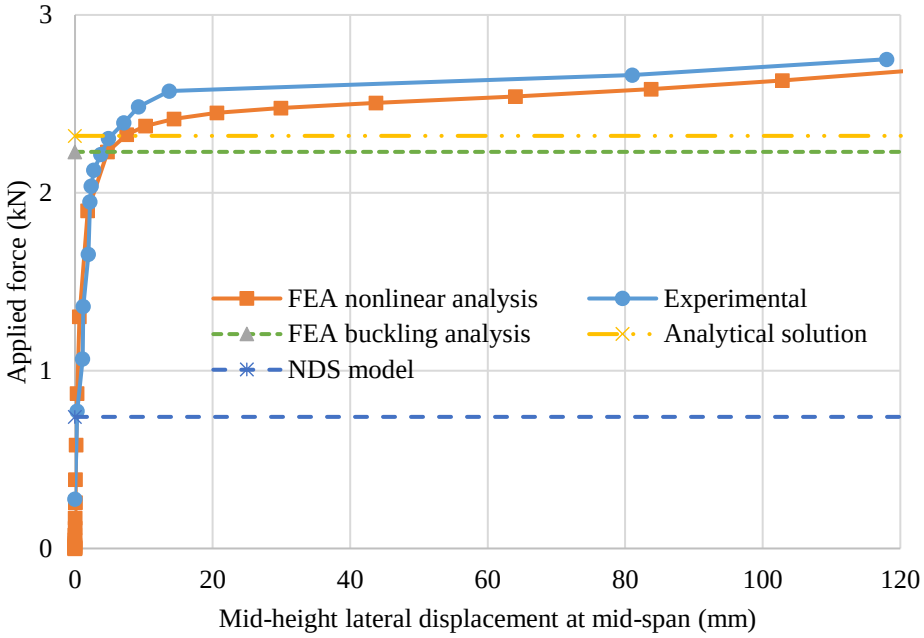

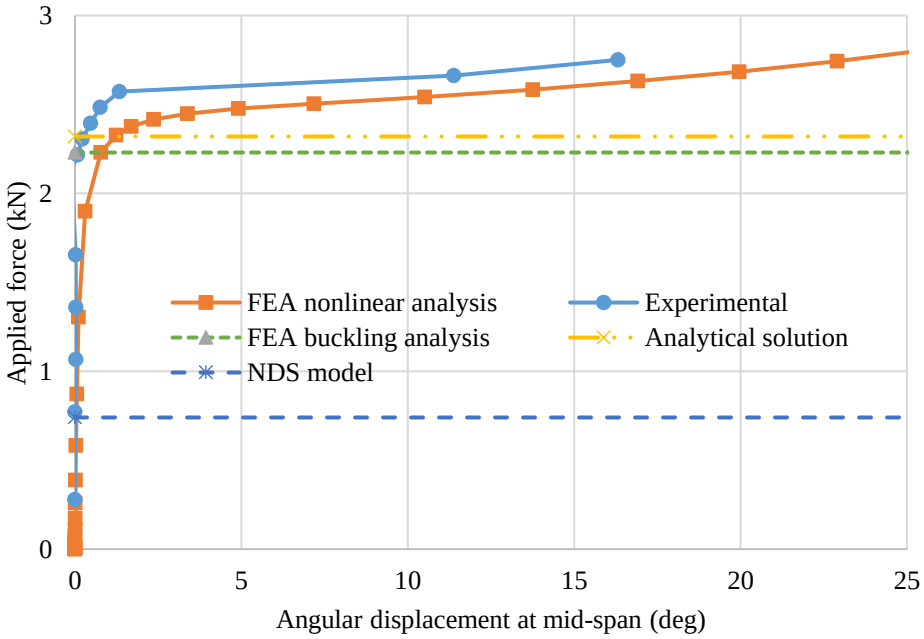

Figure A-25 Buckling displacements of specimen 5-8

Specimen 6 Sample group 8

Table A-26 Buckling displacements of specimen 6-8

Mid-span				Quarter-span
Force (kN)	**Vertical displacement (mm)**	**Lateral displacement at mid-height (mm)**	**Angle of twist (Deg)**	**Lateral displacement at top flange (mm)**
0.28	0.0	0.0	0.0	0
0.77	1.0	0.7	0.0	0.7
1.07	1.7	1.4	0.0	1.5
1.36	2.4	2.0	0.1	1.87
1.65	3.2	3.4	0.3	3.38
1.95	3.9	5.1	0.5	5.3
2.04	4.1	4.6	0.3	4.5
2.13	4.3	4.9	0.4	4.9
2.22	4.6	8.0	0.8	8.1
2.31	4.8	7.0	0.6	6.9
2.39	5.2	17.8	2.5	18.1
2.48	5.9	27.2	3.9	27.5
2.57	6.6	33.6	4.9	33.9
2.66	13.4	86.6	13.1	87.4
2.75	19.2	113.0	17.5	116.8

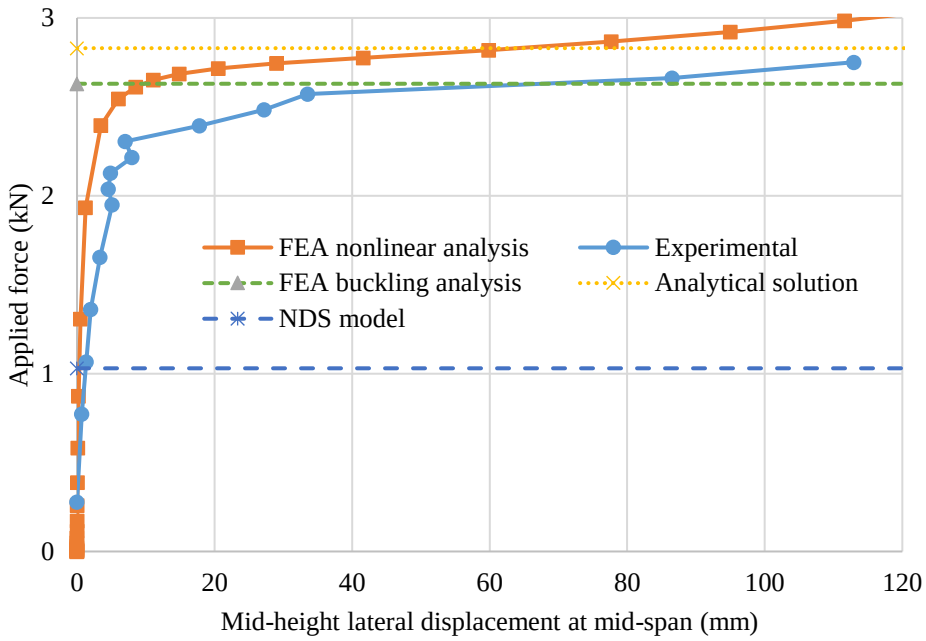

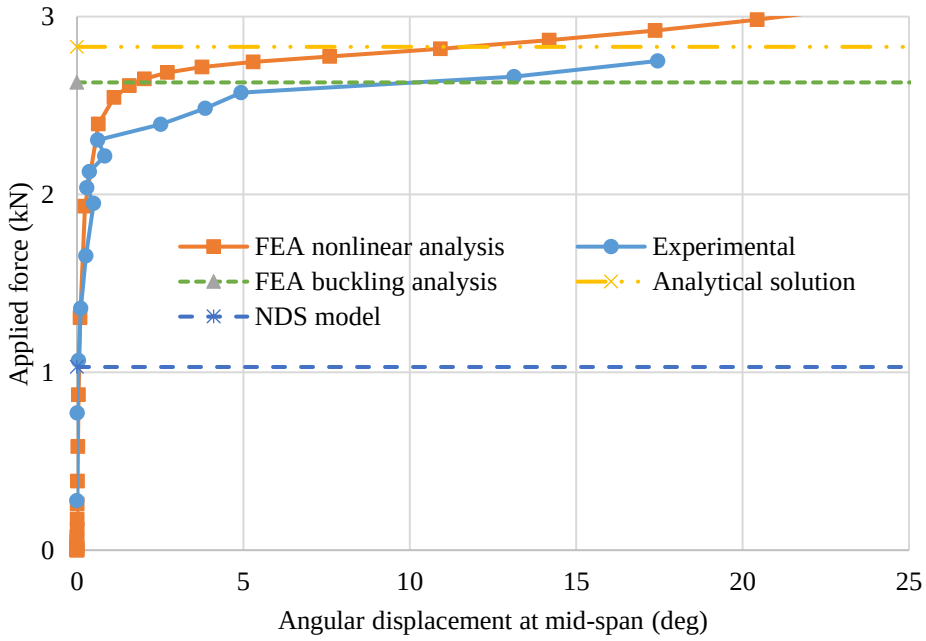

Figure A-26 Buckling displacements of specimen 6-8

Specimen 7 Sample group 8

Table A-27 Buckling displacements of specimen 7-8

Mid-span				Quarter-span
Force (kN)	**Vertical displacement (mm)**	**Lateral displacement at mid-height (mm)**	**Angle of twist (Deg)**	**Lateral displacement at top flange (mm)**
0.28	0.0	0.0	0.0	0
0.77	1.1	2.4	0.2	2.4
1.07	1.8	4.1	0.3	4.3
1.36	2.5	6.7	0.6	6.8
1.65	3.3	10.0	1.0	9.8
1.95	4.1	17.5	2.2	17.6
2.04	4.4	21.4	2.7	21.5
2.13	4.8	24.7	3.0	24.9
2.22	5.5	32.3	4.1	32.5
2.31	6.9	46.0	6.1	46
2.39	8.0	56.0	7.4	55.9
2.48	10.2	71.8	9.6	72.4
2.57	13.7	92.4	12.9	93.9
2.66	17.6	113.0	15.7	116.1

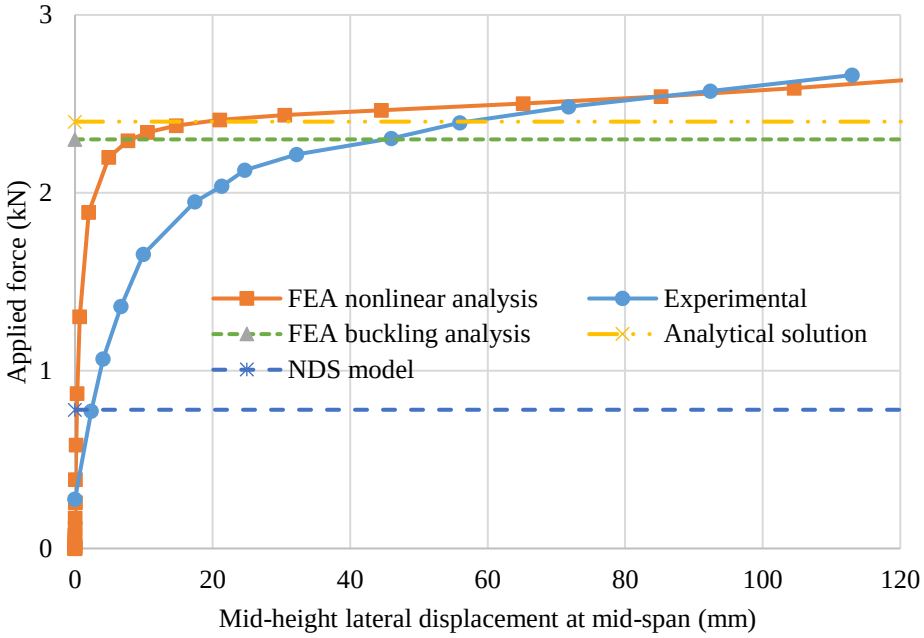

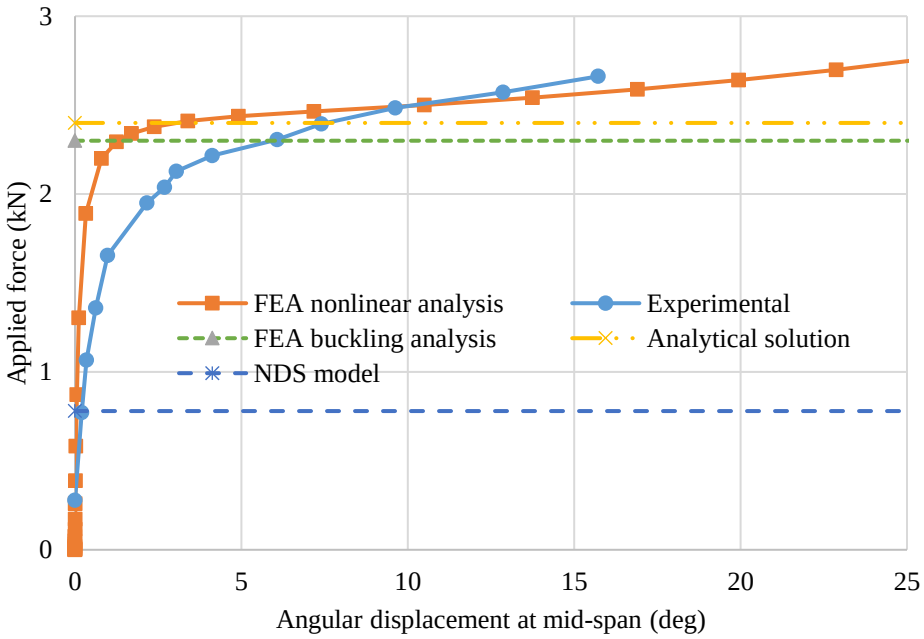

Figure A-27 Buckling displacements of specimen 7-8

Specimen 8 Sample group 8

Table A-28 Buckling displacements of specimen 8-8

Mid-span				Quarter-span
Force (kN)	**Vertical displacement (mm)**	**Lateral displacement at mid-height (mm)**	**Angle of twist (Deg)**	**Lateral displacement at top flange (mm)**
0.28	0.0	0.0	0.0	0
0.77	0.9	0.3	0.1	0.8
1.07	1.6	0.5	0.2	1.1
1.36	2.3	1.8	0.0	2.9
1.65	2.9	3.0	0.2	3.6
1.95	3.5	5.8	0.5	4.9
2.04	3.7	6.9	0.6	5.9
2.13	3.9	7.6	0.7	6.6
2.22	4.1	14.3	1.8	13.7
2.31	4.3	24.7	3.2	24.8
2.39	4.6	29.5	3.8	29.6
2.48	6.5	66.5	9.8	70
2.57	9.9	96.8	14.0	100.4

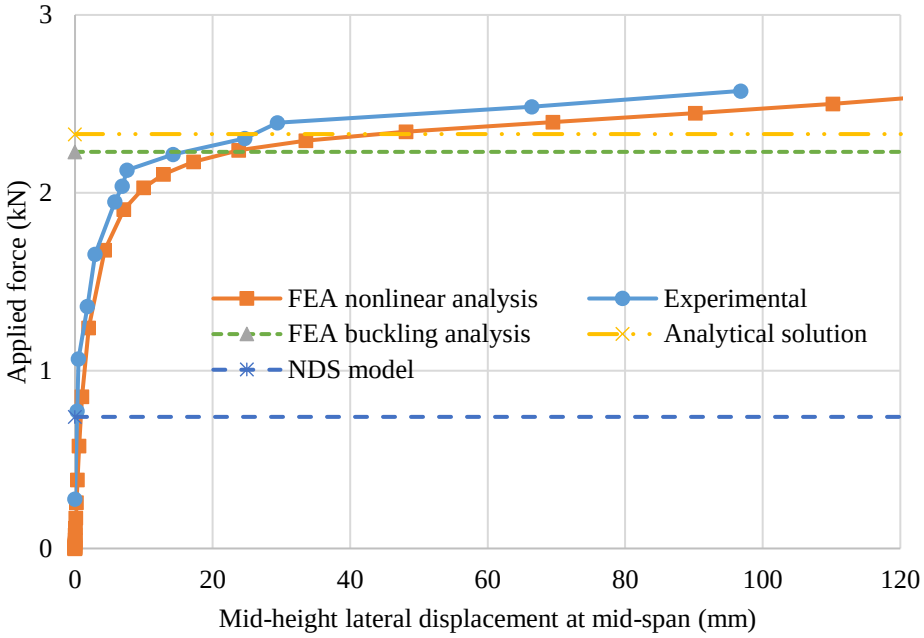

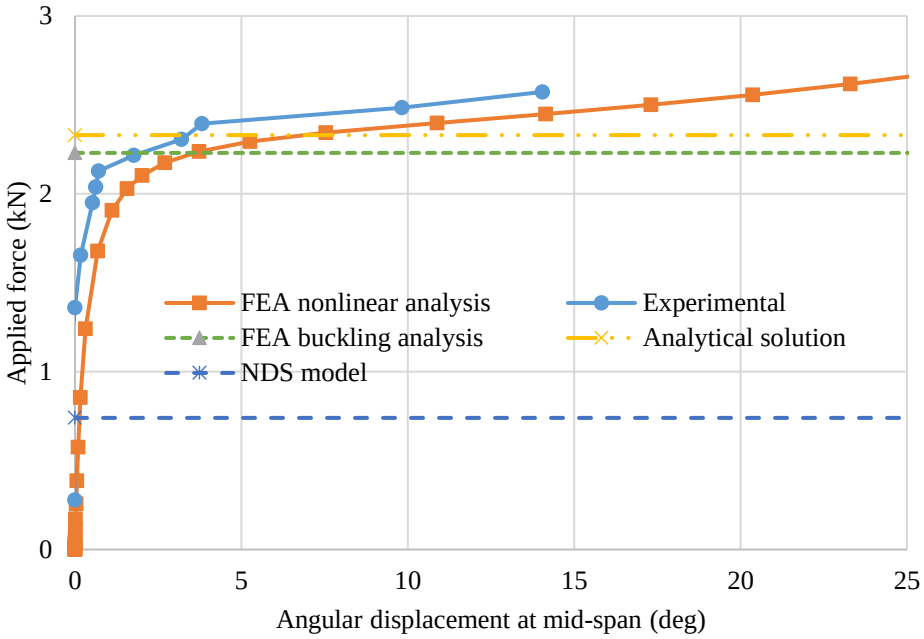

Figure A-28 Buckling displacements of specimen 8-8

Specimen 9 Sample group 8

Table A-29 Buckling displacements of specimen 9-8

Mid-span				Quarter-span
Force (kN)	**Vertical displacement (mm)**	**Lateral displacement at mid-height (mm)**	**Angle of twist (Deg)**	**Lateral displacement at top flange (mm)**
0.28	0.0	0.0	0.0	0
0.77	1.1	0.6	-0.2	0.2
1.07	1.8	1.1	-0.2	1.3
1.36	2.5	2.7	-0.1	2.6
1.65	3.1	3.3	0.0	3
1.95	3.7	7.6	0.5	5.8
2.04	3.8	10.8	1.0	9.3
2.13	3.9	9.2	0.6	7.4
2.22	4.2	13.7	1.3	12.2
2.31	4.5	15.9	1.5	14.3
2.39	5.1	32.3	3.9	31.9
2.48	6.7	56.0	7.3	57.8
2.57	10.8	91.1	12.6	93.6

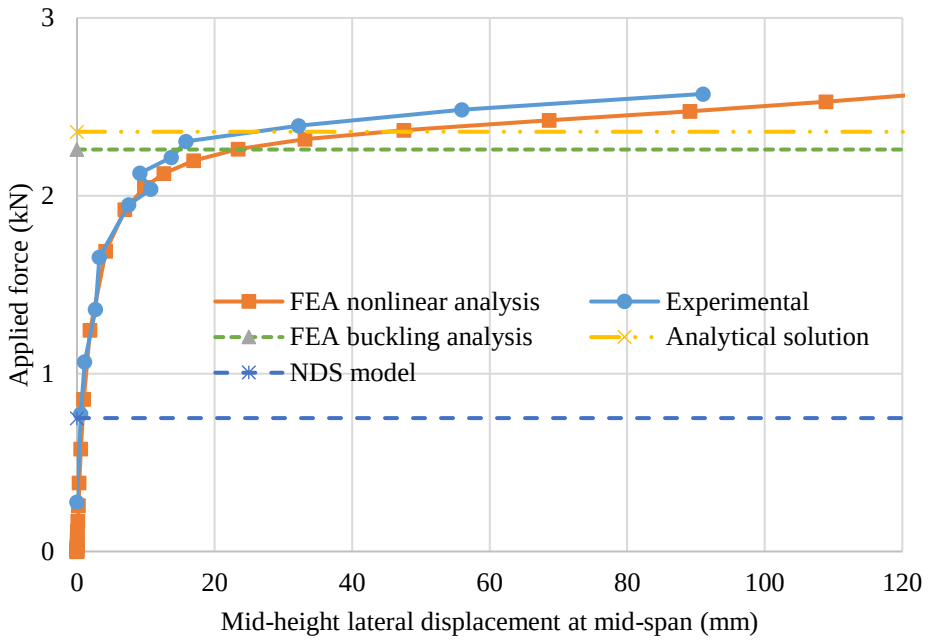

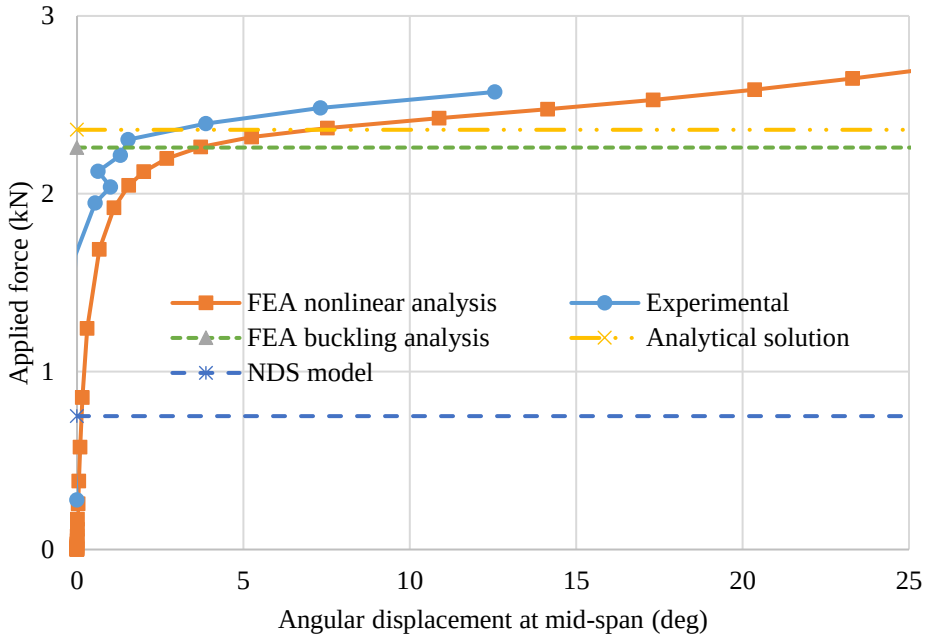

Figure A-29 Buckling displacements of specimen 9-8

Specimen 10 Sample group 8

Table A-30 Buckling displacements of specimen 10-8

Mid-span				Quarter-span
Force (kN)	**Vertical displacement (mm)**	**Lateral displacement at mid-height (mm)**	**Angle of twist (Deg)**	**Lateral displacement at top flange (mm)**
0.28	0.0	0.0	0.0	0
0.77	1.1	0.5	0.4	1.62
1.07	1.4	0.9	0.6	2.1
1.36	2.2	1.6	1.0	3.8
1.65	3.0	3.6	2.1	6.04
1.95	3.9	10.7	1.8	10.05
2.04	4.4	14.7	2.4	14.1
2.13	4.7	16.4	2.7	15.7
2.22	5.6	24.6	3.9	24.1
2.31	6.1	28.2	4.4	27.3
2.39	8.7	50.1	7.7	49.6
2.48	12.3	70.9	11.0	71.03
2.57	16.4	90.7	14.3	91.9
2.66	21.3	111.1	17.4	114.8

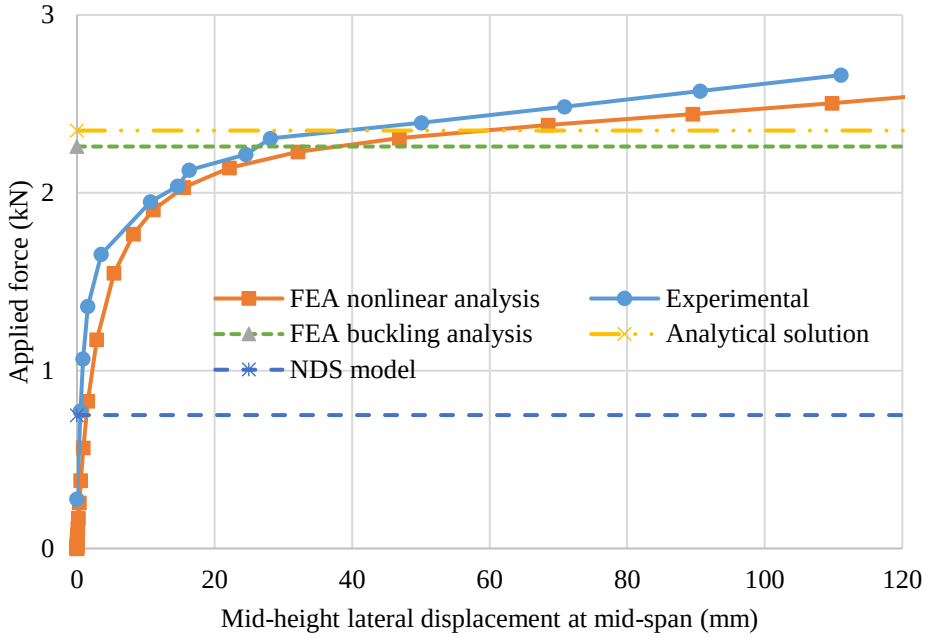

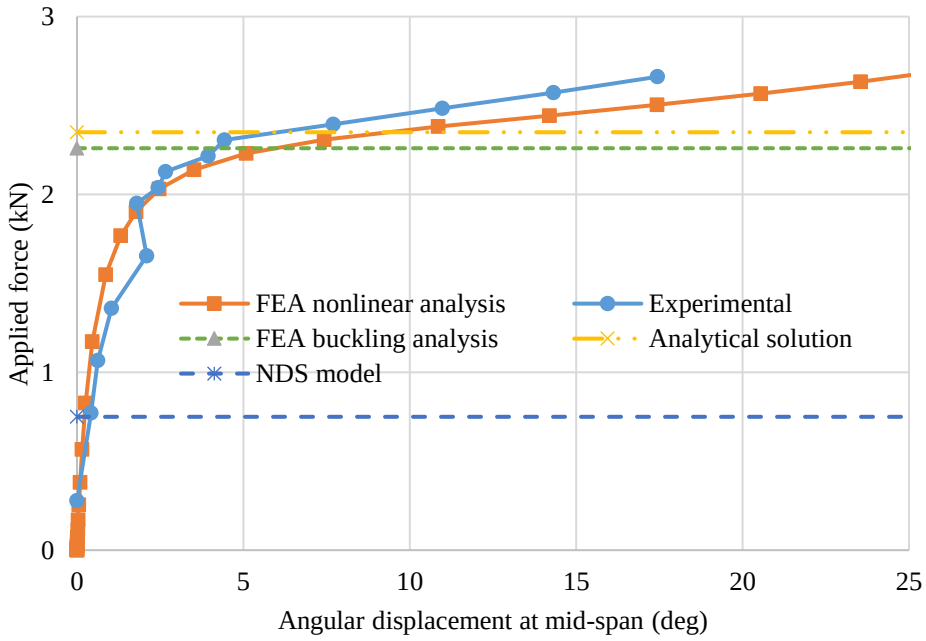

Figure A-30 Buckling displacements of specimen 10-8

Specimen 11 Sample group 8

Table A-31 Buckling displacements of specimen 11-8

Mid-span				Quarter-span
Force (kN)	**Vertical displacement (mm)**	**Lateral displacement at mid-height (mm)**	**Angle of twist (Deg)**	**Lateral displacement at top flange (mm)**
0.28	0.0	0.0	0.0	0
0.77	0.9	2.3	0.2	1.98
1.07	1.7	4.0	0.4	4.2
1.36	2.6	6.6	0.8	6.31
1.65	3.5	11.4	1.5	11.18
1.95	4.8	20.3	2.8	19.6
2.04	5.4	24.4	3.5	24.5
2.13	6.0	29.9	4.3	29.8
2.22	7.6	44.3	6.5	44
2.31	9.5	57.6	8.4	57.8
2.39	12.7	76.9	11.4	78.3
2.48	16.7	98.4	14.7	100

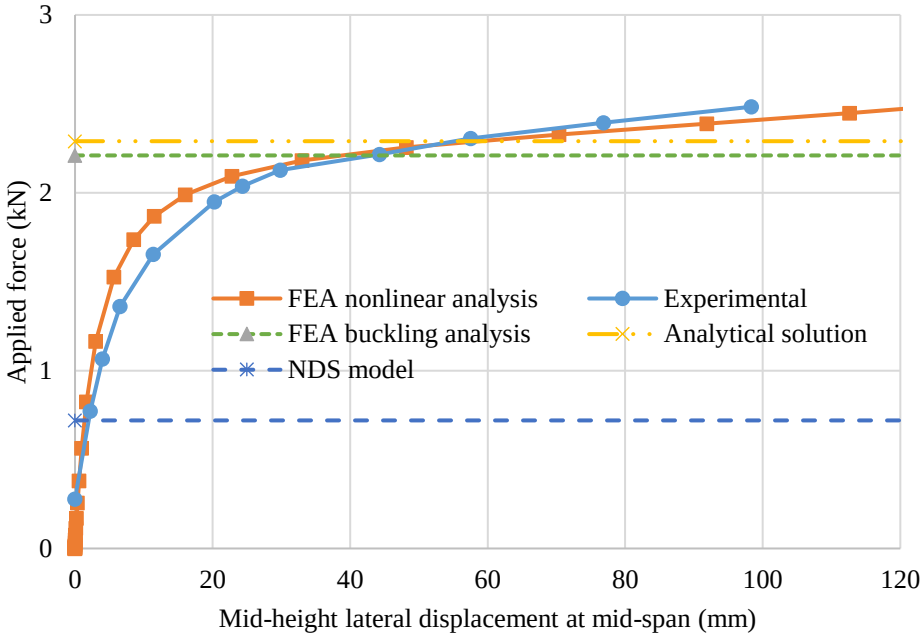

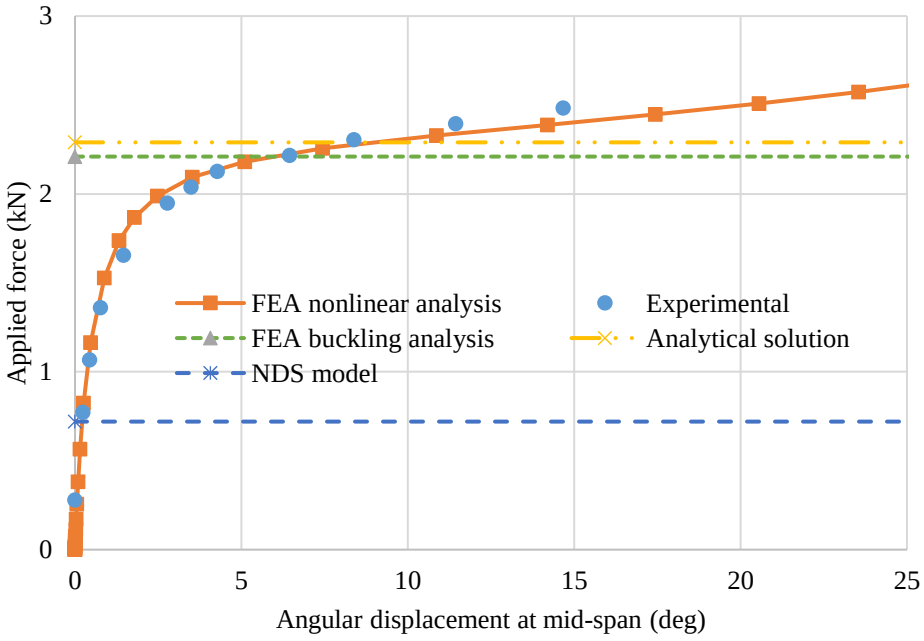

Figure A-31 Buckling displacements of specimen 11-8

Specimen 1 Sample group 16

Table A-32 Buckling displacements of specimen 1-16

Mid-span				Quarter-span
Force (kN)	**Vertical displacement (mm)**	**Lateral displacement at mid-height (mm)**	**Angle of twist (Deg)**	**Lateral displacement at top flange (mm)**
0.46	0.0	0.0	0.0	0
3.32	2.7	6.2	1.2	7.9
3.61	3.0	8.6	1.9	11.4
3.91	3.3	10.0	2.2	13.0
4.20	3.7	12.4	2.7	17.0
4.50	4.0	16.7	3.8	22.7
4.79	4.7	24.7	6.0	33.2
4.88	4.8	25.1	6.0	33.7
4.97	5.3	30.2	7.4	40.4
5.06	5.4	31.7	7.7	42.6
5.14	5.9	36.4	8.9	48.6
5.23	6.6	42.2	10.5	56.6
5.32	7.3	49.5	12.5	65.9
5.41	8.8	60.1	15.5	82.0
5.50	9.7	66.6	17.2	89.8
5.58	10.9	73.4	19.0	98.0
5.67	12.5	81.3	21.0	110.2

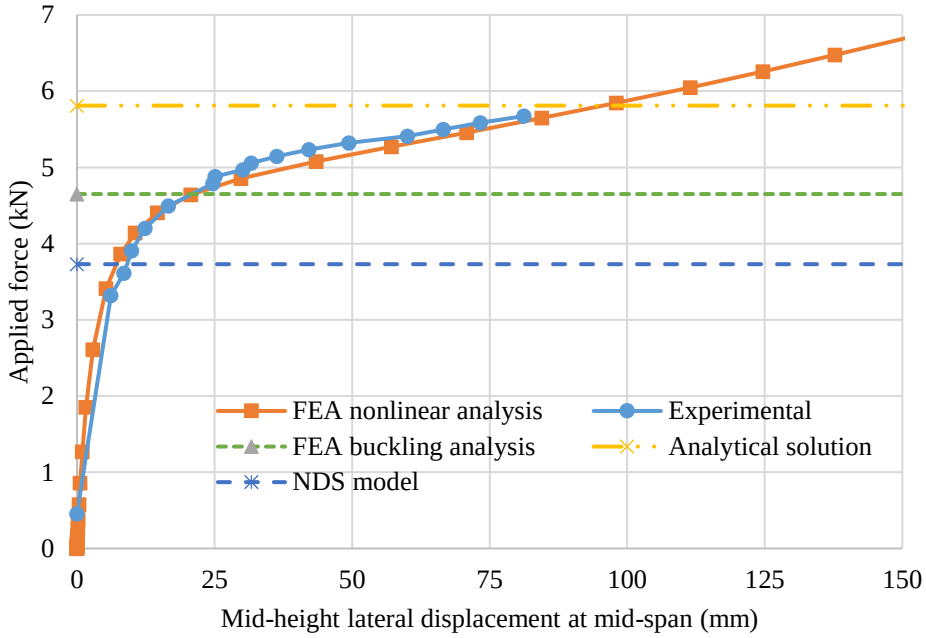

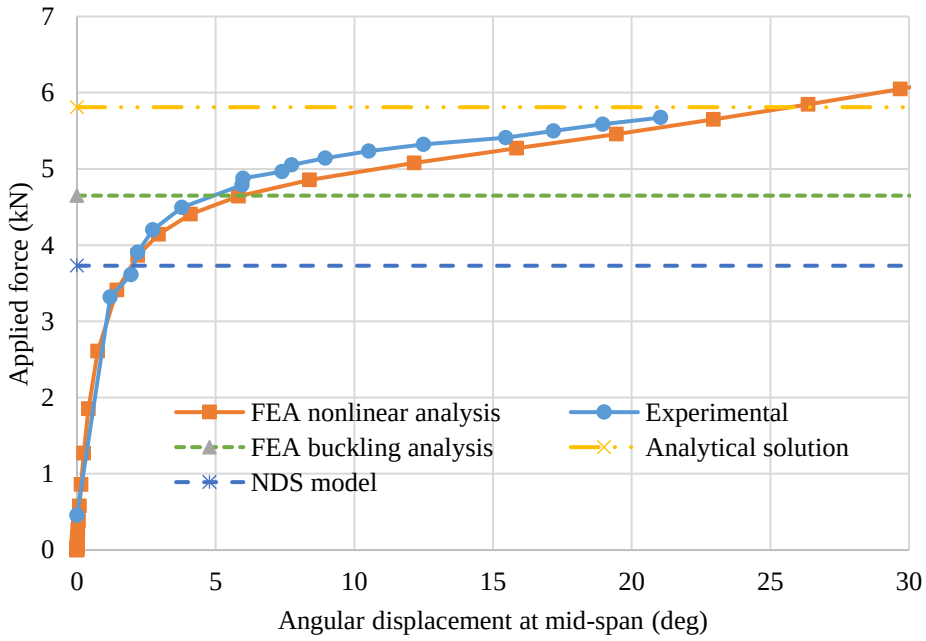

Figure A-32 Buckling displacements of specimen 1-16

Specimen 2 Sample group 16

Table A-33 Buckling displacements of specimen 2-16

Mid-span				Quarter-span
Force (kN)	**Vertical displacement (mm)**	**Lateral displacement at mid-height (mm)**	**Angle of twist (Deg)**	**Lateral displacement at top flange (mm)**
0.46	0.0	0.0	0.0	0
3.32	2.6	6.5	1.1	8.0
3.61	3.0	9.3	1.8	11.9
3.91	3.5	12.3	2.4	16.6
4.20	4.1	17.9	3.8	23.7
4.50	4.9	25.0	5.5	32.8
4.79	6.6	41.0	9.7	53.2
5.08	10.2	65.5	15.8	84.7
5.17	11.2	71.1	17.3	98.0
5.26	13.4	82.6	20.0	106.6
5.35	27.1	183.4	37.2	172.6

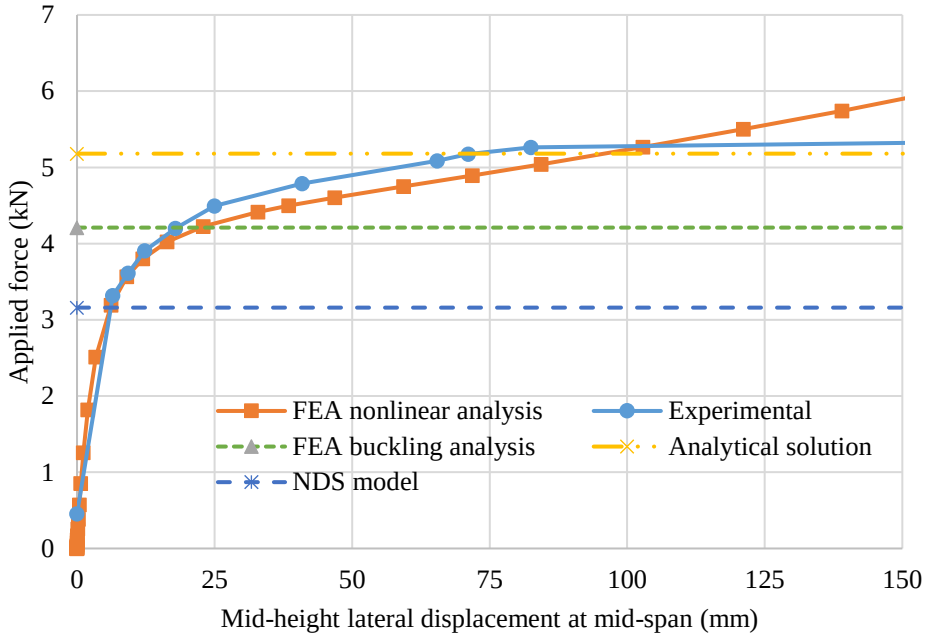

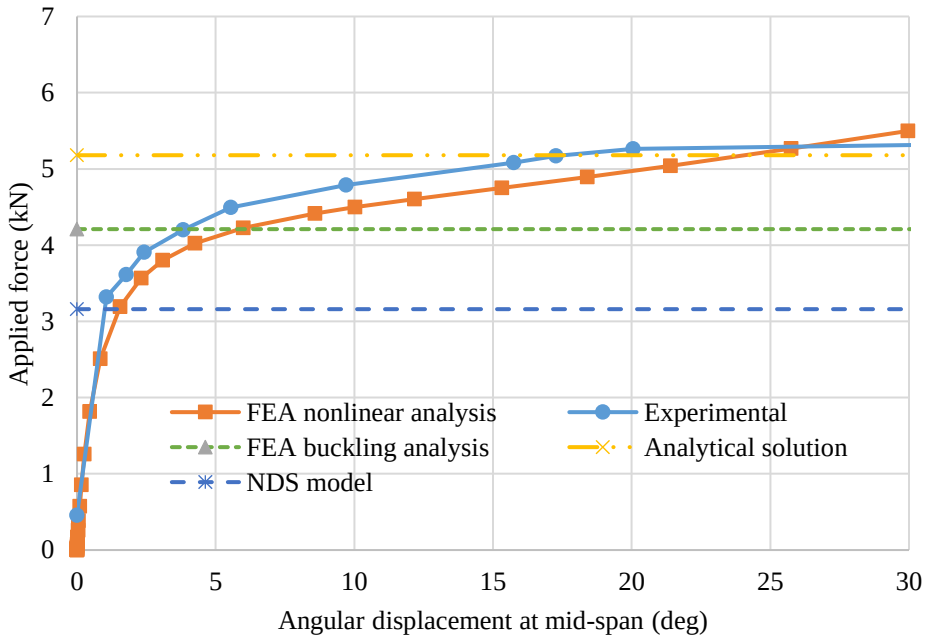

Figure A-33 Buckling displacements of specimen 2-16

Specimen 3 Sample group 16

Table A-34 Buckling displacements of specimen 3-16

Mid-span				Quarter-span
Force (kN)	**Vertical displacement (mm)**	**Lateral displacement at mid-height (mm)**	**Angle of twist (Deg)**	**Lateral displacement at top flange (mm)**
0.46	0.0	0.0	0.0	0
2.33	2.0	5.3	1.2	7.7
2.73	2.4	7.0	1.6	9.5
3.02	2.6	10.0	2.2	13.7
3.32	2.9	13.3	3.0	17.6
3.61	3.4	17.2	3.9	22.8
3.91	4.0	22.1	5.1	28.9
4.20	4.8	29.5	6.9	38.7
4.50	5.9	38.5	9.1	50.7
4.79	7.5	49.4	11.8	65.4
5.08	11.0	70.9	16.7	92.9
5.17	11.9	75.3	18.0	99.2
5.26	12.7	77.9	18.5	103.6
5.35	14.4	86.0	20.5	114.9
5.44	15.5	90.4	21.4	120.8
5.53	17.5	100.0	23.8	133.9

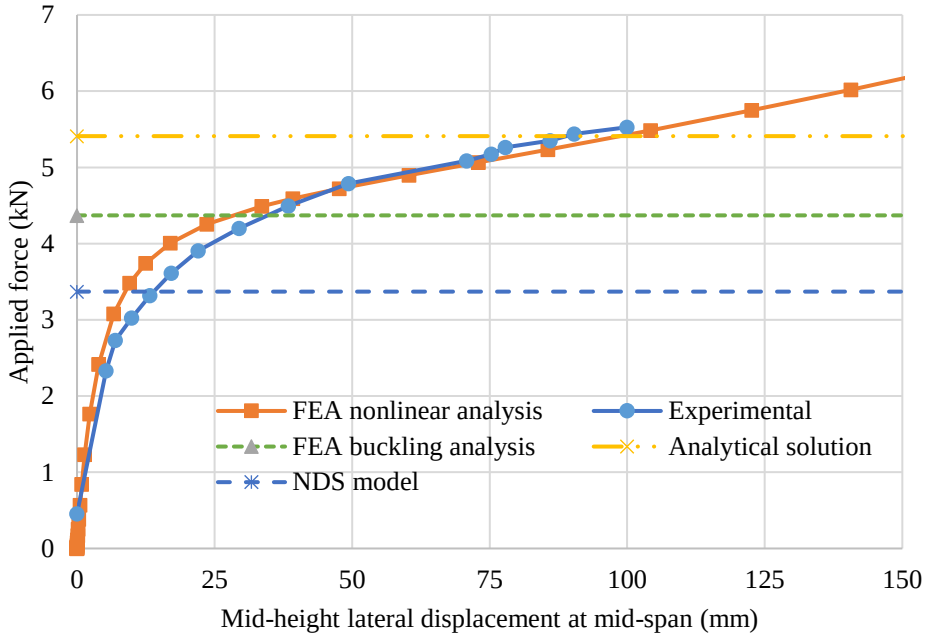

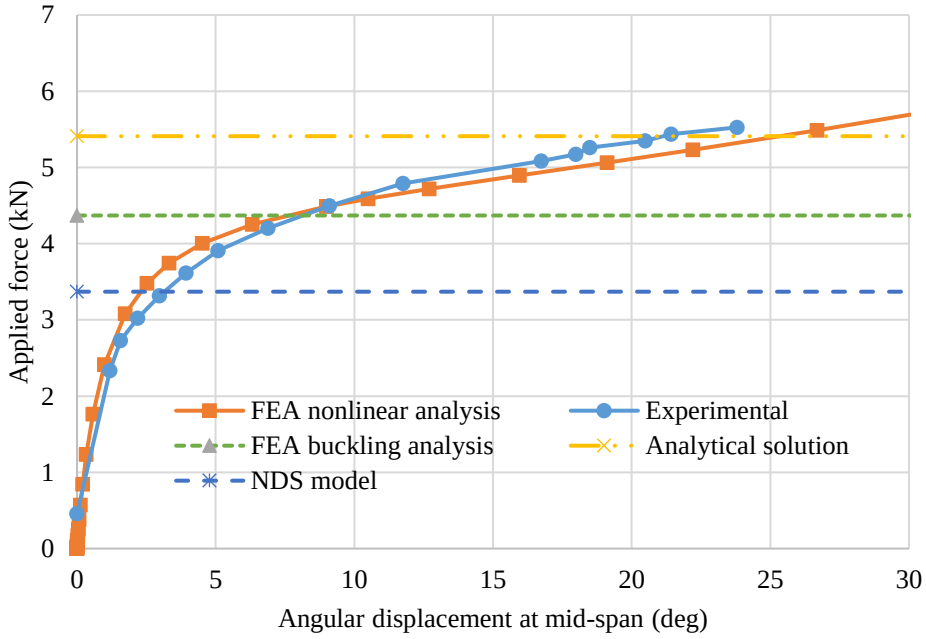

Figure A-34 Buckling displacements of specimen 3-16

Specimen 4 Sample group 16

Table A-35 Buckling displacements of specimen 4-16

Mid-span				Quarter-span
Force (kN)	**Vertical displacement (mm)**	**Lateral displacement at mid-height (mm)**	**Angle of twist (Deg)**	**Lateral displacement at top flange (mm)**
0.46	0	0.0	0.0	0.0
3.32	-0.3	2.1	0.3	0.0
3.91	-0.2	2.6	0.3	0.0
4.20	0.3	2.9	0.7	0.2
4.50	0.4	3.2	0.9	0.2
4.79	1.7	3.5	1.9	0.4
4.88	2.0	3.5	2.0	0.5
4.97	2.4	3.6	2.4	0.6
5.06	2.5	3.7	2.6	0.7
5.14	2.9	3.8	3.0	0.8
5.23	3.6	3.9	3.6	0.9
5.32	6.1	4.0	5.4	1.4
5.41	7.2	4.1	6.4	1.6
5.50	12.0	4.4	10.3	2.5
5.58	72.3	8.2	55.6	14.0
5.67	94.6	11.0	72.9	18.3
5.76	106.6	12.8	81.0	20.3

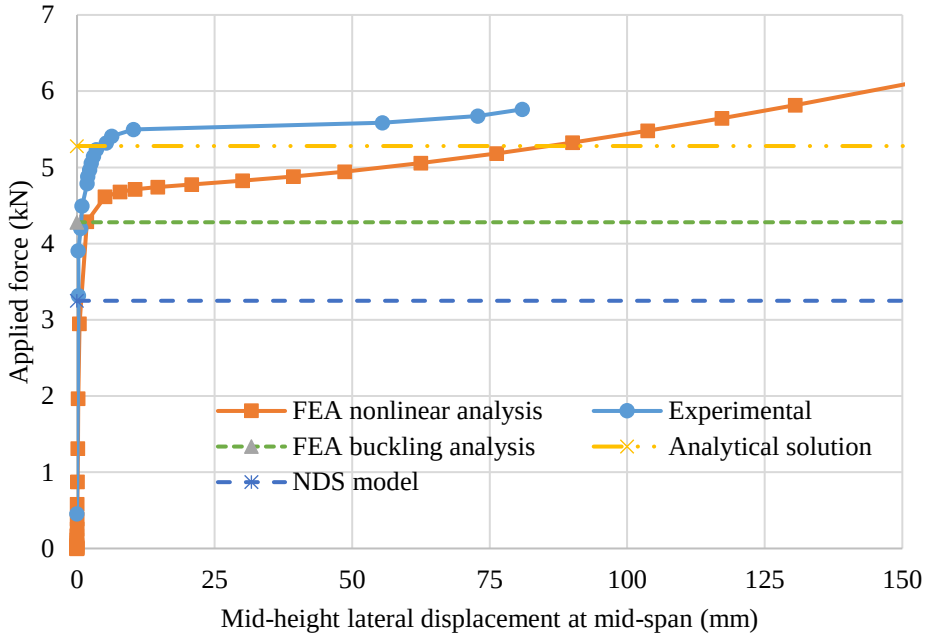

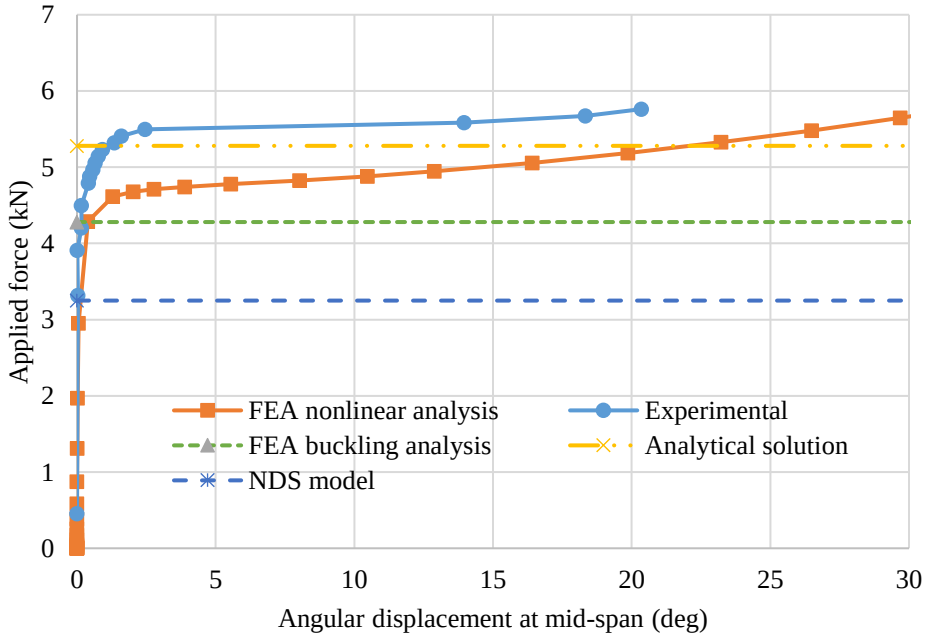

Figure A-35 Buckling displacements of specimen 4-16

Specimen 5 Sample group 16

Table A-36 Buckling displacements of specimen 5-16

Mid-span				Quarter-span
Force (kN)	**Vertical displacement (mm)**	**Lateral displacement at mid-height (mm)**	**Angle of twist (Deg)**	**Lateral displacement at top flange (mm)**
0.46	0.0	0.0	0.0	0
3.32	2.9	22.0	4.9	27.4
3.61	3.3	26.9	6.0	33.7
3.91	4.2	34.7	7.9	42.9
4.20	5.6	44.8	10.4	57.1
4.50	7.7	58.7	13.7	73.6
4.79	10.2	73.6	17.0	93.7
4.88	11.6	80.2	18.5	102.5
4.97	12.9	87.8	20.3	111.6
5.06	14.0	93.5	21.5	119.4
5.14	15.5	101.5	23.3	130.0
5.23	17.6	110.1	25.2	141.8
5.32	18.6	116.3	26.3	149.6
5.41	20.6	126.6	28.3	149.6
5.50	22.0	138.2	30.7	149.6
5.58	22.4	172.3	34.9	149.6
0.46	0.4	24.9	4.3	27.0

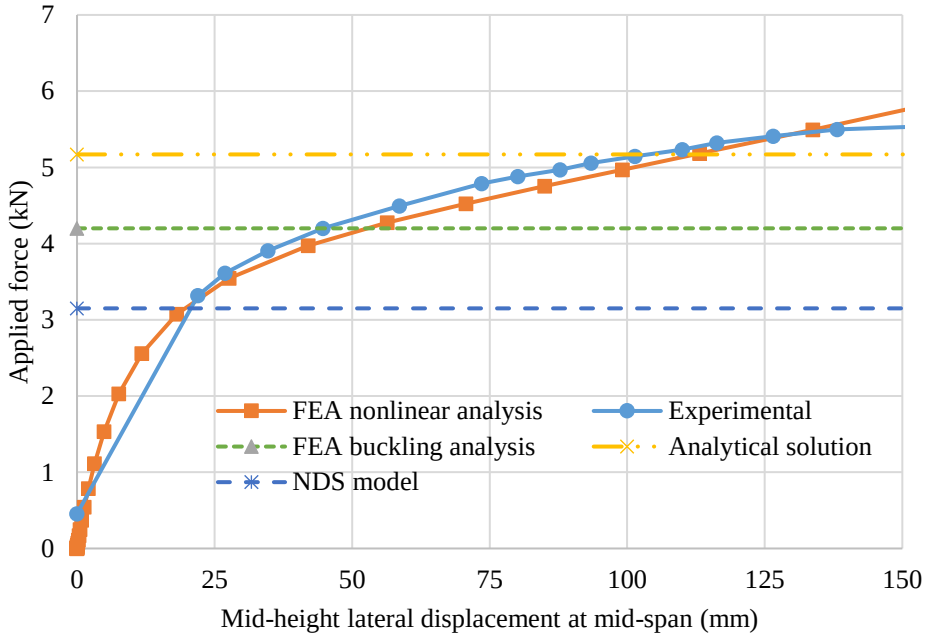

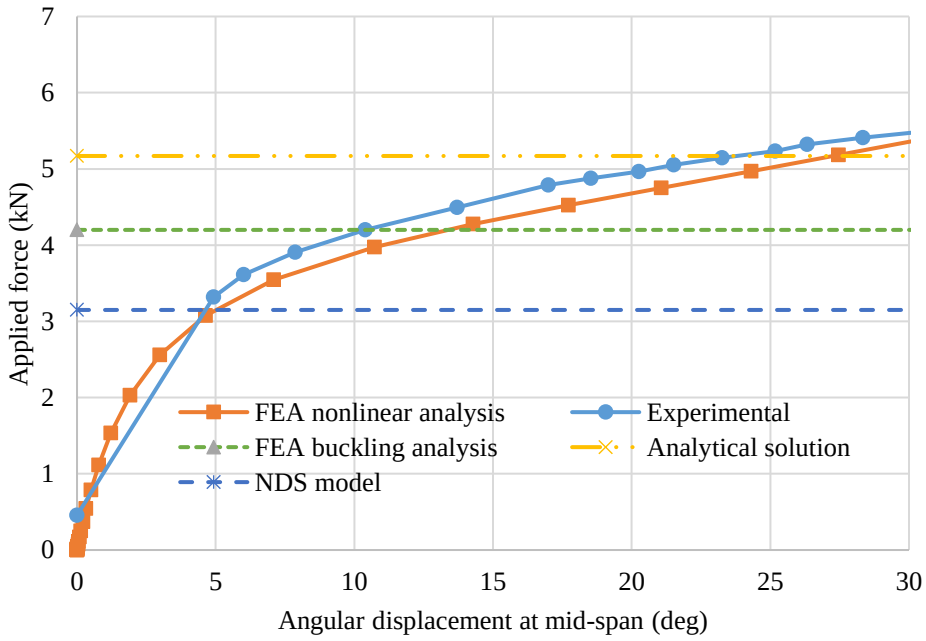

Figure A-36 Buckling displacement of specimen 5-16

Specimen 6 Sample group 16

Table A-37 Buckling displacements of specimen 6-16

Mid-span				Quarter-span
Force (kN)	**Vertical displacement (mm)**	**Lateral displacement at mid-height (mm)**	**Angle of twist (Deg)**	**Lateral displacement at top flange (mm)**
0.46	0.0	0.0	0.0	0
3.32	2.7	4.0	0.8	2.7
3.61	2.9	5.1	1.0	4.1
3.91	3.3	7.7	1.7	7.7
4.20	3.6	9.0	1.9	9.7
4.50	4.0	15.3	3.3	19.9
4.79	4.8	26.2	6.0	33.8
4.88	5.4	34.6	8.1	45.2
4.97	6.3	44.1	10.5	58.3
5.06	7.9	59.4	14.2	78.5
5.14	9.3	69.7	16.7	90.6
5.23	9.9	74.7	17.7	96.3
5.32	10.2	84.2	19.9	108.3
5.41	11.4	92.6	21.8	118.4
5.50	13.1	102.9	24.0	130.9
0.46	0.1	5.0	1.3	0.2

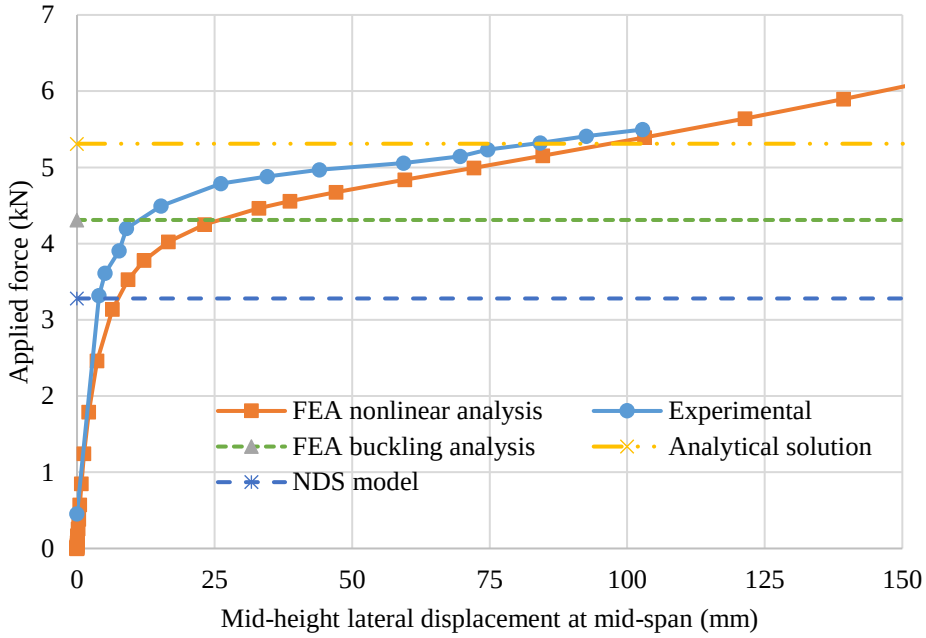

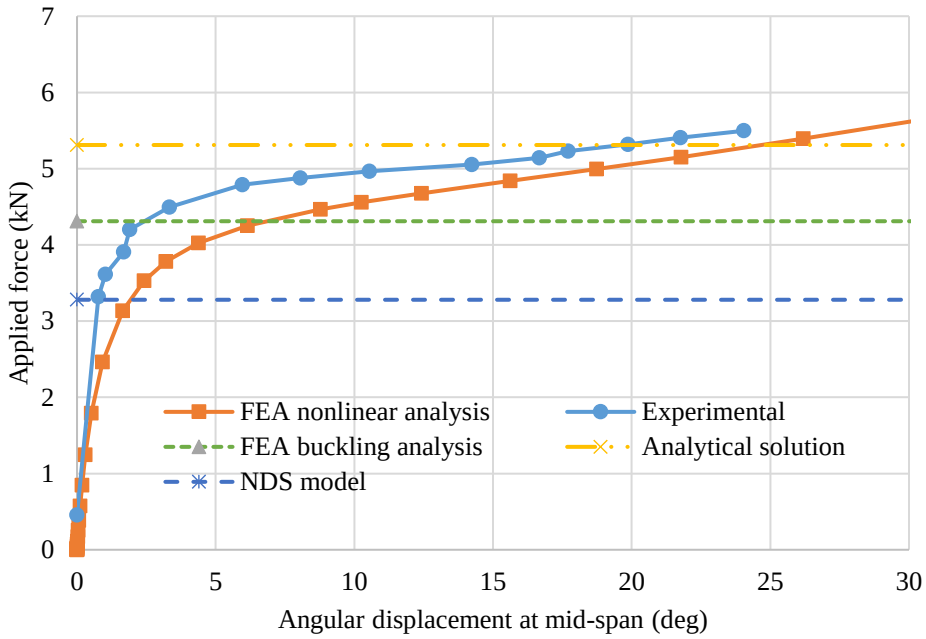

Figure A-37 Buckling displacement of specimen 6-16

Specimen 7 Sample group 16

Table A-38 Buckling displacements of specimen 7-16

Mid-span				Quarter-span
Force (kN)	**Vertical displacement (mm)**	**Lateral displacement at mid-height (mm)**	**Angle of twist (Deg)**	**Lateral displacement at top flange (mm)**
0.46	0.0	0.0	0.0	0
3.32	1.7	3.0	0.8	3.7
3.61	2.0	5.3	1.4	6.6
3.91	2.4	5.7	1.5	7.8
4.20	2.8	8.7	2.3	11.0
4.50	3.1	10.9	2.8	13.9
4.79	4.6	29.7	7.5	37.1
4.88	4.9	31.9	8.0	39.4
4.97	5.3	35.0	8.8	43.2
5.06	6.0	41.3	10.3	51.3
5.14	6.9	48.7	12.3	61.3
5.23	8.3	57.2	14.5	72.7
5.32	9.8	65.8	16.6	83.0
5.41	11.2	73.8	18.7	93.9
5.50	12.9	81.9	20.7	103.8
5.58	14.6	89.7	22.4	114.8
5.67	16.1	95.7	23.8	122.2
0.46	0.7	7.7	2.4	3.1

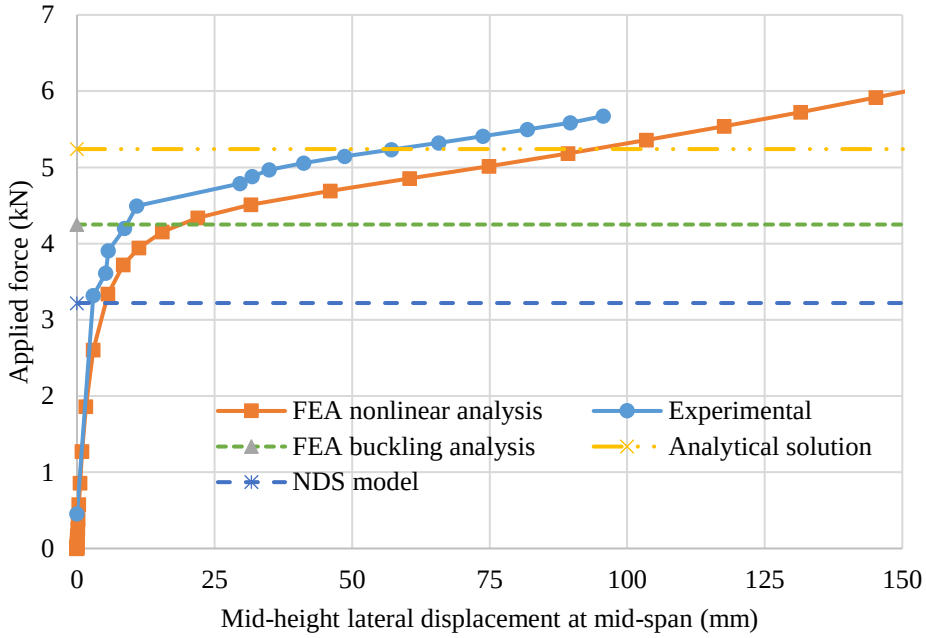

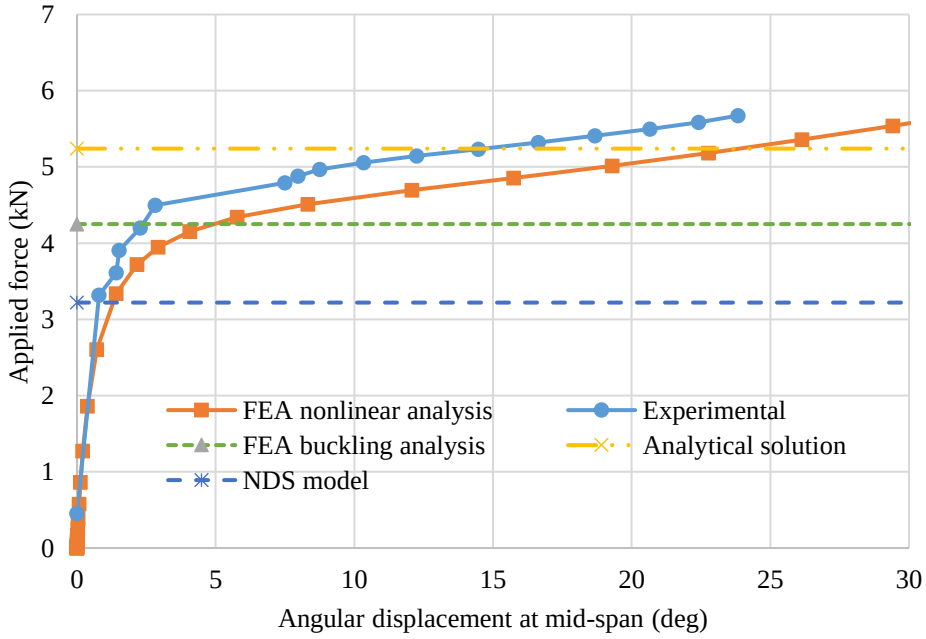

Figure A-38 Buckling displacement of specimen 7-16

Specimen 8 Sample group 16

Table A-39 Buckling displacements of specimen 8-16

Mid-span				Quarter-span
Force (kN)	**Vertical displacement (mm)**	**Lateral displacement at mid-height (mm)**	**Angle of twist (Deg)**	**Lateral displacement at top flange (mm)**
0.46	0.0	0.0	0.0	0
3.32	2.5	0.9	0.1	0.5
3.61	2.6	1.0	0.1	0.4
3.91	2.6	1.2	0.2	0.8
4.20	2.6	1.1	0.1	0.6
4.50	2.6	1.6	0.2	0.8
4.79	2.7	1.7	0.2	0.8
4.88	2.8	1.7	0.2	0.8
4.97	2.8	1.9	0.2	0.8
5.06	2.9	1.9	0.2	0.8
5.14	3.0	2.1	0.3	0.8
5.23	3.1	1.9	0.2	0.8
5.32	3.2	1.8	0.2	0.8
5.41	3.2	7.5	2.8	-12.4
5.50	3.2	4.8	1.8	-8.5
5.58	21.4	189.3	36.1	169.7
0.46	0.9	39.3	7.8	31.1

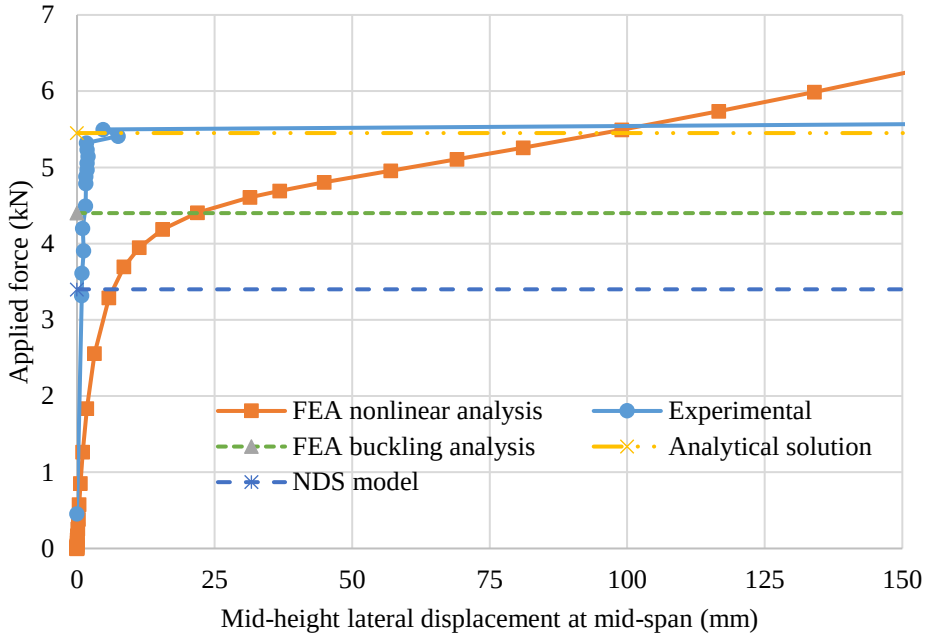

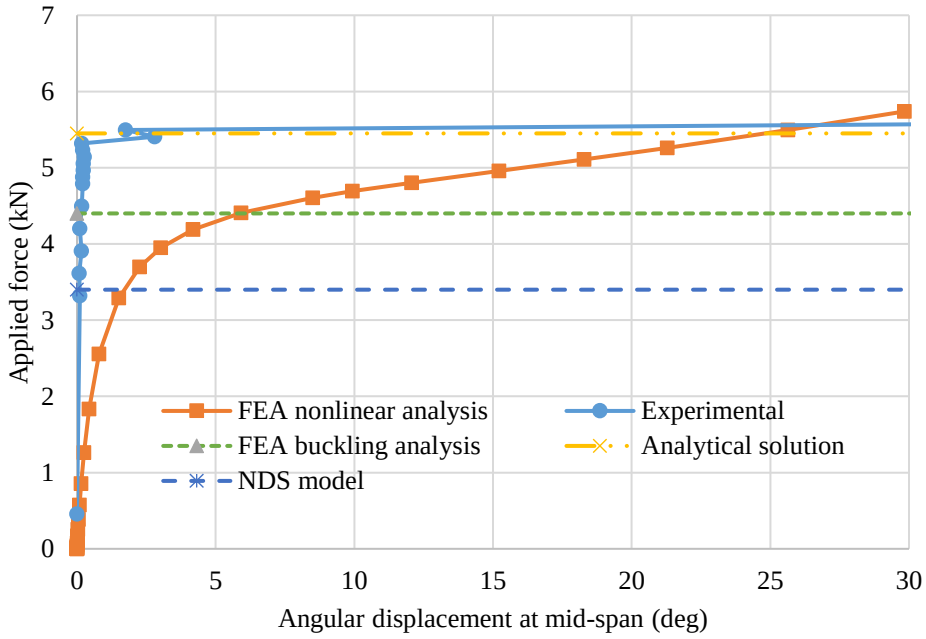

Figure A-39 Buckling displacement of specimen 8-16

Specimen 9 Sample group 16

Table A-40 Buckling displacements of specimen 9-16

Mid-span				Quarter-span
Force (kN)	**Vertical displacement (mm)**	**Lateral displacement at mid-height (mm)**	**Angle of twist (Deg)**	**Lateral displacement at top flange (mm)**
0.46	0.0	0.0	0.0	0
3.32	3.4	16.2	3.8	23.1
3.61	3.9	21.2	4.8	28.8
3.91	4.5	27.5	6.4	38.8
4.20	5.3	34.2	7.9	47.8
4.50	6.6	44.5	10.4	62.1
4.79	8.7	61.2	14.5	82.1
4.88	9.5	65.5	15.6	88.1
4.97	10.2	70.0	16.7	93.9
5.06	11.2	74.5	17.6	101.1
5.14	12.6	81.5	19.3	110.2
5.23	13.5	87.6	20.9	117.5
5.32	15.1	94.0	22.5	126.9
5.41	16.9	104.9	24.9	138.9
5.50	17.9	107.1	25.4	145.0
5.58	18.8	112.4	26.7	150.5
5.67	19.5	116.2	27.4	156.2
5.76	20.8	121.9	28.8	159.1
5.85	21.7	128.7	30.2	159.1
0.46	0.3	3.3	0.9	4.5

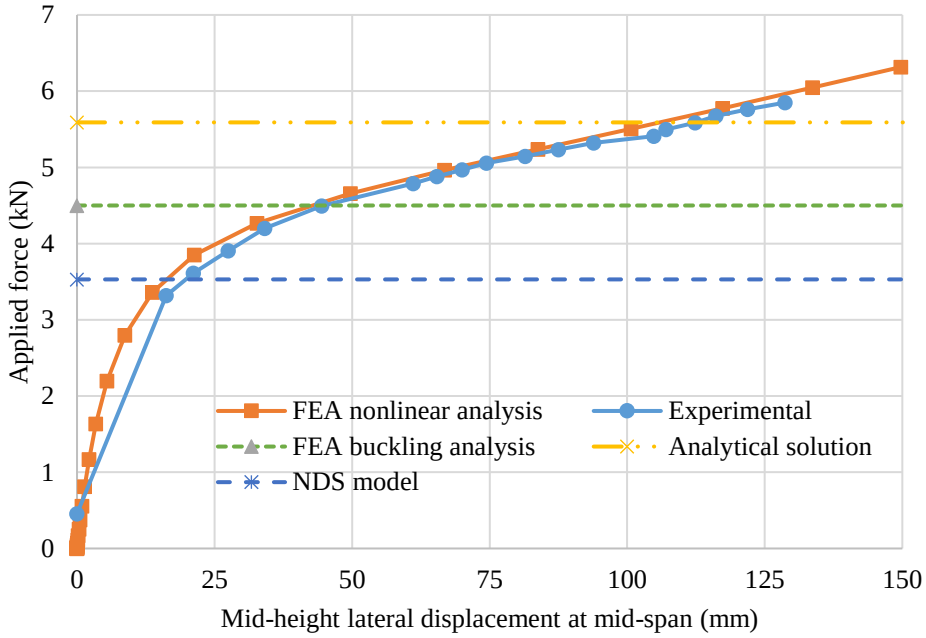

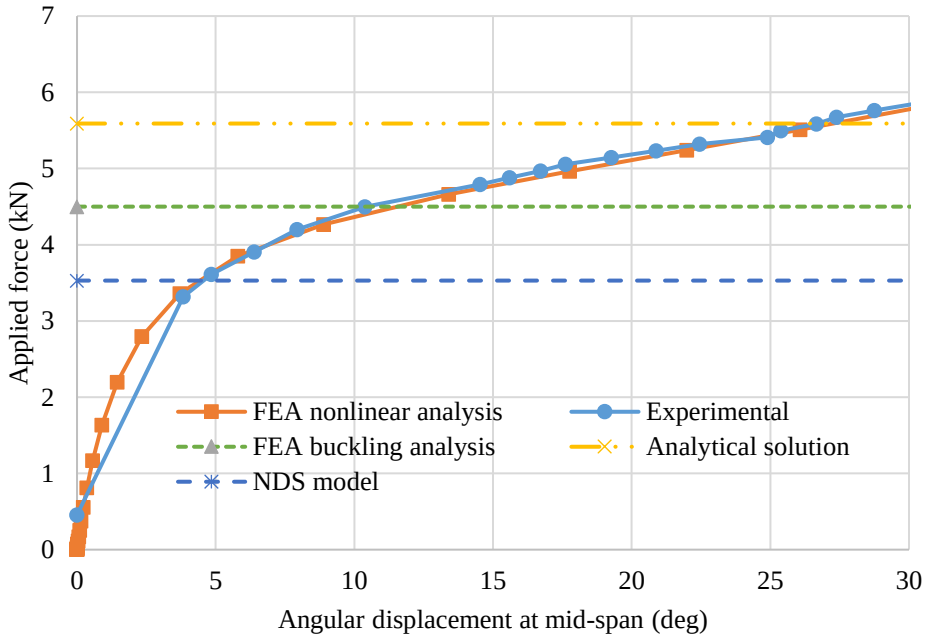

Figure A-40 Buckling displacements of specimen 9-16

Specimen 10 Sample group 16

Table A-41 Buckling displacements of specimen 10-16

Mid-span				Quarter-span
Force (kN)	**Vertical displacement (mm)**	**Lateral displacement at mid-height (mm)**	**Angle of twist (Deg)**	**Lateral displacement at top flange (mm)**
0.46	0.0	0.0	0.0	0
3.32	3.1	2.7	0.6	4.6
3.61	3.4	2.3	0.4	3.9
3.91	3.7	3.9	0.9	5.5
4.20	4.1	6.2	1.4	9.0
4.50	4.5	8.3	1.9	11.8
4.79	4.8	10.7	2.5	15.3
4.88	5.0	13.2	3.0	18.3
4.97	5.3	15.9	3.6	21.4
5.06	7.2	42.2	10.2	57.0
5.14	7.2	52.2	12.9	70.1
5.23	8.7	62.5	15.7	84.6
5.32	10.6	74.2	18.8	100.1
5.41	12.9	84.7	21.6	115.1
5.50	15.2	95.1	24.3	130.2
0.46	6.0	2.9	0.9	5.2

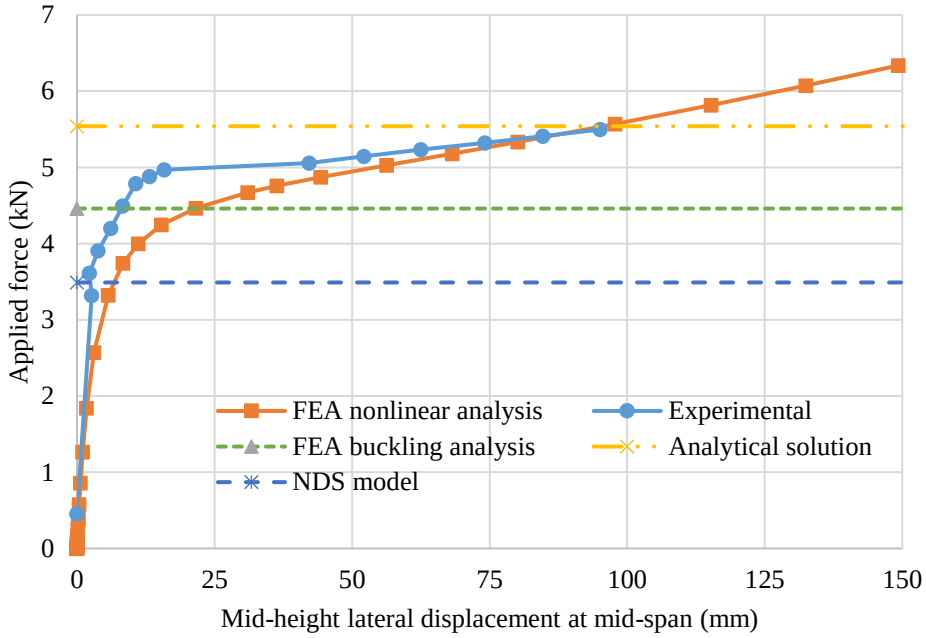

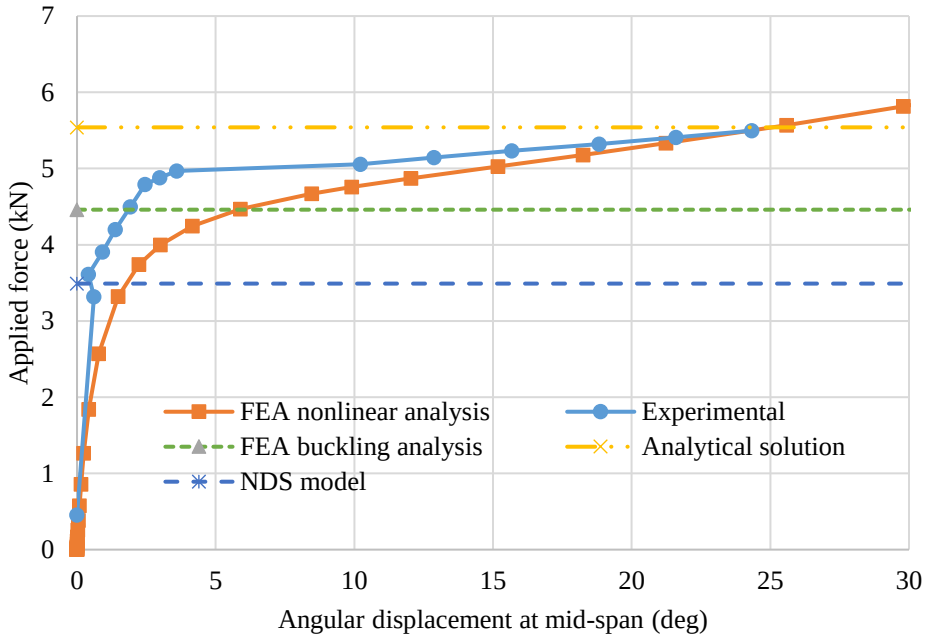

Figure A-41 Buckling displacements of specimen 10-16

Specimen 11 Sample group 16

Table A-42 Buckling displacements of specimen 11-16

Mid-span				Quarter-span
Force (kN)	**Vertical displacement (mm)**	**Lateral displacement at mid-height (mm)**	**Angle of twist (Deg)**	**Lateral displacement at top flange (mm)**
0.46	0.0	0.0	0.0	0
3.32	2.4	11.3	2.4	15.5
3.61	2.7	14.3	2.9	18.6
3.91	3.0	22.1	4.6	28.9
4.20	3.5	29.2	6.3	38.5
4.50	4.1	37.3	8.3	49.8
4.79	5.4	53.0	12.2	71.4
4.88	6.0	56.9	13.2	75.6
4.97	6.3	63.0	14.8	83.1
5.06	6.4	69.4	16.6	92.0
5.14	7.4	75.5	18.2	100.0
5.23	8.5	81.3	19.6	109.2
5.32	9.8	88.5	21.4	118.2
5.41	11.3	96.6	23.4	128.4
5.50	12.1	99.8	24.0	132.9
5.58	13.1	104.9	25.1	139.2
5.67	14.5	111.5	26.9	148.0
5.76	15.2	114.3	27.1	150.4
5.85	16.3	119.4	28.3	----
0.46	0.1	2.8	0.7	3

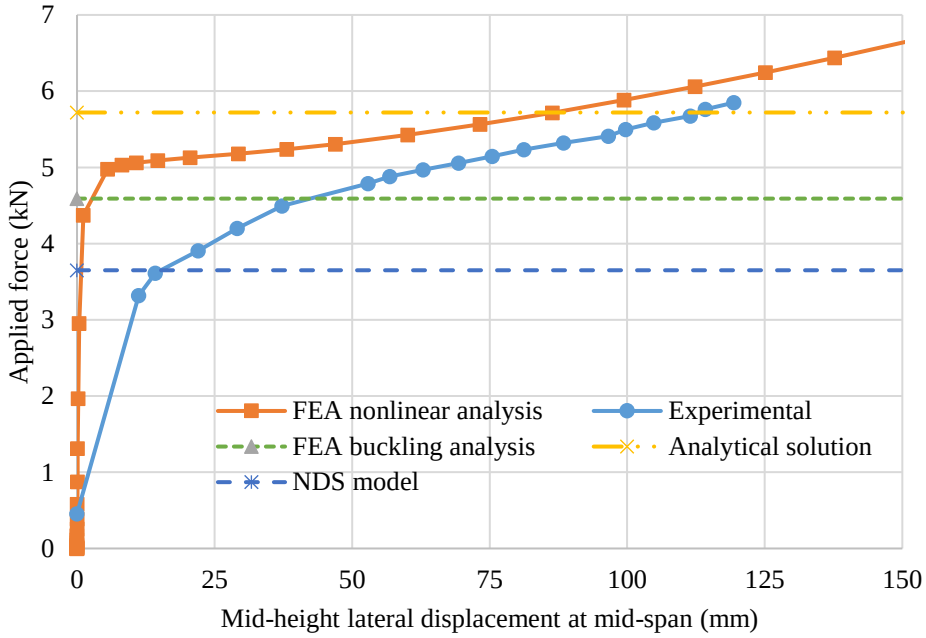

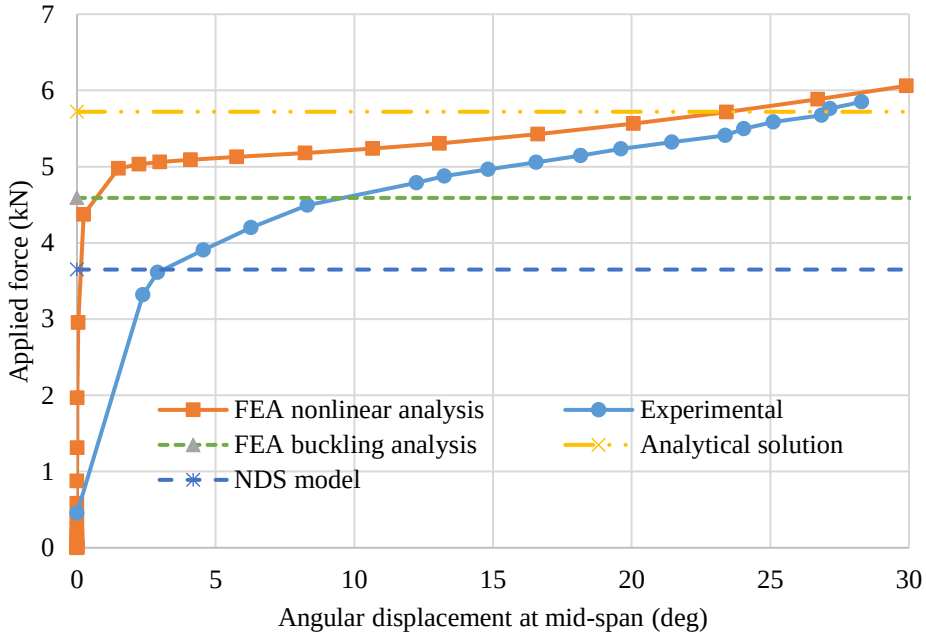

Figure A-42 Buckling displacements of specimen 11-16

APPENDIX B

1.1 *Experimental results of wood I-joist mechanical properties*

Table B-1: Lateral flexural stiffness of wood I-joists

Specimen length (ft)	Specimen #	EI_y x 10^{10} Nmm^2 (16 in. I-joist)			EI_y x 10^{10} Nmm^2 (24 in. I-joist)		
		Side A	Side B	Average	Side A	Side B	Average
6	1	1.98	2.03	2.00	4.47	4.55	4.51
6	2	2.02	2.12	2.07	4.69	4.93	4.81
6	3	2.12	2.06	2.09	5.33	5.36	5.35
6	4	1.98	2.05	2.02	5.10	4.74	4.92
6	5	2.14	2.19	2.17	4.73	4.37	4.55
6	6	1.75	1.75	1.75	5.50	4.86	5.18
6	7	2.18	2.15	2.17	4.63	4.70	4.66
6	8	1.92	1.92	1.92	5.34	5.12	5.23
6	9	2.20	2.21	2.21	5.43	5.23	5.33
6	10	1.95	2.05	2.00	5.14	5.06	5.10
8	1	1.89	1.87	1.88	4.65	4.97	4.81
8	2	1.91	1.94	1.93	4.79	4.84	4.81
8	3	1.95	1.93	1.94	5.08	4.80	4.94
8	4	1.80	1.78	1.79	4.80	4.81	4.80
8	5	2.02	2.05	2.03	4.68	4.95	4.82
8	6	1.88	1.85	1.87	5.23	4.73	4.98
8	7	2.04	2.05	2.04	5.05	4.92	4.98
8	8	2.07	2.12	2.09	5.38	5.30	5.34
8	9	2.10	2.06	2.08	5.15	4.98	5.07
8	10	2.09	2.08	2.09	5.37	5.11	5.24
10	1	1.89	1.89	1.89	4.77	4.61	4.69
10	2	2.08	2.08	2.08	5.01	5.06	5.03
10	3	1.93	1.98	1.95	5.31	5.14	5.23
10	4	2.24	2.22	2.23	5.67	5.53	5.60
10	5	2.00	2.10	2.05	5.35	5.05	5.20
10	6	2.07	2.00	2.04	5.13	5.07	5.10
10	7	1.95	1.98	1.97	5.34	5.40	5.37
10	8	1.92	1.91	1.92	6.23	6.19	6.21
10	9	2.02	2.00	2.01	4.90	4.96	4.93
10	10	2.05	2.03	2.04	4.98	5.01	4.99
12	1	2.04	2.08	2.06	5.09	4.95	5.02
12	2	2.23	2.24	2.23	5.79	5.68	5.74
12	3	2.10	2.10	2.10	5.66	5.68	5.67
12	4	2.11	2.07	2.09	5.45	5.54	5.50
12	5	2.09	2.16	2.13	5.96	5.77	5.86
12	6	2.13	2.13	2.13	5.92	5.81	5.87

12	7	2.21	2.21	2.21	5.25	5.32	5.29
12	8	1.99	1.99	1.99	5.98	6.23	6.10
12	9	2.08	2.09	2.08	5.47	5.35	5.41
12	10	2.25	2.18	2.22	5.29	5.40	5.35
14	1	2.10	2.05	2.07	5.56	5.69	5.62
14	2	2.33	2.06	2.20	4.87	4.94	4.91
14	3	2.30	2.05	2.18	5.54	5.58	5.56
14	4	2.00	1.97	1.98	5.43	5.37	5.40
14	5	2.18	2.15	2.16	5.40	5.30	5.35
14	6	2.23	2.11	2.17	5.42	5.39	5.41
14	7	2.17	2.21	2.19	5.59	5.64	5.61
14	8	2.14	2.32	2.23	5.34	5.25	5.29
14	9	1.98	2.07	2.03	5.83	5.75	5.79
14	10	2.19	2.19	2.19	5.46	5.65	5.55
16	1	2.03	1.93	1.98	5.41	5.60	5.50
16	2	2.16	2.15	2.16	5.61	5.70	5.65
16	3	1.91	1.96	1.94	5.43	5.46	5.45
16	4	1.88	2.14	2.01	5.33	5.29	5.31
16	5	2.12	2.12	2.12	5.18	5.20	5.19
18	1	1.84	1.83	1.84	4.63	4.84	4.73
18	2	2.15	2.19	2.17	4.67	4.87	4.77
18	3	2.09	2.07	2.08	5.02	4.88	4.95
18	4	2.15	2.34	2.25	4.97	4.90	4.94
18	5	1.63	1.99	1.81	5.73	5.82	5.78
20	1	2.24	2.21	2.22	6.15	5.89	6.02
20	2	2.52	2.12	2.32	5.22	4.96	5.09
20	3	2.14	2.47	2.31	5.58	5.28	5.43
20	4	2.08	2.49	2.28	5.30	5.18	5.24
20	5	2.44	2.00	2.22	5.08	5.06	5.07
20	6	3.26	3.00	3.13	5.06	5.52	5.29
20	7	2.39	2.33	2.36	5.08	5.28	5.18
20	8	2.11	2.34	2.23	5.45	5.52	5.49
20	9	2.12	2.44	2.28	5.70	5.69	5.69
20	10	2.32	2.22	2.27	5.36	5.88	5.62
20	11	2.17	2.17	2.17	5.83	5.96	5.90
Average	----	----	----	**2.10**	----	----	**5.27**
COV	----	----	----	**0.087**	----	----	**0.072**